2014

High Frequency AC Power Systems

Huaxi Zheng
University of South Carolina - Columbia

HIGH FREQUENCY AC POWER SYSTEMS

by

Huaxi Zheng

Bachelor of Science
Beijing Jiaotong University, 2007

Master of Science
Beijing Jiaotong University, 2009

Submitted in Partial Fulfillment of the Requirements

For the Degree of Doctor of Philosophy in

Electrical Engineering

College of Engineering and Computing

University of South Carolina

2014

Accepted by:

Roger A. Dougal, Major Professor

Herbert L. Ginn III, Committee Member

Charles W. Brice, Committee Member

Jamil A. Khan, Committee Member

Lacy Ford, Vice Provost and Dean of Graduate Studies

DEDICATION

This dissertation is dedicated to all of the people who have supported me through this process.

I am especially grateful to my wife Yang Yue, whose unconditional love, unstoppable support, and hard work made this possible. You are the most encouraging, wonderful, creative, and thoughtful person I know and I am still amazed that I have the privilege of being your husband. I could not have accomplished any of these without you. Thank you. I wish you could receive an honorary degree with me; you have definitely put in enough work and learned alongside me. I love you.

To my parents, Chongsu Zheng and Yang Zhuang: Thank you for your love, encouragement and pride in my accomplishments. It means more than you know.

To my in-laws, Fuqiang Yue and Xun Zhang: In the end, you were working as hard as I was. I could not have done it without your help.

ACKNOWLEDGEMENTS

I would like to express my most sincere appreciations to my advisor, Dr. Roger A. Dougal, for his professional and patient guidance over the course of my Ph.D. studies. Every time after having a discussion with him, I feel fully inspired by his talents. Thanks for his encouragements and helps in both academic and personal issues. I could not become the person who I am today without his supports.

Many thanks to my Ph.D. committee members: Dr. Charles W. Brice, Dr. Herbert L. Ginn, and Dr. Jamil A. Khan for those invaluable discussions and timely feedback. To Dr. Yucheng Zhang, Dr. Hasan Ali, and Dr. Enrico Santi: thanks for the guidance in the ship baseline modeling work from which I have learned a lot.

Thanks to the faculty and staff of the Electrical Engineering department for their continuous support: Rich, Hope, Blake, Nat, and Lauren. Also, many thanks to my colleagues Pietro, Dan, Antonio, Reza, Tianlei, Blanca, Asif, Rostan, Yuanyuan, Qiu, Phllip and Haroula who were always ready to share and help.

I would like to acknowledge the support of the US Office of Naval Research under the grant N00014-08-1-0080 and the Electric Ship Research and Development Consortium (ESRDC) which funded my research and allowed me to demonstrate the values and importance of my work.

ABSTRACT

High Frequency AC (HFAC) power systems – systems having frequencies higher than the usual 60 Hz – may have advantages in some applications, especially where small size and weight are important (aircraft, ships, etc), or where variable operating speed increases efficiency. While 400 Hz systems are widely used in aircraft, these generally do not include parallel-connected generators that operate at megawatt power levels, which is our domain of interest in this research. In particular, we are interested in micro-grid power systems in the 10-100 MW range, consisting of several generators operating in parallel at system frequencies above 60 Hz. This type of system is of interest for many industrial and commercial applications, especially ship and marine systems.

There is little historic precedent for HFAC power systems, and the operating frequency limits of these systems are not well defined, especially in regard to how intrinsic stability depends on physical factors such as the inertias of rotating machines, the impedances of power buswork, and the operating speeds of circuit protection devices.

In this research, we first explored the benefits of high frequency systems, including how weight and volume of equipment such as synchronous generators are reduced, and found that generator power density scales proportionally with frequency. We also found that as the power density increases, the inertia constant of a rotating machine decreases, and can easily become smaller than two seconds, which threatens stability since stability often depends on a large inertia constant.

Increasing frequency was found to deteriorate rotor angle stability under both large-signal and small-signal conditions. For large perturbations caused by short circuits, the Critical Clearing Time (CCT) was found to scale proportionally to the inverse square-root of system frequency. Thus, successful use of HFAC systems requires development of faster-acting circuit protection devices. The upper limit of operating frequency occurs where the operating time of available short-circuit protection devices equals the CCT. Existing circuit breaker technologies appear to support system frequencies as high as 800 Hz. Large-signal stability, studied via extensive simulation tests, confirmed conclusions drawn from the fundamental analysis - the low inertias in typical micro-grids aggravate the stability problem in higher frequency systems. At the higher angular speeds associated with higher system frequencies, rotor angles can diverge and then quickly exceed the critical value, resulting in the faster loss of synchronism in HFAC systems. This emphasizes the necessity for developing fast-acting circuit protection devices. On the other hand, small-signal stability, studied by eigen-analysis, showed the sensitivity and dependency of stability on some key parameters such as generator damping coefficients or inertia constants. For example, larger inertia constants tend to benefit transient stability but deteriorate the small-signal stability, especially at system frequencies above 1000 Hz. The higher the frequency, the greater the sensitivity; the range of system parameters that permits stable operation of a 3000 Hz system is much narrower than the range of parameters acceptable in a 60 Hz system.

TABLE OF CONTENTS

LIST OF TABLES

LIST OF FIGURES

LIST OF ABBREVIATIONS

AC ..... Alternating Current

CCA ..... Critical Clearing Angle

CCT ..... Critical Clearing Time

DC ..... Direct Current

ESPS ..... Electric Ship Power System

ESRDC ..... Electric Ship Research and Development Consortium

HFAC ..... High Frequency AC

HTS ..... High Temperature Superconducting

PD ..... Power Density

Chapter 1

INTRODUCTION

1.1 RESEARCH OBJECTIVE

This dissertation focuses on High Frequency AC (HFAC) power systems. It aims at finding the frequency limit of HFAC systems and the roots of this limitation, exploring the influence of operating frequency on system stability, and providing reference for building a HFAC power system. Micro-grids in the 10-100 MW range, consisting of multiple directly-coupled synchronous generators with operating frequencies above 60 Hz is our interest. Some significant issues associated with implementing HFAC systems are:

- Increasing speed of electric machines is associated with smaller rotor diameters and smaller moment of inertias, which potentially results in decreased rotor angle stability.
- Increasing system frequency reduces the weight, size and footprint of system equipment, but may trigger system stability problem.
- Choosing a system frequency to best explore the benefits of HFAC systems without sacrificing safe and stable operation.

The research objectives of this study are:

- Determine the over-riding factors that impose practical limits on system frequency.

- Discover the mass and volume improvement of critical components such as synchronous generators by increasing operating frequency; explore the scaling law of inertia constants (one of the most significant generator parameters for system stability) versus frequency.

- Study the fundamental impact of system frequency, generator's inertia constants, and other significant system parameters on rotor angle stability.

1.2 CONTRIBUTIONS OF THIS RESEARCH

The contribution of this research involves two aspects. The first one is related to synchronous generators in HFAC systems. This contribution can be summarized as:

- Developed the trend line for the feasibility area of generators to reflect the maximum power one generator can achieve at different speeds.

- Derived the trend lines for the scaling law of power density of high frequency generators versus system frequency.

- Established the equation for quick estimation of generator's inertia constants which facilitates power system stability analysis without having detailed machine data and extensive knowledge for machine design.

The second aspect is stability characteristics of HFAC systems. This contribution covers the following aspects:

- Showed for the first time that the mathematical relation between Critical Clearing Time and system frequency is inverse square-root.

- Discovered that the capability of system protection devices is the major cause limiting the operating frequency in HFAC systems.

- Showed that fast-acting circuit breakers and wide-bandwidth PID controllers in excitation systems can permit HFAC systems to exhibit large signal rotor angle stability comparable to 60 Hz systems.

- Determined the fact that low inertias, which is a typical problem for stability of many micro-grids, can cause more severe problem in HFAC systems

- Explored the strong sensitivity of small-signal stability of HFAC systems on operating frequency and other system key parameters

- Revealed the range of parameters to ensure the stable operation of HFAC systems is much narrower than normal 60 Hz systems.

1.3 PROJECT SIGNIFICANCE

Terrestrial power systems have been running at 50/60 Hz for over a century. All system components have been designed for this frequency. It is unlikely that grid frequency will change in the near future because it will bring enormous changes to the current grid network that cannot be solved immediately. However, the idea of running a micro-grid at a frequency higher than 50/60 Hz has been raised for over 30 years and has been planned to deploy in some applications currently. Many benefits from the implementation of HFAC systems have been proven and many efforts have been made to develop equipment that runs under high frequency. However, the frequency limit for HFAC systems is unknown as well as the major factors for this potential limitation. The stability characteristics of HFAC systems can be significantly different from that of the 50/60 Hz system. The question of whether the

stability is enhanced or degraded as one increases the nominal operating frequency is an interesting and increasingly important one.

1.3.1 Benefits of HFAC Systems

HFAC power systems deliver electrical power at frequencies greater than 60 Hz. Some advantages of implementing HFAC power over conventional 50/60 Hz counterpart are listed below [1][2][3][4].

- Electric equipment can be much lighter and smaller, therefore cheaper because of fewer materials. For example, doubling the frequency generally permits electric machines to be 75% smaller. This appears to be the greatest benefit of HFAC systems.

- High frequency generators can be directly coupled with prime movers, such as gas turbines, instead of using gearboxes on the shaft to reduce the speed of prime movers. This greatly reduced the maintenance burden especially if the micro-grid is in a remote and distant area. Drivetrain length could be reduced and power loss due to the gearbox will be saved by approximately 2% [5].

- High speed induction motors can be directly used for compressors, high pressure pumps, and turbines.

- Acoustic noise could be reduced dramatically due to higher frequency mechanical vibration.

- Harmonics in HFAC systems will be at higher frequency and can be easily removed through proper filters.

1.3.2 Applications of HFAC Systems

One of the earliest attempts to adopt the concept of HFAC power systems was by NASA's Lewis Research Center in 1983, for the Space Station Freedom program [5] [6]. The motivation was to meet the trend for bigger spacecraft and stations like the space shuttle and the international space station project. Existing dc-based power system at that time were facing limitations in the form of excessive copper cable weight to compensate for the ohmic losses. The proposed HFAC distribution system employed inverters to generate HFAC electric power from a dc source, such as solar panels, instead of directly using HFAC electric machines. But higher crosstalk and higher EMI were challenges to proposed high frequency schemes because it required novel power cables with low inductive reactance, low radiated magnetic field, and the capability of carrying single-phase, 440 V, 20 kHz HFAC current without incurring significant losses due to skin and proximity effects.

Another application involving the content of HFAC electric power is telecommunication [3]. Considering the demand of increasing load levels, compactness, higher complexity, and higher reliability, HFAC scheme is an excellent alternative for current dc solutions. But similar to space station power systems, this HFAC system is only for the purpose of distributing electric power, different from our focus in this study – direct HFAC electric power generation from rotating machines. The power supply is still 50/60 Hz from the grid and HFAC power only exists during the stages of transmission and power conversion.

The oil and gas industry may embrace the advantages of HFAC systems. The power rating of a medium-size oil and gas production platform can easily exceed 10 MW. If the platform is designed for deep water drilling, dynamic positioning systems with power ratings up to 40 MW are required. The compactness of HFAC systems makes it a great fit

for offshore platforms, where space is a valuable commodity. In terms of oil and gas refinery facilities, pumps, compressors, and blowers [5] [8], driven by synchronous or induction motors, require large and heavy speed-up gearboxes. Increasing generator frequency to remove the gearboxes will be very beneficial. This is especially meaningful to reduce the maintenance workload for the cases in which oil and gas processing facilities are in remote areas.

The HFAC power system was proposed as one of the three candidates for the Next Generation Integrated Power System (NGIPS) for electric ships [4] [9]. The other two competing candidates are Medium Voltage AC (MVAC) and Medium Voltage DC (MVDC). Figure 1.1 is NGIPS master plan showing the three candidates [4].

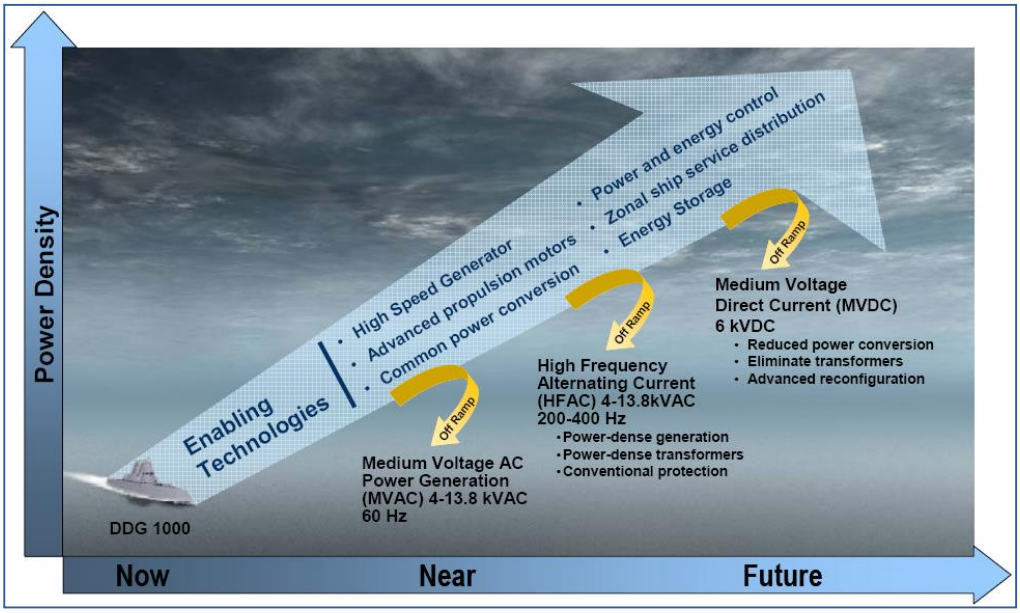

Figure 1.1 NGIPS master plan

As the implementation of MVDC on all-electric ship requires the industry and the Navy to address a number of technical challenges, a HFAC system serves as a risk-reduction alternative for near term. Figure 1.2 depicts the diagram for notional electric power system

proposed by the ESRDC [10]. The proposed HFAC power system deploys high frequency synchronous generators to produce electric power at a fixed frequency between 60 Hz and 400 Hz. The voltage at distribution ring bus is either 4.16 or 13.8 kV.

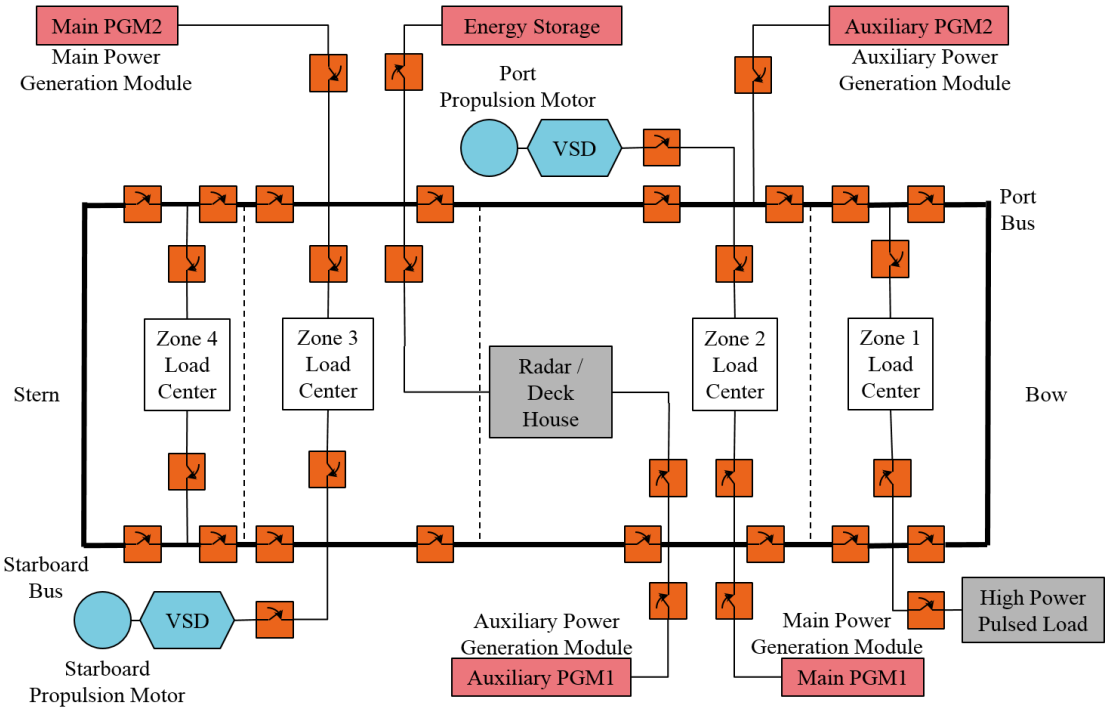

Figure 1.2 Notional ship power system diagram

1.4 SUMMARY

The objective of this study is to find frequency limit in HFAC systems and to discover the potential impact of increasing system frequency on system stability. The focus of our study is micro-grids in the MW-range with multiple synchronous generators operating in parallel. Such HFAC systems are especially beneficial for applications where size and weight are the priorities for system designers. Significant applications of HFAC systems include offshore oil and gas platforms and electric ship power systems.

Chapter 2

LITERATURE REVIEW AND BACKGROUND

In this section the literature concerning HFAC power systems and power system stability will be reviewed. The concept of using HFAC as the link or a way of transmission in the micro-grid will be presented. The issues of power system stability for both utility systems and the promising application of HFAC systems – an electric ship power system will be summarized.

2.1 HFAC POWER SYSTEMS

2.1.1 HFAC DISTRIBUTION SYSTEMS

HFAC distribution systems deliver electric power at frequencies up to multi-kHz via cables. The earliest HFAC distribution system was proposed in 1980s for the power system of the International Space Station [11] [12] [13] with a power rating of 120 kW. The HFAC distribution architecture utilized a resonant converter to convert the 160 V dc power from solar panels to single-phase 440 V/20 kHz ac power. The choice for the frequency of 20 kHz was due to the good balance among power rating per module, audio noise considerations, and component sizing, considering the available technology at that time.

Japanese scholars performed research on the concept of HFAC distribution system during that time as well. Takahashi [1] proposed a 500 Hz power system for applications of industrial zones, intelligent buildings, commercial areas, etc. An experimental model system was built to test system performance under certain faults. Takahashi's experiment revealed

many benefits of HFAC power systems, such as dramatic reduction in the size and weight of transformers, filters, circuit breakers and other system components, reduced power distortion due to the filtering effect of 500 Hz power converters, etc. In [2], Takahashi continued to investigate the applications and needs for HFAC distribution system. Experiment demonstration showed that energy saving, space reduction, and high performance can be achieved by the implementation of higher frequency in fluorescent lightings, amorphous metal core transformers, dc power supplies, and naturally commutated cycloconverters. But similar to the International Space Station, Takahashi's HFAC distribution system did not include HFAC electric generators. Instead, power converters were used to convert 50/60 Hz grid power to 500 Hz one.

In the last two decades, micro-grids have been emerging as a new form of terrestrial grid system as deregulation policies encourage distributed power generation to be close to the end-users. It consists of multiple power sources, such as solar panels, fuel cells, and micro wind turbines. Its operation capability, either interconnected with the grid or independently, renders it an ideal application for HFAC transmission architecture. In [14][15][16], Chakraborty studied single-phase 1 kHz HFAC micro-grids which integrated several renewable energy sources. Figure 2.1 shows the diagram for the studied HFAC micro-grid distribution system. A HFAC link was used to integrate loads and all sources, such as photovoltaic, wind, fuel cells, etc. To compensate for reactive power, load current harmonics, and voltage distortions, p-q theory-based active filters, i.e. Universal active Power Line Conditioner (UPLC) and Unified Power Quality Conditioner (UPQC), were implemented to address the issues of power flow and power quality. In [16], a Distributed Intelligent Energy Management System (DIEMS) acted as an optimizer of operating costs.

Results from [14][15][16] demonstrated the successful implementation of HFAC micro-grids with expected power flow and power quality control, as well as the optimization of operation cost by the proposed DIEMS.

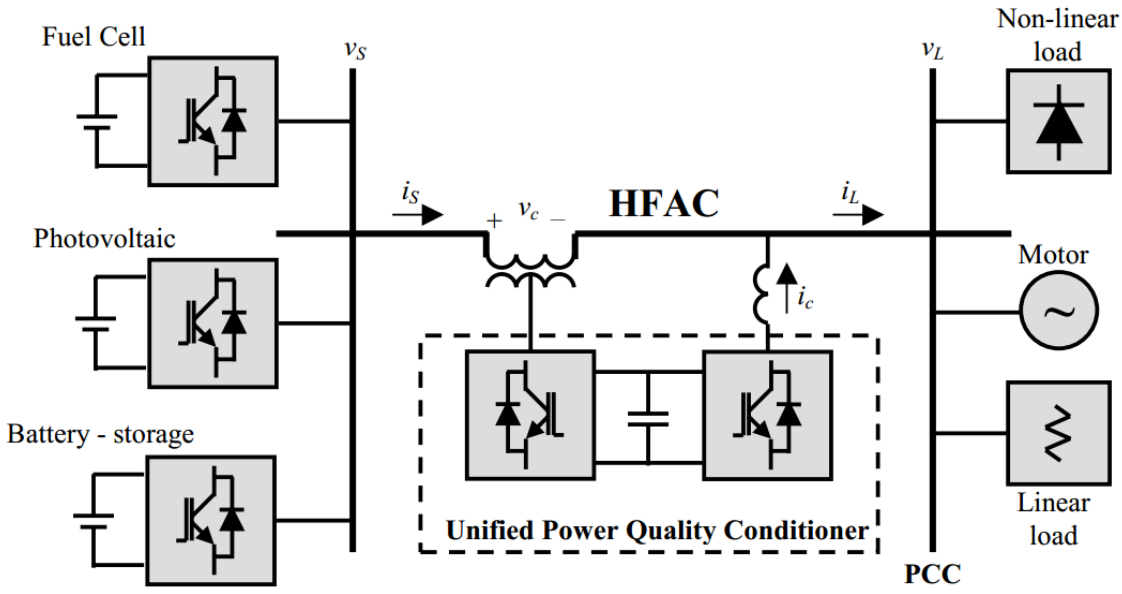

Figure 2.1 HFAC micro-grid studied by Chakraborty

2.1.2 HFAC Power Systems with Direct Power Generation from High Frequency Electric Generators

A more "complete" HFAC power system consisting of line-connected high frequency generators operating in parallel was adopted by electric ship power systems (ESPSs). Under the supervision of the ESRDC (Electric Ship Research and Development Consortium), some work has been done for the baseline model of HFAC power systems for next generation electric ships. In [17], a model of an 80 MW electric ship HFAC power system that generates and distributes electric power at 240 Hz was developed. This detailed system model includes several gas-turbine-generator units, two propulsion power trains, several power distribution and conversion units, a super-capacitor energy storage module, a high-power pulse load, and multiple service loads. Four scenarios were tested to understand the

performance of this HFAC system: partial loss of generation, the application of a large step load, power restoration to a vital load, and the operation of energy storage module. Some benefits of the HFAC architecture were highlighted. But the authors did not discuss the impact of HFAC generation on system stability and other stability issues related to this HFAC power system.

As the key component of HFAC systems, high frequency generators with power ratings in the MW-range were studied by R. M. Calfo since 2002. In [18], Calfo proposed a ship propulsion system having high frequency generators with close-coupled rectifiers. Significant improvements in system weight, volume, and efficiency with frequency increase were presented. Following [18], Calfo proposed concepts to improve power density of a gas-turbine-generator set in [19]. Sixty-one generator designs over four generator types (air-cooled wound field, water-cooled wound field, permanent magnet and high-temperature superconducting) were assessed for different distribution architectures of electric ship. In this paper, power density was given priority. Efficiency, acoustics, and total system cost were evaluated. Calfo concluded that a water-cooled generator can achieve close to the same level of performance and power density as permanent magnet and high-temperature superconducting designs, but it showed more strengths in other aspects such as compatibility with shipboard application, requiring significantly less development, cost, etc. In [20], considering available prime movers such as MT30 and LM2500+, Calfo explored the combinations of prime movers and advanced generators to satisfy the requirement of HFAC power systems defined in NGIPS's master plan. Calfo again substantiated that high frequency generators offered up to 75% savings on size and weight as compared with 50/60 Hz generators. In [21], Calfo compared the cost of high power density and high frequency

generators with that of conventional ones, and showed that the major advantages of power dense electric generators, the size and weight reduction, benefit the affordability of the machine as well. But no discussion on frequency limits of HFAC systems and the feasibility area of high frequency generators was given in Calfo's publications.

2.2 POWER SYSTEM STABILITY

Power system stability is understood as the ability to remain in an equilibrium operating state under normal operating conditions, and to regain an equilibrium state after being subjected to a physical disturbance [22] [23]. Traditionally, a satisfactory system's operating condition is that all synchronous generators operate in synchronism, but instability may also occur while synchronism is maintained. The definition and classification of power system stability could be different based on specific considerations. In terms of the physical nature of the resulting instability, rotor angle and voltage are the two categories of power system stability. Based on the size of the disturbance considered, rotor angle can be sorted into two categories: small-signal and large-signal stabilities. An example for small-signal disturbance would be a small load change while system faults are the typical incidents for large-signal stability study. Similarly, voltage stability can be categorized into large-disturbance and small-disturbance stabilities. If the time span of the system's dynamic operation is considered, mid-term and long-term stabilities can be defined for study period of several minutes and tens of minutes correspondingly. Figure 2.2 shows the classification of power system stability [22].

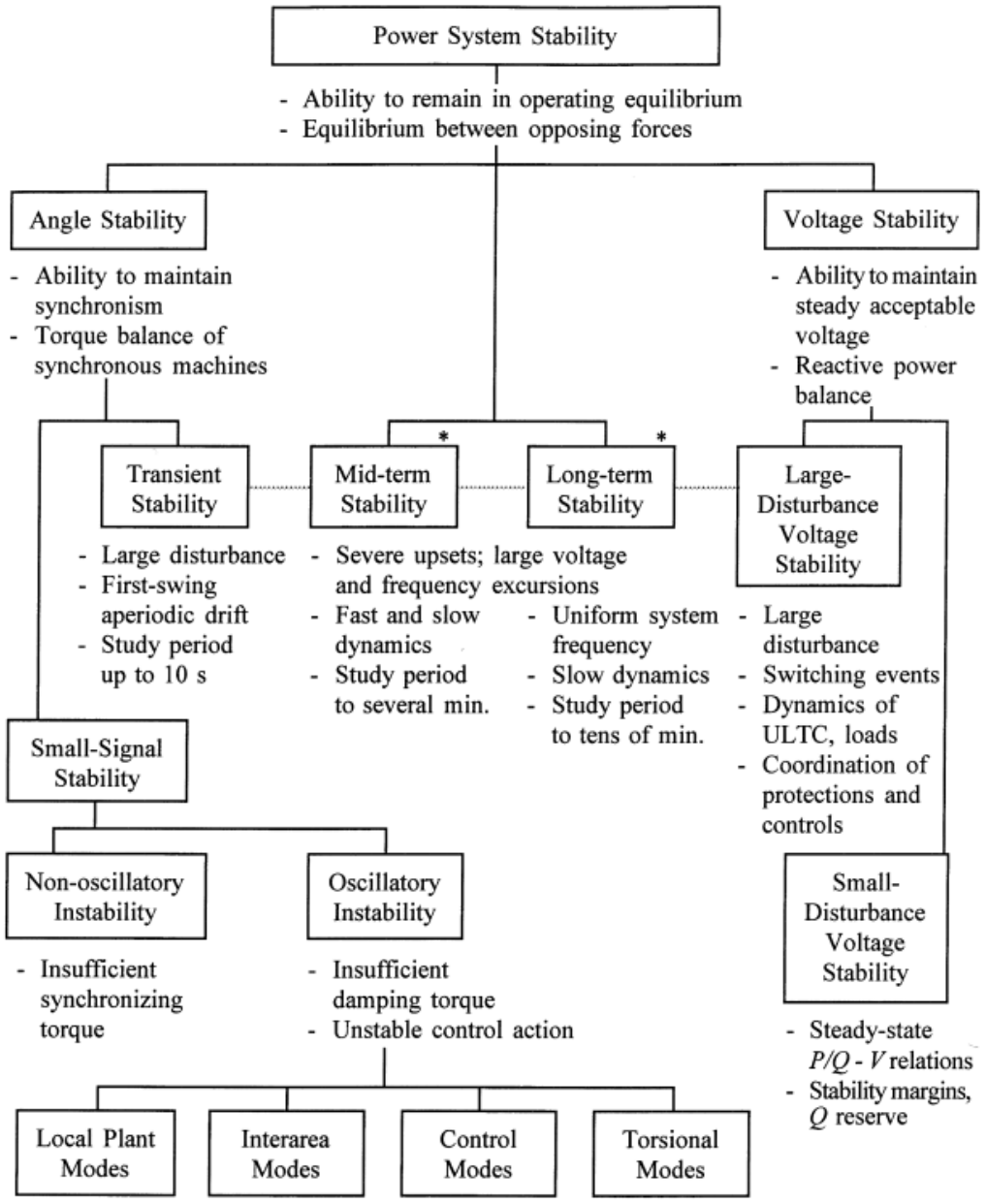

Figure 2.2 Classification of power system stability

2.2.1 ROTOR ANGLE STABILITY [22][24]

When multiple synchronous generators operate in parallel to supply electric power to loads, the system's ability to maintain synchronism is defined as rotor angle stability.

Physically, the requirement for being stable from rotor angle aspect is that all connected synchronous generators are rotating at the same speed, which is termed synchronous speed. Since electrical frequency is proportional to mechanical speed for synchronous generators, in real utility systems this common synchronous speed determines the system electrical frequency to be at 50/60 Hz. When these interconnected synchronous generators reach steady-state, equilibrium occurs between input mechanical power and output electrical power for each generator. Once subjected to a disturbance, the rotors will accelerate or decelerate according to the laws of motion. Rotor angular position between different generators will change accordingly, resulting in the load transferring from slow generators to fast generators based on the power-angle curve. Once the angular position increases over a certain limit, further increase in angular position will result in the fact that at least one generator is unable to go back to stable operation state.

Rotor angle stability is commonly defined as two categories: small-signal stability and large-signal stability (also termed "transient stability"). The following sections will address them from the aspects of phenomena and methods to investigate them.

2.2.1.1 SMALL-SIGNAL STABILITY

Small-signal stability focuses on the ability for maintaining synchronism during small disturbance such as a small load step change. The time span of interest is about 10~20 seconds after the disturbance. In this category, the disturbance is regarded as small enough that the nonlinear system can be adequately represented by a model that is linearized about the operating point. Instability which may occur in this category may result from two aspects: lack of sufficient damping torque, or lack of sufficient synchronizing torque. In modern power system networks, small-signal stability problems are usually raised by

insufficient damping torque. This can be explained by the equations of damping power and synchronizing power. Consider the one-machine-infinite-bus system in Figure 2.3. Ignoring rotor saliency, the damping power P_D and synchronizing power P_S of the generator can be expressed as the following [24]:

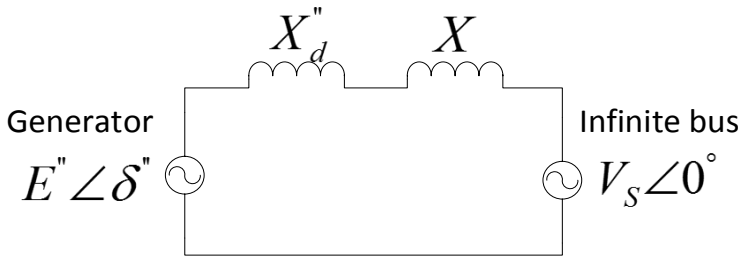

Figure 2.3 One-machine-infinite-bus system

$$P_D = V_S^2 \frac{X_d' - X_d''}{(X + X_d'')^2} \frac{X_d'}{X_d''} \frac{T_d'' \Delta\omega}{(1 + T_d'' \Delta\omega)^2} \tag{2.1}$$

$$P_S = \frac{E'' V_S}{X + X_d''} sin\delta'' \tag{2.2}$$

where $X_d^{'}$ is the generator's transient reactance, $X_d^{''}$ is the generator's subtransient reactance, X is the reactance of transmission line and transformer, $T_d^{''}$ is the subtransient short-circuit time constant of the generator, $\Delta\omega$ is the rotor speed deviation, V_S is the voltage of infinite bus, $E^{''}$ is the subtransient voltage behind $X_d^{''}$, and $\delta^{''}$ is the angle between $E^{''}$ and V_S under a subtransient state. It can be seen that the squared value of network reactance X occurs in the denominator of P_D, while it has much less influence in P_S. Considering the size of current power grid, it is common that transmission line impedance X is a large value. In a HFAC micro-grid with relatively short transmission cables, X may still be large if the frequency is very high, so insufficient damping torque can be an important issue.

The popular method for studying small-signal stability is eigen-analysis by which the eigenvalue and eigenvalue sensitivity of system state matrices are evaluated to learn the system characteristics. In Chapter 4, this method will be introduced and applied to study the small-signal stability of HFAC systems

2.2.1.2 TRANSIENT STABILITY [22][24]

The ability of a power system to recover from large disturbances is termed as transient stability. Such large disturbances involve different types of system contingencies at widely varying degrees of severity. Large disturbances commonly encountered in power systems involve loss of large portion of a transmission system, loss of major power generations/loads, and system faults. Three-phase-to-ground faults are the most severe faults in a power system network. The time span of interest for 60 Hz grid system is usually 3~5 s after the disturbance, while in some very large power systems it will be extended to 20 s. The large disturbance will trigger a system response such as large excursion of generator's rotor angles and frequencies. The ability for a power system to sustain synchronism through a contingency is determined by its initial operating status, the level of severity of the contingency, fault clearing time, post-contingency system structure, the aids from system equipment, etc.

Transient stability problems are highly nonlinear and highly dimensional. Two methods for evaluating transient stability involve indirect and direct methods. Time-domain simulation, which is the most popular and widely used in modern power system analysis, is in the category of indirect method. It utilizes mathematical models for power system devices to establish a power system model. Then the time domain solutions for non-linear and algebraic equations can be computed step by step. The accuracy of the solutions and the

speed of simulation depend on the choice of solver and the level of detail of the mathematical representation for each system component. Eventually the stability could be learned by observing the simulation results. The indirect method is reliable but cannot be used for finding the stability margin.

The direct method utilizes Lyapunov Energy functions to assess stability. The results of stability regions given by various direct methods are usually too conservative and smaller than the real boundary. Moreover, constructing a Lyapunov Energy function is not easy, especially when the target power system includes some models in great detail. Each direct method applies different characteristics of the stability boundary to locate the stability region. [25] and [26] present comprehensive discussions on direct methods.

2.2.2 VOLTAGE STABILITY

Voltage stability is the ability of a power system to maintain desired voltage at all buses during small or large disturbances [22][27]. The capability of a power system to meet the requirements of reactive power will determine the voltage stability. The basic criterion for assessing voltage stability is that under a specific operating point, the magnitude of the bus voltage (V) in every bus of a power system will increase as the reactive power (Q) injection increases. This so-called V-Q sensitivity needs to be positive for each bus of the investigated power system. Voltage stability is classified into two categories: large-disturbance voltage stability and small-disturbance voltage stability. The "large-disturbance" refers to large load step changes, power system faults, loss of generation, etc., while the "small-disturbance" refers to small perturbations such as incremental load changes. Both large-disturbance and small-disturbance stabilities depend on system characteristics, system controls, and

protections. Voltage stability and rotor angle stability often occur together so that it is difficult to make the distinction.

2.3 REVIEW OF POWER SYSTEM STABILITY RESEARCH

The research on power system stability dates back to the year 1920 [28][29][30][31]. The instability at that time was mainly due to insufficient synchronizing torque which resulted from long transmission lines. After that, the equal-area criterion and other methods were developed to tackle simple power system analysis, such as a system containing two generators. In 1930, the development of a network analyzer made it possible for power flow analysis, which served as an extremely useful tool for emerging large interconnected power systems in this early age. 1956 saw the first computer software for power system stability analysis which facilitated detailed modeling of power system equipment such as synchronous machines, excitation systems, and governors. In 1965, the famous northeast blackout emphasized the significance of power system stability to power system engineers and researchers [32]. About the same time, power system stabilizers were introduced [22][24] to mitigate the adverse impact on small-signal stability brought by high-response excitations that greatly improved transient stability.

Modern power system networks and operation have resulted in new types of stability problems. For example, as renewable energy becomes popular in power systems, a lot of studies for power system stability have been focused on the impact of renewable energy penetration on large interconnected power systems[33][34][35][36]. The main concern is that power electronics converters, serving as interfaces between the power grid and different energy sources, decouple the connection and therefore lower the system inertia, which is

very important for system rotor angle stability. Some mitigation methods such as controller improvements have been proposed to address potential stability problems [35][36].

In the meantime, voltage instability and low-frequency inter-area oscillations in modern power systems become more common than in the past. Long-term stability, system controls, and protections are attracting more attentions as well [22][24][37][38].

2.3.1 SHIPBOARD POWER SYSTEM STABILITY

As stated in Chapter I, ESPSs are a significant application for HFAC systems. With strong support from US Office of Naval Research, the stability of ESPSs has been widely researched.

One of the main issues that draws attentions is the stability problem caused by power electronics converters. Converters are widely used in dc and ac ESPSs and they present a behavior of Constant Power Load (CPL) which will cause negative-impedance voltage instability. [39] reviewed and discussed the methods for analyzing this stability issue and it focused on the design of load-side power converters. [40] implemented a dedicated control algorithm to prevent the MVDC ESPS from negative-impedance instability. Power converters were disconnected when they started to cause MVDC systems running into unstable regions. Arcidiacono in [41] presented an innovative control system which was designed to control generators, gas turbines, and power converters in an integrated way so that stabilization of a dc bus in MVDC systems can be achieved.

Other important literatures covering the stability of ESPSs include [37], [51], [42], and [43]. In [42], the Lyapunov linearization method was adopted to identify the stable region for a simplified version of an ESPS which included a generator-motor set. In [51], Li

proposed an automated detection method based on RTDS simulation and Prony analysis (a curve-fitting method) to study ESPS stability. The stability boundary was determined by the maximum allowable magnitude of the pulsed load. The obtained boundary was found as conservative as from the Lyapunov method. In [43], Amy used a composite system method which was based on the Lyapunov direct method to assess the stability of an MVAC ESPS. The proposed method could be applied to study HFAC system stability but exhibits some limitations and inaccuracies, such as the close proximity of shipboard system components requiring higher order models for capturing dynamics. The implementation of the co-energy concept needs more research work as well. In [37], Qi presented two new indices for voltage stability assessment for the ship power system application: Static Voltage Stability Index (SVSI) and Dynamic Voltage Stability Index (DVSI). Qi also discussed rotor angle stability for the case when an ESPS has multiple generators with the same power rating. The main conclusion was that rotor angle stability were not an issue in shipboard systems because the generators have the same inertia and rating. But as ESPSs start to use generators with significantly different ratings, such as the current baseline system proposed in [10] having two main and two auxiliary generators, such conclusion may not be valid.

2.4 SUMMARY

This chapter addresses the literature work concerning HFAC systems, critical equipment for HFAC systems, and power system stability issues. No report has been found to discover the stability characteristics of HFAC systems.

.

Chapter 3

SYNCHRONOUS GENERATORS IN HFAC SYSTEMS

This chapter discusses the impact of system frequency on the size and weight of synchronous generators. Trend lines will be derived for illustrating the scaling laws of generator's output power and power density versus frequency. The Inertia Constant is one of the most important parameters for power system stability. An equation which facilitates quick estimation of inertia constants of high frequency generators will be established.

3.1 SCALING LAW OF GENERATOR POWER DENSITY VERSUS FREQUENCY

High frequency synchronous generators are the power sources of HFAC systems. In general, increasing generator frequency tends to make the generator more compact.

3.1.1 POWER DENSITY IMPROVEMENT OF SYNCHRONOUS GENERATORS IN HFAC SYSTEMS

The basic relation among the number of output electrical frequency (f in Hz), the number of magnetic poles (p), and mechanical rotational speed of generators (N in RPM) can be expressed as:

$$f = \frac{Np}{120} \tag{3.1}$$

It is apparent that there are two ways to increase generator output frequency: to rotate the rotor faster (higher N), or to add more magnetic poles to the rotor (higher p). Another

important equation relating the nominal output power of a synchronous generator to its weight and volume is:

$$P = K(pf)ABD^2LN \tag{3.2}$$

where *K* is the unit conversion factor, *pf* is the power factor, *A* is the stator surface current density in A/m, *B* is the peak air gap flux density in T, *D* is the rotor diameter in m, *L* is the stator core length in m, and *N* is the mechanical rotational speed in RPM.

In this study, Power Density (*PD*) is defined as the electrical output power divided by the generator weight (weight power density) or volume (volumetric power density) and used as the metric to evaluate the impact of higher frequency on a generator's weight and size:

$$PD = \frac{P}{m_{gen}\ or\ V_{gen}}\ (kW/kg\ or\ kW/m^3) \tag{3.3}$$

Based on (3.2) and (3.3), three ways can be discovered to achieve more compact design and higher *PD* [18][21][52]:

- As the rotational speed (*N*) increases, output power increases proportionally which leads to *PD* increase.

- If the size of the generator shrinks, generator mass can be reduced resulting in *PD* increase. Increasing pole count will result in a smaller and shorter stator.

- If the stator surface current density (*A*) and the air gap flux density (*B*) are increased, higher output power and *PD* can be achieved. The three ways will be explained in detail in the following sections.

3.1.1.1 OBTAINING HIGHER *PD* BY INCREASING MECHANICAL SPEED

If we define the surface speed of the rotor as:

$$v_r = \frac{\pi DN}{60} \tag{3.4}$$

(3.2) can be re-written as:

$$P = \frac{K}{\pi}(pf)ABDLv_r \tag{3.5}$$

If rotational speed can be increased by increasing the speed of the prime mover, surface speed will be increased to achieve higher output power. The maximum surface speed is determined by the rotor structure and materials. For solid-rotor and laminated-rotor synchronous generators, the maximum surface speeds limited by the mechanical strength of electrical steels are 400 m/s and 250 m/s correspondingly [44][45]. If the yield strength of rotor material improves, the output power limit can be increased. As long as the surface speed does not exceed the maximum speed, higher *PD* could be achieved.

3.1.1.2 OBTAINING HIGHER *PD* BY INCREASING GENERATOR POLE COUNT

Compact generators could be acquired by increasing the number of magnetic poles. Assuming the rotor diameter remains constant, as the pole number increases, the pole pitch decreases proportionally. Since the backiron of the stator core and the overall length of the stator winding end turns change proportionally with the pole pitch length, increase in pole number will result in a shorter generator. Preliminary design study in [18] showed that if the pole number of a 20 MVA, 3600 RPM generator increases from two to four, the weight and length reductions are 32% and 13% respectively. The extent of the reduction will be determined by practical limit in the minimum size of the stator core thickness, end turn length, and magnetic air gap.

3.1.1.3 OBTAINING HIGHER *PD* BY BETTER COOLING SCHEME AND HIGH SATURATION MAGNETIC MATERIALS

According to (3.2), stator surface current density and peak air gap flux density are significant factors in determining how much power could be drawn from a synchronous generator. Maximum current density is determined by the cooling method of the generator system. Currently the popular cooling schemes involve air-cooling and liquid-cooling. Air-cooling methods are commonly used in a wide range of applications in modern industry. Its high reliability and low reliance on complex auxiliary systems have been proven by decades of design work and operation. Liquid-cooling method adopts direct liquid cooling of stator and rotor windings. It dramatically reduces the space that must be allocated for air passage inside the generator. It provides an opportunity for significantly increasing the current density and thus achieving higher power density. Although liquid-cooled generators were tested by some companies in the 1970s and there are many industrial applications in the market, challenges for implementation still exist, such as the insulation of tube connectors to withstand significant centrifugal force and the supply of deionized water to the rotor through a rotary union. Table 3.1 lists some typical values for current densities of electrical machines with different cooling schemes [45].

Table 3.1 Current densities for copper-winding electrical machines with different cooling systems

Cooling system	Current density, A/m
Total enclosed machine, natural ventilation	4.5 to 5.5
Total enclosed machine, external blower	7.5 to 11.0
Through-cooling machine, external blower	14.0 to 15.5
Liquid-cooled machine	23.0 to 30.0

Peak air gap flux density is another important parameter which is closely related to the magnetic lamination materials a generator uses. Traditional synchronous generators utilize silicon iron steel lamination. To increase the air gap flux density in high speed generators, high saturation magnetic materials such as the cobalt steel alloy lamination is required. Hiperco 50 [46] is such a material that is widely used in aircraft generators. Its saturation point is as high as 2.4 T. This type of materials also makes it possible for smaller stator teeth and larger stator slots, which eventually lead to more conductors in the windings and higher current loading.

The discussions in the previous sections illustrate that higher rotational speed and higher pole count will result in higher output power and higher power density. After reaching the maximum speed and maximum pole count, if high efficiency cooling methods and high-saturation lamination materials could be adopted, output power and power density can be further increased.

3.1.2 Trend Lines for Scaling of Power, Mass and Volume vs. Frequency

The previous section describes how the power density of generators can be improved by several design factors. This section will derive the trend lines for the relation of generator's output power and power density versus generator frequency.

Manipulating (3.2) and (3.4), and defining k_{DL} as the ratio of rotor diameter (D) and length (L) yields the following expression for scaling generator's output power:

$$P = \frac{60^3 K}{\pi^3 k_{DL}} (pf) A B v_r^3 \frac{1}{N^2} = K_{PN1} \frac{1}{N^2} \tag{3.6}$$

Output power is inversely proportional to the squared rotor speed (N), assuming that the other parameters remain the same. K_{PN1} is the coefficient relating generator speed and power. If K_{PN1} can be obtained, the trend line for the boundary of generator's output power versus frequency could be drawn. Table 3.2 lists the major parameters of some well-designed MW-range round-rotor-type synchronous generators from machine designers ([18][19][20]).

Table 3.2 Parameters for well-designed generators

No.	Speed (RPM)	Power (kW)	Pole count	Frequency (Hz)	PD (kW/kg)	Weight (kg)	PD (kW/m^3)	Volume (m^3)	Cooling
1	3600	18000	2	60	0.33	54430	n/a	n/a	air
2	3600	18000	4	120	0.48	37194	n/a	n/a	air
3	3600	18000	8	240	0.61	29483	n/a	n/a	air
4	3600	18000	4	120	0.42	42637	n/a	n/a	air
5	4800	18000	4	160	0.53	34246	n/a	n/a	air
6	7000	18000	4	233.3	0.68	26308	n/a	n/a	air
7	7200	18000	4	240	0.68	26308	n/a	n/a	air
8	4800	18000	6	240	0.72	24948	n/a	n/a	air
9	3600	18000	8	240	0.61	29484	n/a	n/a	air
10	7000	14000	4	233	0.77	18182	962.90	15	air
11	7000	14000	4	233	0.64	21875	859.73	16	air
12	7000	14000	4	233	1.25	11200	2101.03	7	water
13	7000	14000	4	233	1.07	13084	1929.13	7	water
14	3600	36000	8	240	0.64	56160	534.89	67	air
15	3600	36000	8	240	1.41	25492	2958.96	12	water
16	3600	36000	2	60	0.43	83536	442.01	81	air
17	6200	25000	4	206.7	0.53	47488	415.44	60	air
18	6200	25000	4	206.7	1.47	17025	2900.35	9	water
19	3600	26000	2	60	0.35	74097	371.64	70	air
20	3600	25000	8	240	0.54	46160	424.94	59	air
21	3600	25000	8	240	1.23	20248	2361.66	11	water
22	3600	26000	2	60	0.35	74097	371.64	70	air
23	7000	10000	4	233.3	0.43	23029	255.64	39	air
24	7000	10000	4	233.3	1.02	9761	1771.27	6	water
25	3600	8000	2	60	0.14	57204	191.30	42	air

After examining the original data, it is found that the rotor surface speeds of these machines are all close to the maximum value with enough redundancy so they are on the edge of boundary curve for output power vs. speed. Substituting the generator data of No. 18 (four-pole) and No. 15 (eight-pole) into (3.6) will find that the K_{PN1} for four-pole and eight-pole generators are $9.61*10^{11}$ and $4.67*10^{11}$ respectively. Using the two values, the curve can be drawn for the output power limit vs. generator speed, as shown in Figure 3.1. The cross marks in the figure represent the other four-pole or eight-pole generators in Table 3.2. The vertical axes for the output power and weight are logarithmic.

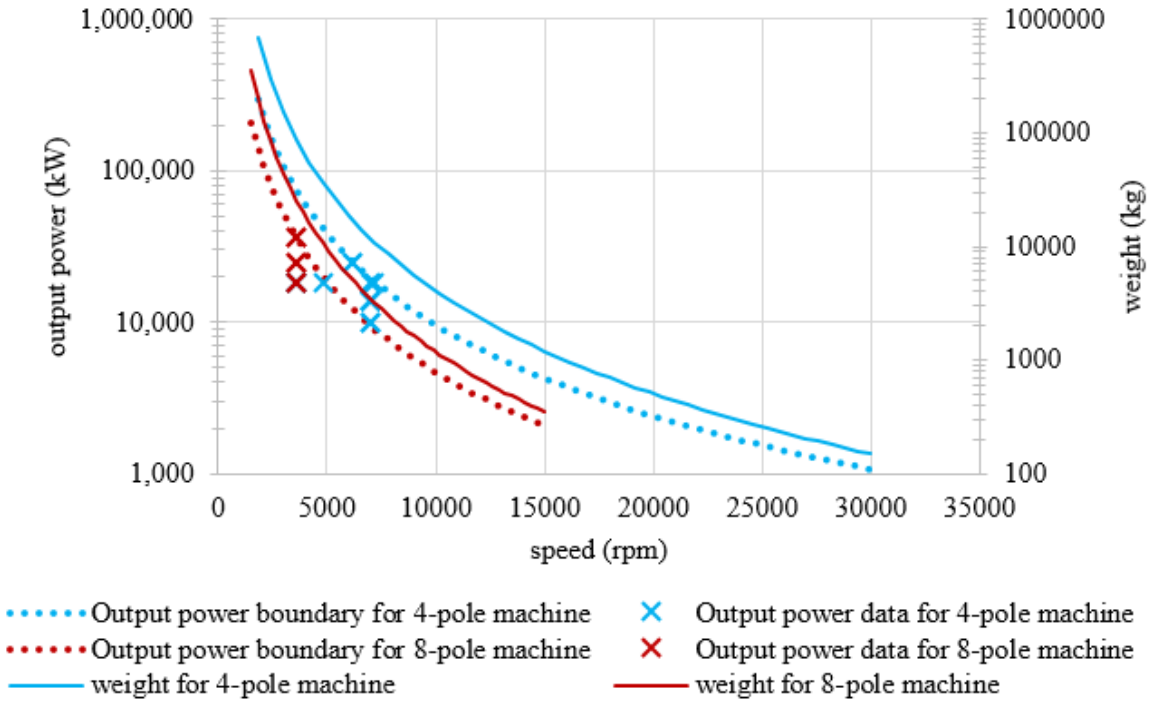

Figure 3.1 Trend lines for output power limit vs. generator speed

Considering increasing the frequency only by increasing rotor speed and keeping the same pole count, the output power limit vs. frequency can be obtained by replacing the axis of speed in Figure 3.1 with generator frequency, as shown in Figure 3.2.

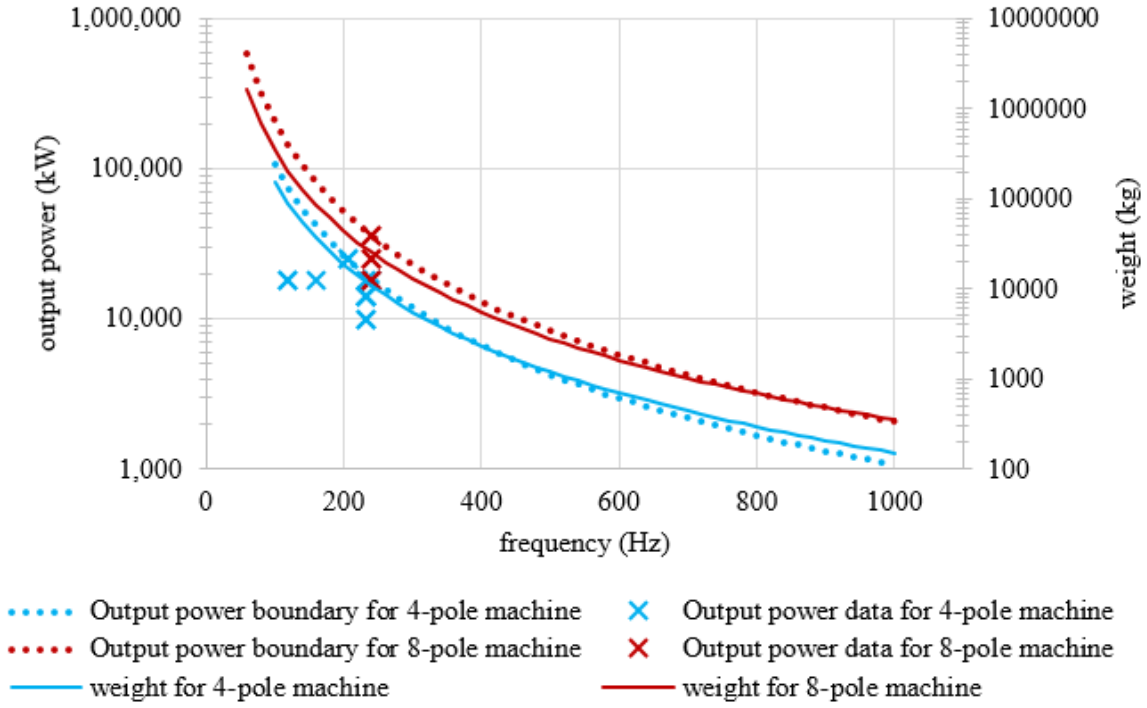

Figure 3.2 Trend lines for output power limit vs. generator frequency

If we define k_{SR} as the ratio of stator diameter to rotor diameter and rearranging (3.2), (3.3) and (3.6), the relation between power density and generator speed can be derived:

$$PD = \frac{4K(pf)AB}{\pi\rho k_{SR}^2}N = K_{PN2}N \tag{3.7}$$

where ρ is the mass density of the generator, and K_{PN2} shows the proportional relation between generator speed and power density. Similar to the method used for obtaining output power limit vs. speed (and frequency) in Figure 3.1 (and Figure 3.2), the data for Generator No. 18 and No. 15 in Table 3.2 are used to plot the trend lines for power density vs. generator speed (and frequency).

Figure 3.3 and Figure 3.4 indicate that as generator speed and frequency increase, both weight and volumetric power density of the generators will increase. However, in practice, this power density improvement will have a threshold limit, which is due to the challenges

of miniaturizing various components and extracting thermal losses from a small area [47]. The black lines (solid and dotted) in Figure 3.3 and Figure 3.4 represent this effect.

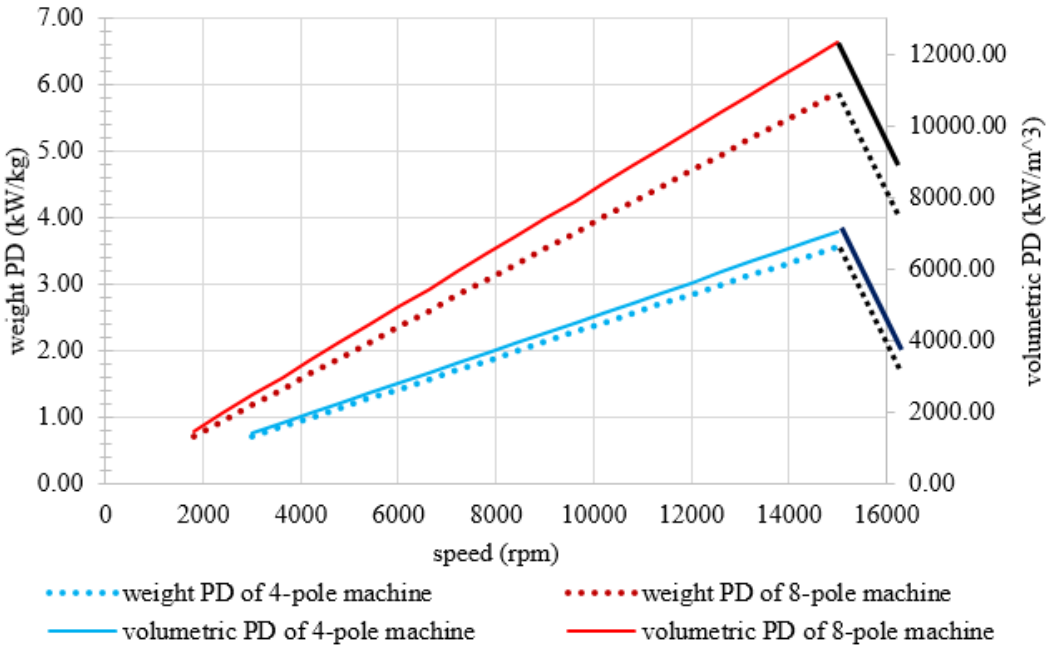

Figure 3.3 Trend lines for scaling weight and volumetric power density vs. generator speed

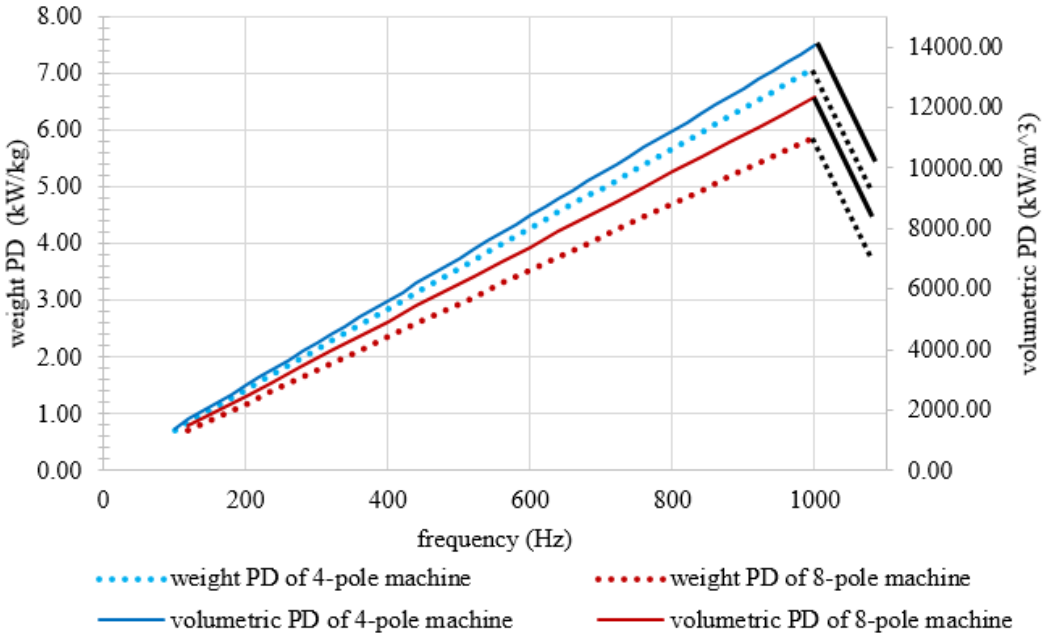

Figure 3.4 Trend lines for scaling weight and volumetric power density vs. generator frequency

It should be noted that all the scaling trend lines in this section are based on existing, or well-designed generators in the literature. As the design technique keeps moving forward, the cooling scheme becomes more efficient, and the material technology advances, the trend lines will move upward, introducing more feasible areas for generators with higher power rating and speed.

3.2 INERTIA CONSTANTS OF HIGH FREQUENCY GENERATORS

Inertia constants of synchronous generators are extremely critical to power system stability [22]. However, since there are few existing or well-designed high frequency generators available, the lack of data for inertia constants constrains HFAC system planners from conducting system stability studies. A useful method for estimating the inertia constants is highly desired. In this section, an equation that relies on parameters that can be easily obtained and facilitates quick estimation of generator inertia constants is developed.

The inertia constant is defined as kinetic energy at rated generator speed divided by the rated output power. The mathematic expression for inertia constant is [22]:

$$H = \frac{1}{2}\frac{Jw_m^2}{S} * 10^{-6} \tag{3.8}$$

where J is the rotor's moment of inertia in kg·m^2, w_m is the rotor mechanical speed in rad/s, S is the power rating of the generator in MVA. Considering the generator rotor as a solid cylinder with radius of r, its moment of inertia can be calculated as:

$$J = \frac{1}{2}m_r r^2 \tag{3.9}$$

where r is in meters and m_r is the mass of rotor in kg. Substituting (3.9) into (3.8) yields:

$$H = \frac{1}{4}\frac{m_r v_r^2}{S} * 10^{-6} \tag{3.10}$$

where v_r is the surface speed of rotor in m/s. It is mainly limited by the centrifugal stress the rotor can withstand for its material and structure. High frequency generators will have the same limit from surface speed as normal 60 Hz generators (same v_r). But since they are usually lighter (smaller m_r) as discussed in Section 3.1, the inertia constants will be smaller, according to (3.10).

If we further define the mass ratio (k_r) as the rotor mass divided by that of overall generator:

$$k_r = \frac{m_r}{m} \tag{3.11}$$

and relate the mass of overall generator to power factor (*pf*), rated output power (*S* in MVA), and power density (*PD* in kW/kg),

$$m = \frac{pf * S * 10^3}{PD} \tag{3.12}$$

The equation for inertia constants (3.8) can be arranged into the following format:

$$H = \frac{1}{4}\frac{(mk_r)v_r^2}{S} * 10^{-6} = \frac{1}{4}\frac{\frac{pf * S * 10^3}{PD}k_r v_r^2}{S} * 10^{-6} = \frac{1}{4}\frac{pf * k_r v_r^2}{PD} * 10^{-3} \tag{3.13}$$

Both (3.8) and (3.13) can be used to calculate *H*. (3.8) requires the knowledge of three parameters, among which the moment of inertia is very difficult to obtain for most power system engineers. It requires people to go through the design process or to have extensive knowledge of machine design. (3.13) needs four variables to calculate *H*. But the four variables in (3.13) can be found or estimated more easily. *Pf* is a design parameter that

commonly locates between 0.8 and 1 for most of the generators. K_r depends on the structure and it can be estimated by some well-designed machines in the same type. V_r is limited by the type of machine, and its critical values were presented earlier in this section. *PD* can be known by collecting the data of similar machines. Statistics [18][19][20] indicate that most of traditional 60 Hz synchronous generators have *PD*s less than 0.6 kW/kg while high frequency generators usually have *PD*s higher than 1 kW/kg. Thus, we can use (3.13) to quickly estimate *H*s of high frequency generators. Table 3.3 lists the estimated values for four MW-range generators in two types: traditional round-rotor and advanced high-temperature superconducting (HTS) generators. Generators 1 and 2 are based on the data of high frequency generators designed by machine engineers in Westinghouse [20], while Generator 3 and 4 are for HTS generators developed by researchers at GE Global Research Center [47]. The numbers in bold are our estimations for learning the possible range of inertia constants. All of the estimated inertia constants are smaller than 2 s. Statistics [22] show that normal 60 Hz synchronous generators in MW-range operating in current power systems usually have *H*s higher than 4 s. Therefore, high frequency generators in HFAC power systems can easily have much lower *H*s which may potentially threaten system stability.

Table 3.3 Estimated inertia constants of synchronous generators in HFAC systems

Generator No.	*pf*	k_r	v_r (m/s)	*PD* (kW/kg)	Estimated Inertia Constants (s)	Type
1	0.9	**0.10**	200	1.1	0.8	Round-rotor type
2	0.9	**0.25**	200	1.1	2.0	Round-rotor type
3	**0.9**	**0.05**	652	8.7	0.55	HTS
4	**0.9**	**0.10**	652	8.7	1.1	HTS

3.3 SUMMARY

This chapter analyzed the power density improvement of high frequency generators by increasing system frequency. Trend lines were developed for scaling the generator output power and power density versus generator frequency. Due to the lack of data for high frequency generators, and in order to facilitate stability analysis for HFAC systems, an equation that can quickly estimate inertia constants was established. High frequency generators were found to have much smaller inertia constants than normal 60 Hz generators.

Chapter 4

TRANSIENT STABILITY OF HFAC POWER SYSTEMS

Power system stability is often characterized in terms of rotor angle divergence in response to either large or small disturbances. Transient stability is tested when the power system is subjected to a large disturbance while small signal stability describes the response to incremental changes to the operating point. Power system stability has been heavily researched for several decades. However, there is no description of the fundamental dependence of stability on system frequency, considering that characteristic properties of the system components will also vary with the design frequency. This chapter will define the frequency limit of HFAC systems to system faults and current circuit breaker technologies, based on the critical clearing time. The impact of higher system frequencies on transient stability will be discussed.

4.1 FUNDAMENTAL ANALYSIS OF TRANSIENT STABILITY

Consider a simple micro-grid composed of two synchronous generators having different inertia constants (H_{LG} and H_{SG}) and a load equal to the total power rating of the two generators. At steady state, a three phase bolted fault occurs on the buswork between the generators and the load. Then the subsequent rotor angle [22] is governed by:

$$\begin{cases} T_{mLG} - T_{eLG} = J_{LG} * \alpha_{mLG} \\ T_{mSG} - T_{eSG} = J_{SG} * \alpha_{mSG} \\ J_{LG} = \dfrac{2 * H_{LG} * S_{LG}}{\omega_{mLG}^2} \\ J_{SG} = \dfrac{2 * H_{SG} * S_{SG}}{\omega_{mSG}^2} \\ pf = \dfrac{P_{LG}}{S_{LG}} = \dfrac{P_{SG}}{S_{SG}} \\ T_{mLG} = \dfrac{P_{LG}}{\omega_{mLG}} \\ T_{mSG} = \dfrac{P_{SG}}{\omega_{mSG}} \\ \theta_{mLG} = \omega_{mLG} * t + \dfrac{1}{2} * \alpha_{mLG} * t^2 + \theta_{m0} \\ \theta_{mSG} = \omega_{mSG} * t + \dfrac{1}{2} * \alpha_{mSG} * t^2 \\ |\theta_{mLG} - \theta_{mSG} - \theta_{m0}| = \theta_{mr} = \dfrac{\theta_{er}}{p/2} \\ \omega_{mLG} = \omega_{mSG} = \dfrac{2 * \pi * f}{p/2} \\ k_H = \dfrac{H_{LG}}{H_{SG}} \end{cases} \tag{4.1}$$

where the subscripts "*LG*" and "*SG*" denote Large Generator and Small Generator, respectively. For each generator, T_m is the mechanical torque, T_e is the electrical torque which is assumed to be zero during the fault transient, J is the rotor's moment of inertia, α_m is the rotor angular acceleration, H is the inertia constant, S is the rated apparent power, ω_m is the nominal rotor angular speed, pf is the power factor of generators, P is the rated active power, θ_m is the absolute mechanical rotor angle from the onset of a disturbance that produces constant accelerating torque, θ_{mr} and θ_{er} are the mechanical and electrical rotor angle differences between the two generators, f is the generator rated frequency, p is the pole number of the generators, t is the time to reach the rotor angle difference θ_{er}, θ_{m0} is the initial rotor angle difference, and k_H is the ratio of Hs of two generators. After the fault, the

rotor angle will begin to diverge from its initial value (θ_{m0}) due to any difference of the angular accelerations of the two generators. Algebraic manipulation of (4.1) yields the equation for the time to reach a given rotor angle difference:

$$t = \sqrt{\frac{2 * \theta_{mr}}{|\alpha_{mLG} - \alpha_{mSG}|}} = \sqrt{\frac{2 * \theta_{er}}{pf * \pi * f * \left|\frac{1}{H_{LG}} - \frac{1}{H_{SG}}\right|}} = \sqrt{\frac{2 * \theta_{er} * H_{SG}}{pf * \pi * f * \left|1 - \frac{1}{k_H}\right|}} \tag{4.2}$$

If we substitute the critical clearing angle (CCA) for θ_{er} into (4.2), the calculated time becomes the critical clearing time (CCT).

$$CCT = \sqrt{\frac{2 * CCA * H_{SG}}{pf * \pi * f * \left|1 - \frac{1}{k_H}\right|}} \tag{4.3}$$

The CCT is a popular and important measure for power system stability, which is defined as the latest time to isolate the fault without losing transient stability. The longer the CCT, the longer time the protection systems and devices have to respond to system faults, and therefore the better the system stability. In practice, for a fixed power system, the power angle curve will not change a lot so that the CCA will not vary in a wide range. Therefore, observations on (4.2) indicate that smaller inertia constant (H_{SG}), higher frequency (f), and larger ratio of inertia constants (k_H) lead to smaller CCT. In Chapter 3, it is explained that the inertia constants for generators in HFAC systems tends to be much smaller than normal 60 Hz power systems due to their compactness. They can normally locate in the range less than two second. With that conclusion in mind and considering the increasing frequency in (4.3), the CCT in HFAC systems will be much less than normal 60 Hz systems under the same system fault, which means HFAC systems are potentially and inherently more unstable than normal 60 Hz systems. In other words, HFAC systems approach the stability

boundary faster than 60 Hz systems and thus require faster protection devices to deal with the contingencies.

In order to better illustrate the findings above, a 3D figure based on (4.2) is drawn in Figure 4.1, illustrating the dependence of CCT on two of three variables: the system frequency and the ratio of *H*s of two generators. To draw this figure, H_{SG}, *pf*, and CCA in (4.3) are chosen as 1 s, 0.8, and 60 degree, respectively. The vertical axis represents the CCT. An assumption made here is that H_{LG} is always larger than H_{SG} since usually the *H* will increase when the generator size increases. Observing each plane of system-frequency-versus-CCT, it is learned that for a fixed ratio of *H*s, the CCT decreases as frequency increases, which means a higher frequency system is inherently less stable than a lower frequency system. A similar conclusion can be obtained by observing the planes of ratio-of-inertia-constants-of-two-generators-versus-CCT: if the system frequency is fixed, higher ratio of *H*s shortens the CCT, requiring the protection devices to react faster. This finding is further augmented through extensive simulation experiments as described in the following sections.

It should be also noted that excitation systems will help to increase the CCA [24][27] so that power systems with well-tuned excitation systems can have more time to react to the contingency. But this benefits brought by excitation systems vary case by case and the tuning of PID controllers in excitation systems affects the ultimate improvement as well. For the purpose of fair comparison, the positive effect of excitation systems is ignored in this analytical study.

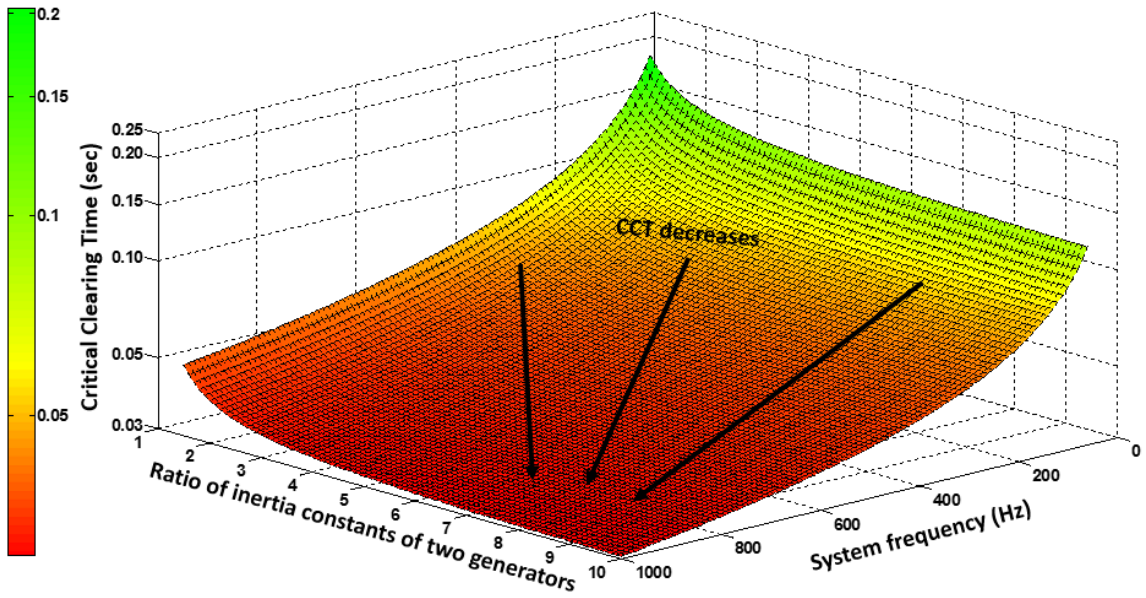

Figure 4.1 CCT decreases with system frequency increases, manifesting system inherent stability decreases.

4.2 SIMULATION STUDIES BASED ON A TWO-MACHINE SYSTEM

The most practical method for studying transient stability is time-domain simulation [22], similar to that used in the rest of this chapter. In this section, simulation tests are based on a two-generator system. A three-phase-to-ground fault is set to incite potential instability. Three sets of generator inertia constants are designed to gain a thorough understanding of system characteristics. For judging system stability, the responses of rotor angle difference and generator frequency are observed and quantified by two stability indices. The effect of tuning the PID controller in an excitation system is evaluated by a sensitivity index.

4.2.1 POWER SYSTEM MODEL

Our reference system, a simplified HFAC notional system [10][48] with parallel-connected generators, is shown in Figure 4.2. It consists of one large generator (LG) having rated power of 36 MW, one small generator (SG) with rated power of 4 MW, and a 33.5 MVA linear load with power factor of 0.95 representing system loads. The LG is driven by

a twin-shaft gas turbine engine, as shown in Figure 4.3 [48]. The SG is powered by a single-shaft gas turbine engine, as shown in Figure 4.4 [10]. The excitation system uses a simplified IEEE Type AC8B exciter as shown in Figure 4.5 [49]. The details of the notional system and its component models can be found in [10][48]. In the reference system, LG and SG each connect to a 10-m cable, then to a common bus. The cable between the common bus and the load bus is 20-m long. The impedance of each cable for the 60 Hz system is 37+j0.6 μ Ω/m (Caledon Type). The same cable is used in a higher frequency system, meaning that the cable impedance increases proportionally with frequency. Stable operation of the system is perturbed by a three phase bolted fault at location A. We have considered four different frequencies (60 Hz/120 Hz/180 Hz/240 Hz) of the generators. All simulation cases considering the same fault will be described in the next section. Assuming the number of poles of generator is fixed at two, the generator speeds corresponding to 60 Hz, 120 Hz, 180 Hz and 240 Hz are 3600 RPM, 7200 RPM, 10800 RPM and 14400 RPM, respectively. The same structures of governor control and excitation system were used for different system frequencies. In order to eliminate the effect of the controller, the parameters of the PID controller in excitation system were tuned for different system frequencies so that the bandwidth of voltage control loop is proportional to system frequency. But the parameters of the engine governor controller remain the same considering that the engine and its speed control are limited by physics that do not change with system frequency and that evolve at speeds much slower than the excitation system. Table 4.1 lists generator parameters.

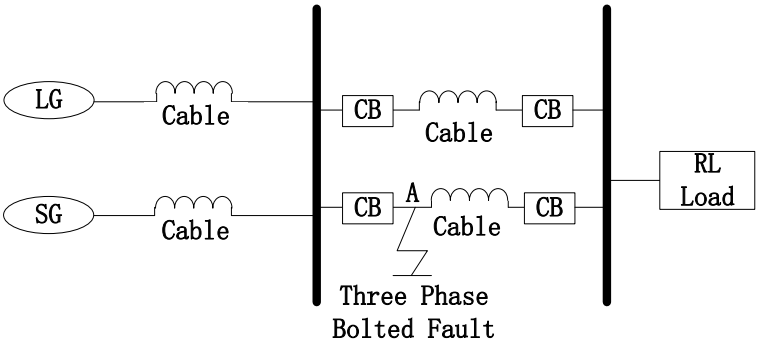

CB = Circuit Breaker, LG = Large Generator
SG = Small Generator

Figure 4.2 Reference system structure.

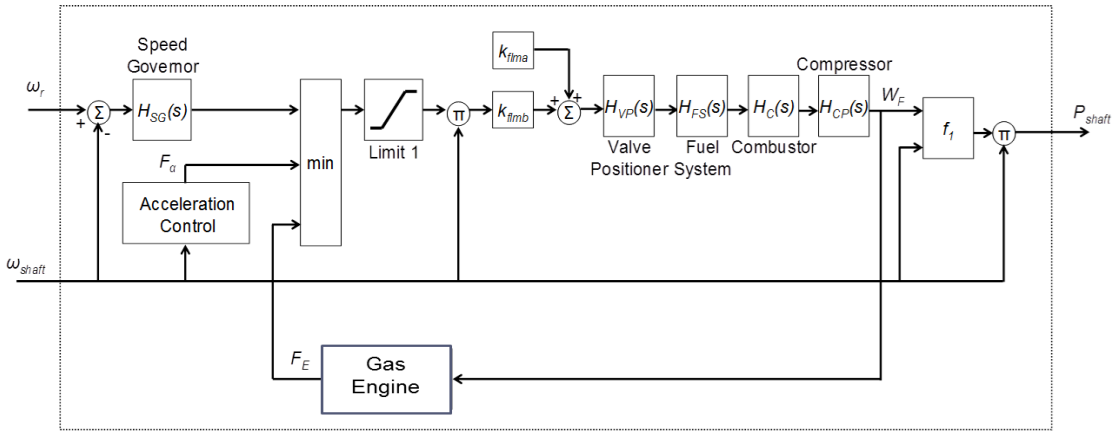

Figure 4.3 Model of twin-shaft gas turbine engine.

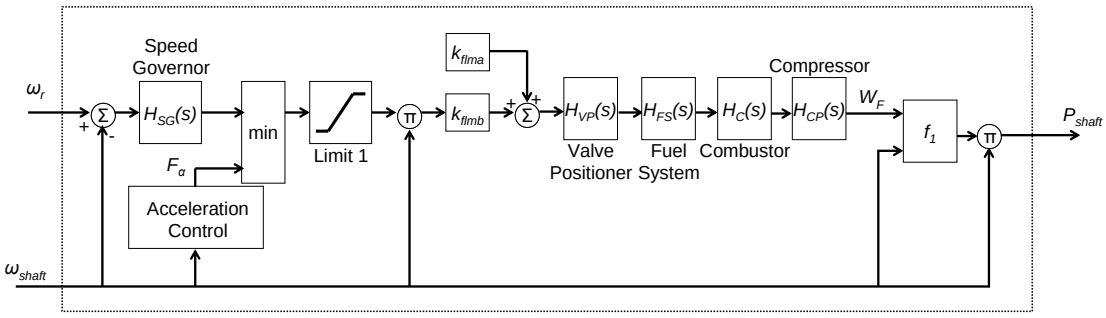

Figure 4.4. Model of single-shaft gas turbine engine.

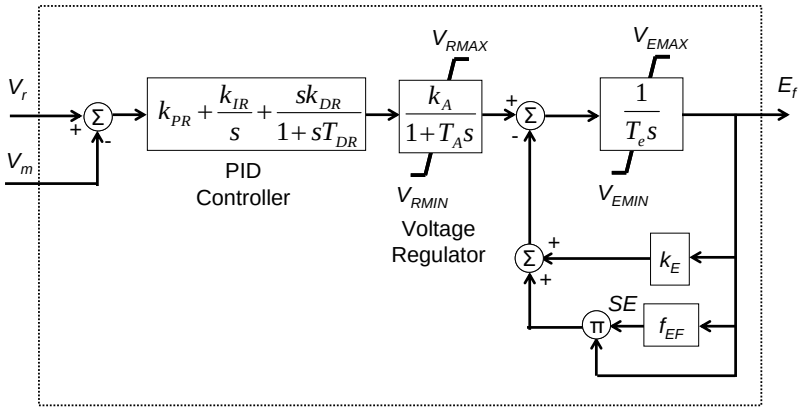

Figure 4.5 IEEE type AC8B exciter model.

Table 4.1 Generator parameters

Specifications	Large Generator (LG) – round-rotor type	Small Generator (SG) – round-rotor type
Power (MVA)	47	5
Speed (RPM)	3600/7200/9600/14400	3600/7200/9600/14400
Number of poles	2	2
Frequency (Hz)	60/120/180/240	60/120/180/240
Voltage (kV)	4.16	4.16
Power factor	0.8	0.8
Stator winding resistance (p.u.)	0.002	0.005
Stator winding leakage inductance (p.u.)	0.135	0.09
Stator d-axis mutual inductance (p.u.)	1.35	0.9
Stator q-axis mutual inductance (p.u.)	1.35	0.9
Field-winding resistance (p.u.)	0.001	0.001
Field-winding leakage inductance (p.u.)	0.081	0.045
d-axis damper resistance (p.u.)	0.045	0.04
d-axis damper leakage inductance (p.u.)	0.0225	0.018
q-axis damper1 resistance (p.u.)	0.01	0.04
q-axis damper1 leakage inductance (p.u.)	0.0405	0.018
q-axis damper2 resistance (p.u.)	0.01	0.04
q-axis damper2 leakage inductance (p.u.)	0.0405	0.018
Friction factor (N.m.s)	0.04	0.04

4.2.2 Three Tests and Discussions

4.2.2.1 Test Configurations

Three tests were conducted to study the influence of system frequencies upon system transient stability, namely a) sensitivity of critical clearing time (CCT) to scaling of inertia constants (*H*) with system frequency (generator speed), b) sensitivity of system stability to system frequency assuming that circuit breakers operate at speeds proportional to system frequency, and c) sensitivity of system stability to system frequency assuming that circuit breakers operate at speeds independent of system frequency.

4.2.2.2 Sensitivity of Critical Clearing Time (CCT) to Scaling of Inertia Constants

CCT is the latest time at which a circuit breaker can open to clear a fault and the system will remain stable. If the circuit breaker opens after the CCT, the rotor angle difference will continue to increase and the system will become unstable. The larger the CCT, the more time a circuit breaker has to respond to a fault.

Although in the previous chapter we found that the *H*s of high frequency generators may become very small, it is still not clear that whether *H* should naturally tend to increase or decrease with increasing system frequency. As CCT depends strongly on *H* as stated in the section of 4.1, we have considered three cases in this test: one in which *H*s are presumed to increase with increasing frequency, one in which they are presumed to decrease with increasing frequency, and one in which they are presumed independent of system frequency. On the other hand, observational data does suggest that the inertia constant of a high-power generator is generally larger than that of a lower-power generator. We therefore designed a

matrix of test cases for comparison to the baseline case in which *H*s were assigned typical values of 3 s for the large generator and 2.5 s for the small generator (at 60 Hz). Then we explored the scenarios in which *H* variously increased or decreased with frequency by incrementing or decrementing *H* (somewhat arbitrarily) by 0.3 s for every 60 Hz increment of frequency. In this way, we were able to test the trend of CCT with frequency and with *H*. It should be noted that the *Hs* used in the simulation studies in this chapter are larger than the values that were estimated from Section 3.2. The reason is that the total *H*s in power system simulations should include the inertias of prime movers (gas turbines in this case). Our estimations were based on some statistics from literature, and the baseline modeling work for next-generation ESPSs [10][48], which is funded by Office of Naval Research.

Table 4.2 shows the results of these tests. The first column shows the test frequencies ranging from 60 Hz to 240 Hz. The second, third, and fourth columns indicate the values of CCT found for each of the test cases. From Table 4.2 it is evident that, regardless of how *H* scales, as frequency increases CCT decreases. Circuit breakers must therefore respond more quickly at higher system frequencies in order to maintain system stability. This might be interpreted to mean that higher frequency systems are inherently more unstable, about which we will explain more after defining quantitative stability indices in the next section.

Table 4.2 Critical Clearing Time (CCT) for different frequencies

Frequency (Hz)	Case 1: *H* decreases with increasing frequency		Case 2: *H* independent of frequency		Case 3: *H* increases with increasing frequency	
	*H*s of MG/AG	CCT	*H*s of MG/AG	CCT	*H*s of MG/AG	CCT
60	3/2.5	1.713	3/2.5	1.713	3 /2.5	1.713
120	2.7/2.2	1.014	3/2.5	1.150	3.3/2.8	1.297
180	2.4/1.9	0.678	3/2.5	0.897	3.6/3.1	1.125
240	2.1/1.6	0.332	3/2.5	0.752	3.9/3.4	1.043

4.2.2.3 Sensitivity of System Stability to System Frequency with Respect to Circuit-Breaker-Speed Using Constant-Cycle Circuit Breaker

We tested the sensitivity of system stability to circuit breaker operating speed in two ways: constant-cycle and constant-time. Two measures for quantifying transient stability are a history index and the Transient Rotor Angle Severity Index (TRASI) [36]. The history index shown in (4.4) is based on the 10-second integration of waveforms of rotor angle difference and generator frequency after the fault:

$$History\ index = \int_0^{10} |x - X_0|^2\, dt \tag{4.4}$$

where x and X_0 are the transient value and steady state value, respectively, for both the rotor angle difference and generator frequency. From (4.4) it is apparent that the smaller the index, the better the system stability. TRASI is based on the maximum deviation of rotor angle difference after the fault:

$$TRASI = \left(\frac{360° - max\left(\delta_{max\_d}^{pos}\right)}{360° - \delta^{pre}}\right) \tag{4.5}$$

where $\delta_{max\_d}^{pos}$ and δ^{pre} denote the post-fault maximum rotor angle difference and pre-fault rotor angle difference. From (4.5), it is apparent that TRASI varies from 0 to 1, with values closer to one considered to be more stable because angular separations between the generators are less compared to the pre-fault values. The fundamental difference between the history index and TRASI is that the former one is based on the system transient performance over a period but the latter one is based on one point (maximum deviation) during that period.

Another sensitivity index [36] evaluating the effect of tuning the PID controller in excitation system on system stability is:

$$Sensitivity = \left(\frac{max\left(\delta_{max\_d}^{no\_PIDtuning}\right) - max\left(\delta_{max\_d}^{PIDtuning}\right)}{\delta^{pre}} \right) \tag{4.6}$$

where $\delta_{max\_d}^{no\_PIDtuning}$ and $\delta_{max\_d}^{PIDtuning}$ represent the maximum rotor angle difference for the cases without PID controller tuning and with PID controller tuning. A positive sensitivity corresponds to an improvement on stability.

In this test, we assumed that it is possible to build a circuit breaker having an operating speed that is commensurate with system frequency; i.e. if a circuit breaker can be designed to open in five cycles at 60 Hz, then one can also be designed to open in five cycles at 240 Hz even though the second case corresponds to a much shorter time. Our test was conducted according to the following protocol: the circuit breaker opens five cycles after the fault occurs, it recloses forty-five cycles after opening; if the fault persists, it reopens in another five cycles. Although according to current technology a typical circuit breaker might not be able to respond as fast as our assumption, this consideration is still very useful for the purpose of this study. In practice, the fault duration should be relatively independent of system frequency and depends instead on the physical nature of the fault and/or on whether or when enough electric energy is deposited into the fault to clear it by explosive force. Since any particular fault could be cleared at any time (if it is cleared at all), we configured this test to measure how the system performance depends on system frequency, scaling of generators' *H*s, and fault duration. Experiments were done for five different values of fault duration ranging from "short" (faster than the circuit breaker's opening time) to "long" (well after the circuit breaker has reclosed). Figure 4.6 illustrates how these five fault duration

times (0.0167 s, 0.0667 s, 0.15 s, 0.5 s and 0.95 s corresponding to Case 1, 2, 3, 4 and 5, respectively) relate to the circuit breaker actuation times at the various system frequencies. The twelve bold points in the three dotted curves represent the circuit breaker opening, reclosing, and re-opening times at the four system frequencies. Three sets of *H*s corresponding to three sub-cases were tested under each case, i.e. *H*=3 s/2.5 s, 4 s/3.5 s, and 5 s/4.5 s (*H* of the large generator/*H* of the small generator).

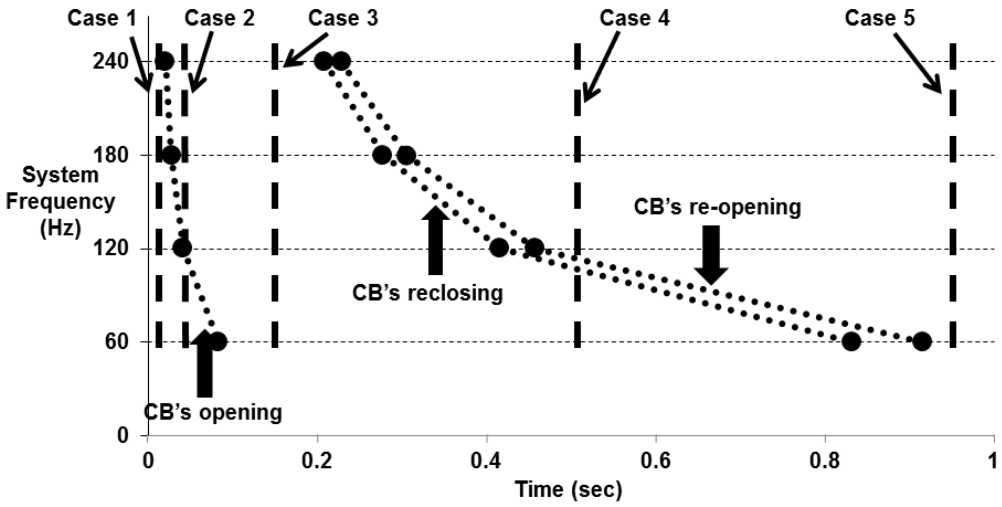

Figure 4.6 Case definitions for Constant-Cycle-Circuit-Breaker test

Figure 4.7 corresponds to Case 3 where the fault duration time is 0.15 s. The history index for rotor angle difference and TRASI both indicate that system stability improves as system frequency increases. It can also be learned that if the system frequency is fixed, as the inertia constants of generators increase, the system stability improves. Figure 4.8 and Figure 4.9 show the responses of the rotor angle difference and large generator's frequency, respectively, corresponding to the sub-case of *H*=4 s/3.5 s in Case 3. In this case, the fault occurs at *t*=1 s. It is apparent that since the 240 Hz system has the shortest circuit breaker opening time, it has the smallest transient oscillation resulting in the smallest history index and the largest TRASI. The same trend was observed in the results from other cases under

Constant-Cycle-Circuit-Breaker test. The history index for rotor angle difference, the history index for generator frequency and the TRASI all agree on this trend. From these results it is clear that the system transient stability depends strongly on the circuit breaker opening time; if it is possible to design circuit breakers that have opening speed in direct proportion to system frequency, then higher frequency systems have better transient stability than lower frequency systems.

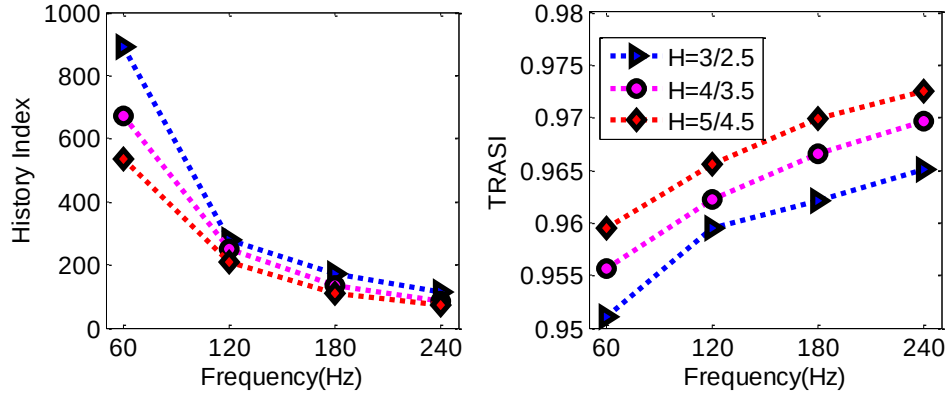

Figure 4.7 History index and TRASI for Case 3 (Fault Duration=0.15 s).

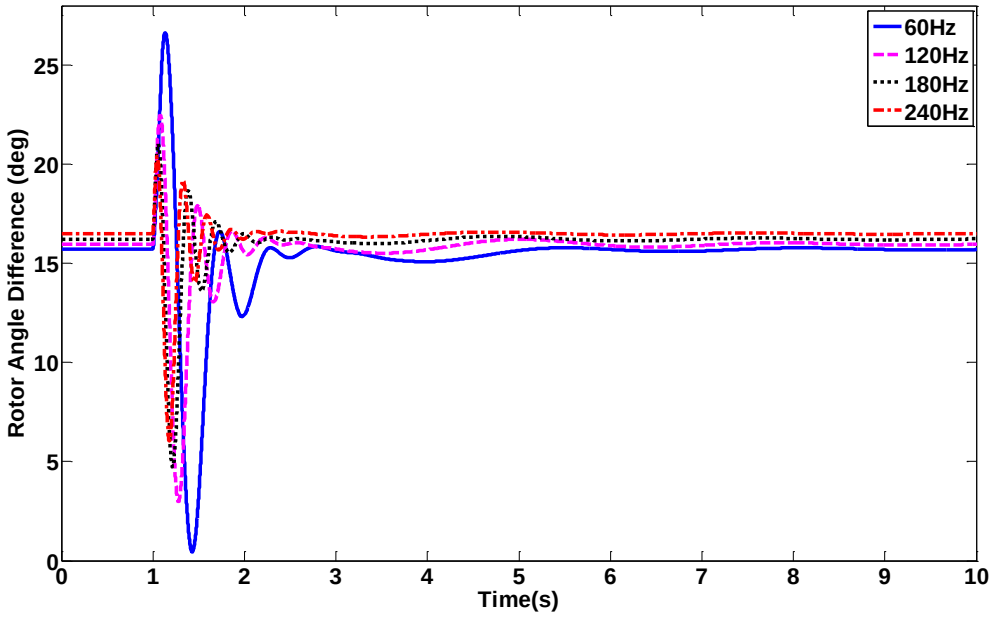

Figure 4.8. Transient response of rotor angle difference for Case 3 with *H*=4 s/3.5 s.

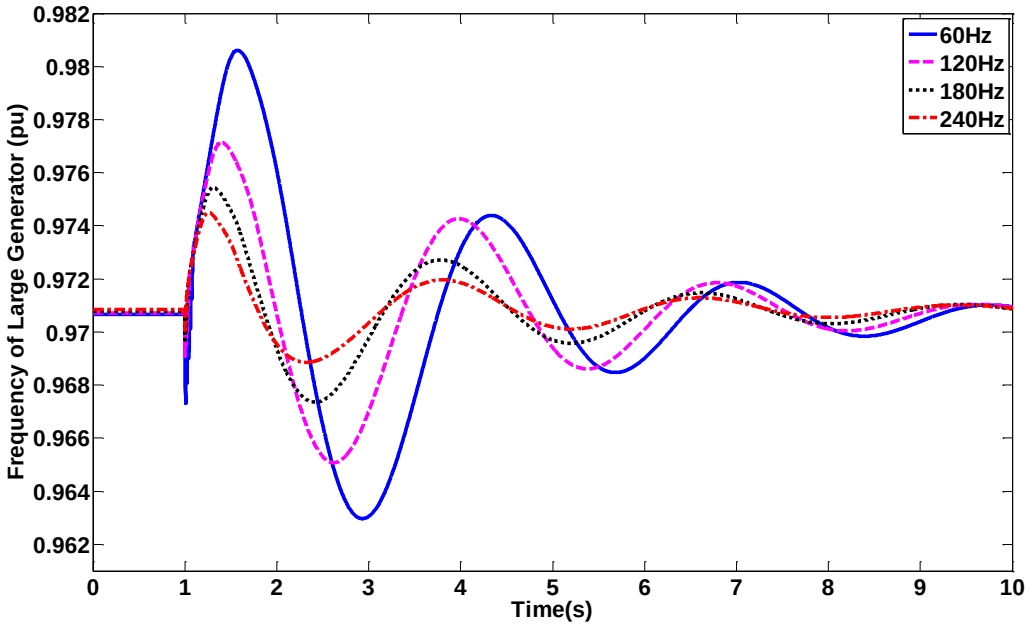

Figure 4.9. Transient response of the frequency of the large generator for Case 3 with H=4 s/3.5 s.

4.2.2.4 Sensitivity of System Stability to System Frequency with Respect to Circuit-Breaker-Speed Using Constant-Speed Circuit Breaker

It might not be possible to build circuit breakers for 240 Hz systems that open four times faster than existing 60 Hz circuit breakers, and therefore the final interpretation of the previous section would be wrong. So we examined how the stability indices depend on frequency when the circuit breaker opening time is independent of system frequency. In this test, the circuit breaker opening time was assumed to always be 0.0833 s (corresponding to five cycles at 60 Hz) at every system frequency, reclosing at 0.833 s (fifty cycles at 60 Hz), and reopening at 0.916 s (fifty five cycles at 60 Hz) if the fault persists. Similar to the Constant-Cycle-Circuit-Breaker test, experiments were done for three different values of fault duration (0.0167 s, 0.5 s, and 0.95 s corresponding to Case 6, 7, and 8, respectively). Three sets of H corresponding to three sub-cases have again been considered, as in the Constant-Cycle-Circuit-Breaker test.

Figure 4.10 shows the history index for rotor angle difference and TRASI calculated for Case 7. Figure 4.11 and Figure 4.12 show the responses of the rotor angle difference and large generator's frequency, corresponding to the case of H=4 s/3.5 s in Case 7 where the fault occurs at t=1 s. It is difficult to infer a significant general trend from these results, and the other cases in this test were similarly ambiguous – there is no strong dependence of stability on system frequency. This conclusion was consolidated by all calculated TRASI and history index.

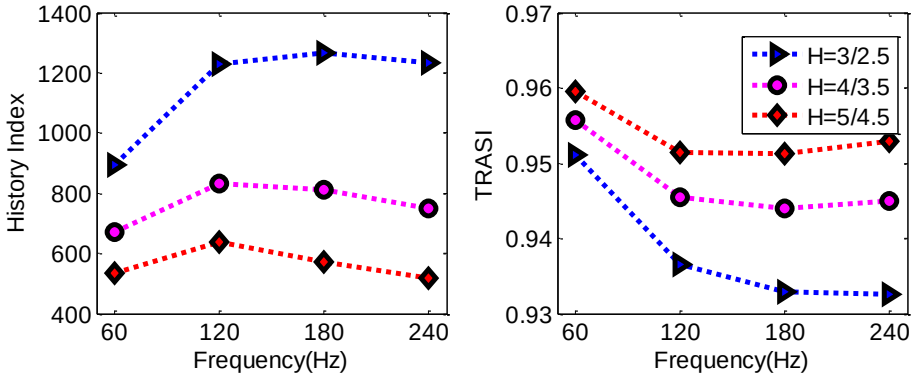

Figure 4.10. History index for rotor angle difference and TRASI for Case 7 (Fault Duration=0.5 s).

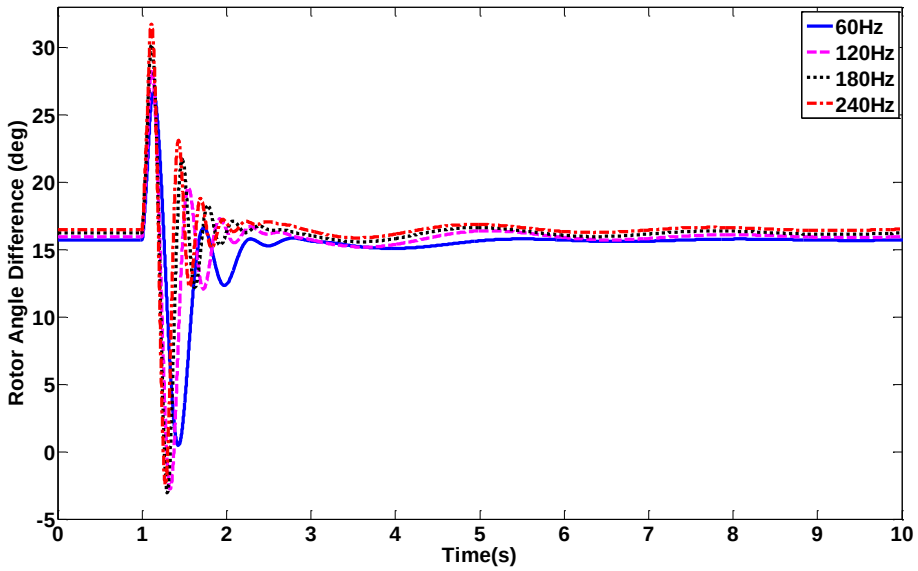

Figure 4.11. Transient response of rotor angle difference for Case 7 with H=4 s/3.5 s.

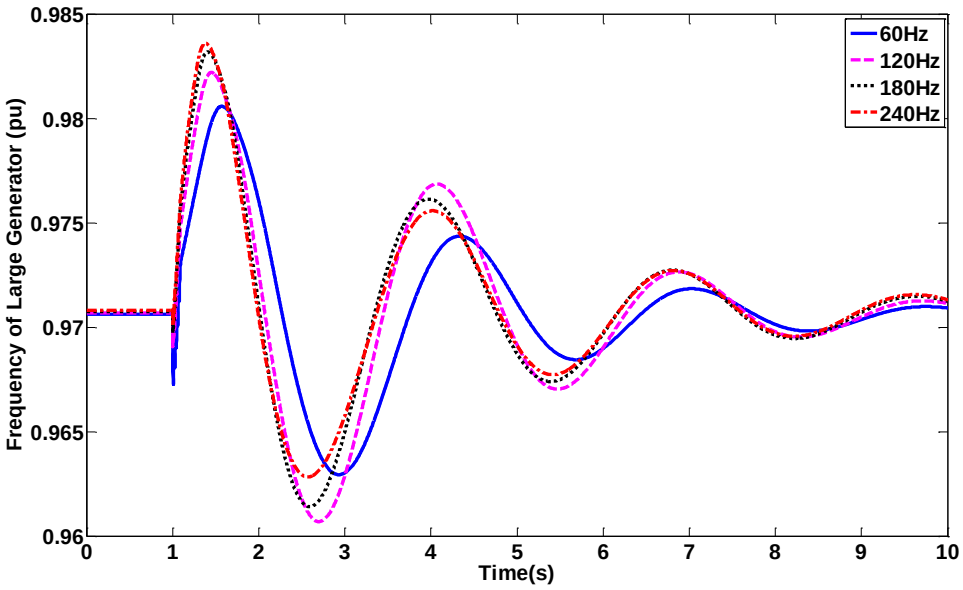

Figure 4.12. Transient response of the frequency of the large generator for Case 7 with H=4 s/3.5

Meanwhile, we performed comparative tests to study whether tuning the PID controller in the excitation system has impacts on system stability in Case 6, 7 and 8. In comparison groups, the same PID controller was deployed for systems with different frequencies, i.e. using the same PID controller for higher frequency system as used in the 60 Hz system. The finding shows that if the PID controller is not tuned specifically for each frequency, larger frequency oscillations occur as system frequency increases. This was consolidated by larger values in history index for generator frequency. An example of this can be illustrated by Figure 4.13 and Figure 4.14. Figure 4.13 indicates that with PID controller tuning less oscillation is present during the transient. From Figure 4.14 it is apparent that without tuning the PID controller, the generator frequency oscillates more as system frequency increases. This can be interpreted as system stability deteriorating as system frequency increases. Therefore, tests of Case 6, 7, and 8 and its comparison groups indicate that tuning the PID controller in an excitation system can help improve system stability in higher frequency

systems. A further comprehensive investigation was done for the effect of tuning the PID controller for all cases (Case 1 through Case 8), which is documented in [50].

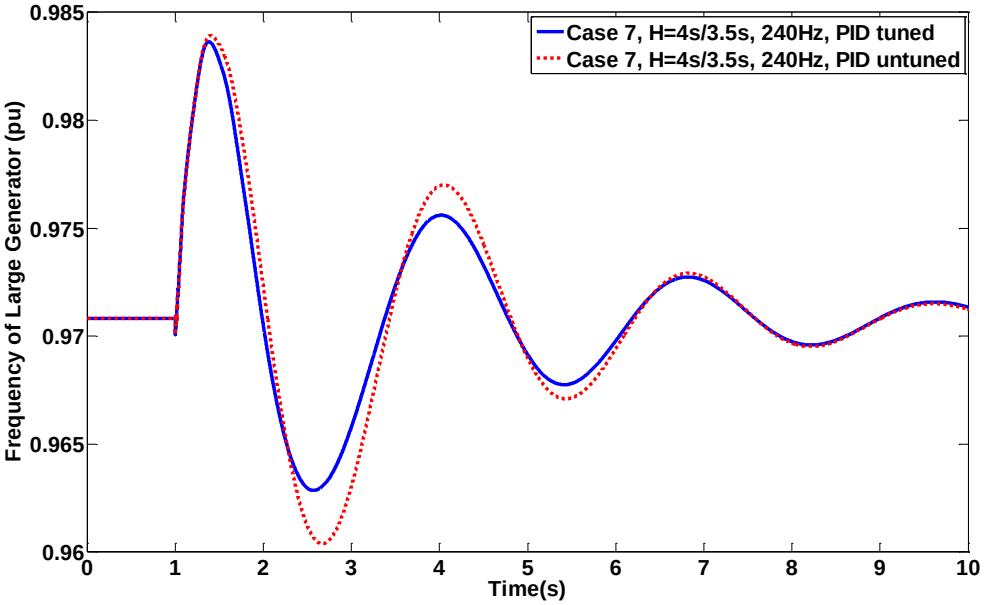

Figure 4.13. Impact of tuning PID controller on transient response of large generator frequency.

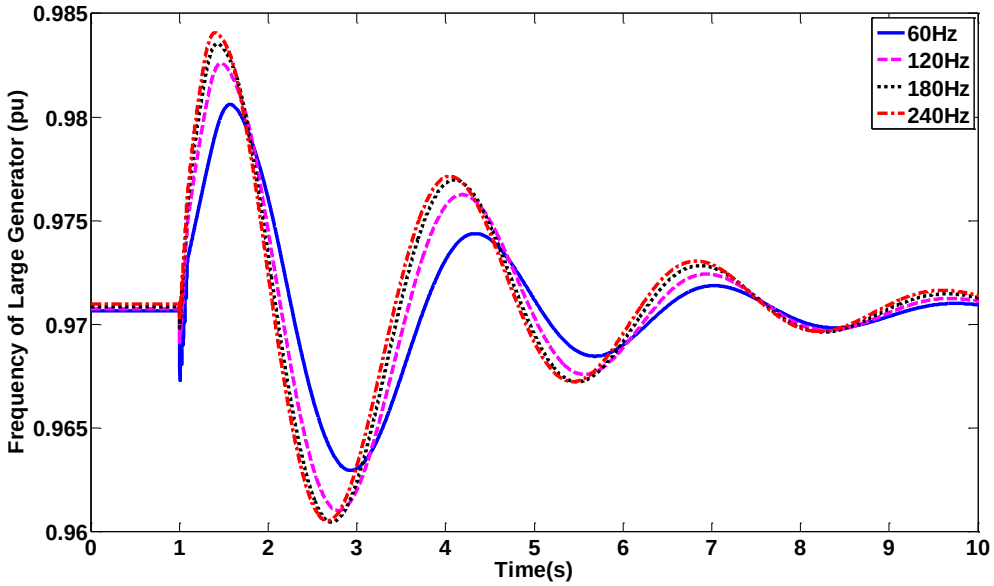

Figure 4.14. Transient response of large generator frequency for Case 7 with *H*=4 s/3.5 s and PID controller untuned.

4.3 SIMULATION STUDIES BASED ON A LARGER SYSTEM - ELECTRIC SHIP POWER SYSTEM

In this section, the transient stability of HFAC systems will be studied based on a large system – a four-generator electric ship power system [48]. The purpose is to verify the findings from the previous section in a larger-scale and more complex micro-grid.

4.3.1 POWER SYSTEM MODEL

The reference system structure is shown in Figure 4.15. It is based on an electric ship power system [48]. The generation module model, including the gas turbine, exciter, and the synchronous generator, is the same as in 4.2.1. The large generators (Gen1 and Gen2 in yellow) are powered by a twin-shaft gas turbine each (Figure 4.3). The small generators (Gen3 and Gen4 in blue) are connected to a single-shaft gas turbine each (Figure 4.4). The parameters of generators are listed in Table 4.1. The total system generation capacity is 80 MW and the total consumption is 68 MVA with power factor of 0.95. The four load zones and propulsion loads are represented by lumped RL loads. Each of four load zones consumes 5% of the total system consumption while each propulsion load consumes 40%. In Figure 4.15, the blocks in magenta represent circuit breakers. The cables are in green, with the numbers beside them showing the length of each cable. The incident that may trigger the potential system instability is the same three-phase-bolted fault as used in the tests earlier in this chapter, which is occurring on the top branch of the ring bus system (in red).

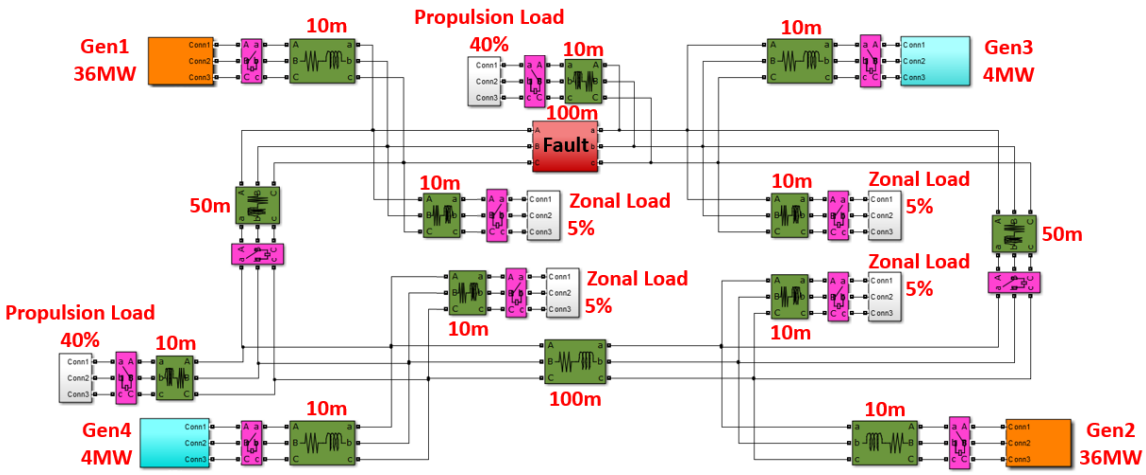

Figure 4.15 Reference system structure

4.3.2 Three Tests and Discussions

4.3.2.1 Test Configurations

Similar to 4.2.2, three tests were conducted to study the influence of system frequencies upon system transient stability, a) sensitivity of critical clearing time (CCT) to scaling of inertia constants with system frequency, b) sensitivity of system stability to system frequency assuming that circuit breakers operate at speeds proportional to system frequency, and c) sensitivity of system stability to system frequency assuming that circuit breakers operate at speeds independent of system frequency.

In this section, the frequency range is extended to 800 Hz. The four system frequencies under tests were chosen as 60 Hz/240 Hz/400 Hz/800 Hz. Three scenarios of inertia constants are slightly different from the tests in 4.2.2, which is defined in Table 4.3. The scenario of Base-Case represents the system having synchronous generators with normal values, which is the same as one of the settings in 4.2.2. The scenario of Large-Ratio represents the case that the generators have much different inertia constants, which is 10:1. The scenario of Both-Small has the same ratio of inertia constants as Base-Case but the

absolute values are smaller. The total number of cases for each sensitivity test is twelve (four frequencies and three scenarios of inertia constants).

Table 4.3 Three Scenarios of Inertia Constants

Scenario	*H*s of large generator / small generator
Base-Case	5 s/4.5 s
Large- Ratio	5 s/0.5 s
Both-Small	3 s/2.75 s

4.3.2.2 Sensitivity of Critical Clearing Time (CCT) to Scaling of Inertia Constants

Figure 4.16 shows the test results. The similar trend as in 4.2.2.2 can be observed: regardless of the scenarios of inertia constants, CCT decreases as system frequency increases; the systems with the scenario of Large-Ratio inertia constants have the smallest CCT. The CCT for 800 Hz of the scenario of Both-Small inertia constants is 0.06 s. Current MW-range circuit breaker technology allows a three-phase-bolted fault to be isolated within four cycles of 60 Hz, which includes one cycle (0.017 s) for fault detection and three cycles (0.050 s) for opening the contact physically and extinguishing the arc. The one cycle for fault detection is related to system frequency because it requires the fault current to cross "zero". But the contact opening time is relatively independent of system frequency. If we consider the same contact-opening capability of 60 Hz circuit breakers to be applied to 800 Hz system, its opening time will be 0.0543 s, which is the sum of one cycle for fault detection in 800 Hz (0.0013 s) and 0.050 s for contact opening. According to Figure 4.16 that the smallest CCTs for 800 Hz is 0.06 s, this type of circuit breaker can ensure the fault in 800 Hz system to be cleared timely and survive the 800 Hz system through the fault.

Further increase in frequency will result in CCT decreasing to a value smaller than circuit breaker opening time, which means that the system cannot maintain synchronism in the end.

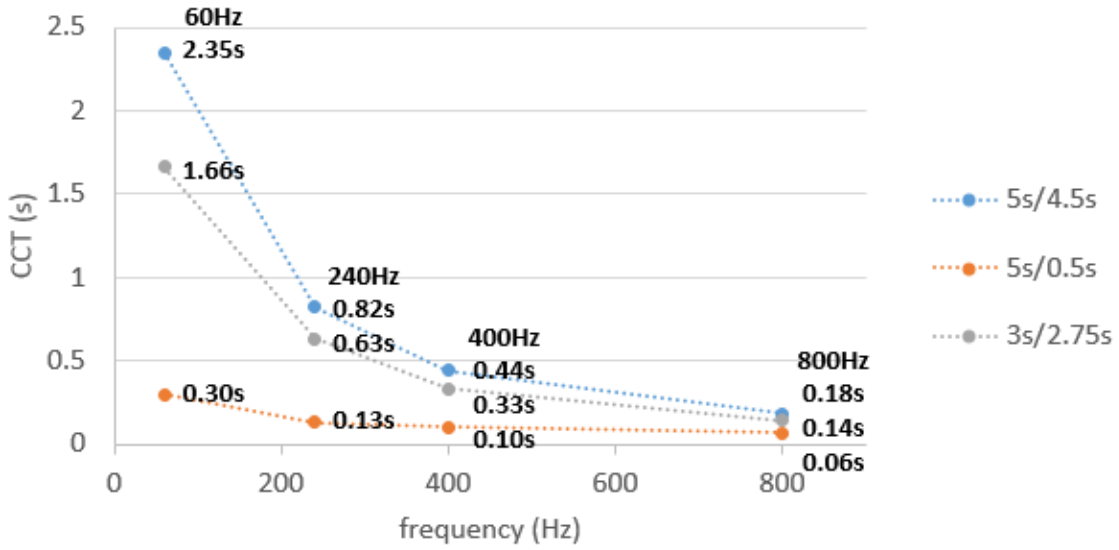

Figure 4.16 Results of CCT Tests

The reason for the fact that higher frequency systems have lower CCTs can be explained by Figure 4.17. Figure 4.17 (a) shows the frequency difference between Generator 1 and 2 after the fault occurs at t=1 s, while Figure 4.17 (b) shows the rotor angle between them. It can be learned that although the per unit frequency difference in low-frequency system is equal to or larger than higher frequency system, the rotor angle between the two generators in higher frequency system such as 800 Hz system are accumulating much faster than low-frequency system, such as 60 Hz, due to the increasing operating frequency, resulting in the rotor angle reaching the Critical Clearing Angle (CCA) faster. The CCA does not change a lot once the system structure and system parameters are relatively fixed. Therefore, the CCTs in higher frequency systems are shorter than lower frequency systems.

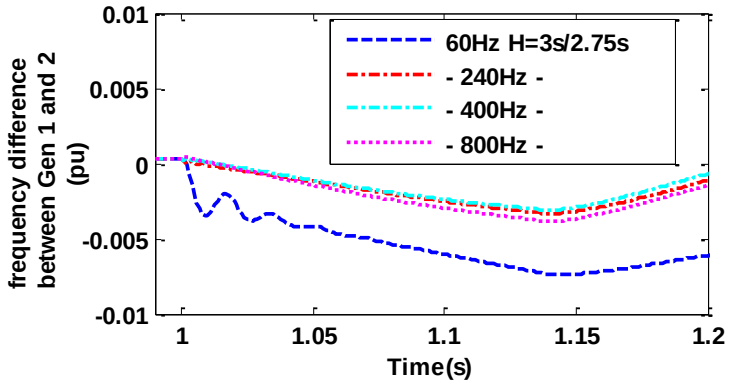

(a) Frequency difference between Generator 1 and 2

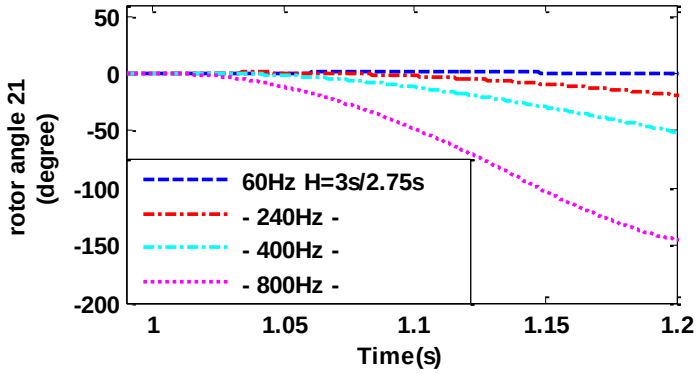

(b) Rotor angle between Generator 1 and 2

Figure 4.17 Explaining the frequency impact on CCT, fault occurs at 1 s

4.3.2.3 Sensitivity of System Stability to System Frequency with Respect to Circuit-Breaker-Speed Using Constant-Cycle Circuit Breaker

Similar to 4.2.2, two different types of circuit breakers were tested in the following two sections: the constant-cycle-circuit-breaker in this section and the constant-speed-circuit-breaker in the next section. In this section, the circuit breakers were configured to open in five cycles, reclose in fifty cycles, and reopen in fifty-five cycles if the fault persists. Three scenarios corresponding to three fault-self-clearing times were configured in all four frequency systems. They are: Fast Self-Clearing in which the fault is self-cleared before the opening of the circuit breaker, Normal Self-Clearing in which the fault is cleared between

the circuit breaker's opening and reclosing, and Permanent Fault in which the fault will not be cleared by itself and the circuit breaker is required to reopen after reclosing. Two stability indices, history index and TRASI as shown in (4.4) and (4.5), were used to quantify the waveforms of rotor angle and generator frequency which are the measures of transient stability.

Figure 4.18 and Figure 4.19 show the TRASI and history index calculated for rotor angle between Generator 1 and 3 under the scenario of Normal Self-Clearing. Figure 4.20 presents the history index for the frequency of Generator 1. Recall that 4.2.2.2 described that larger TRASI and smaller history index represent the better stability. These figures prove that as frequency increases, regardless of the values for inertia constants, if the circuit breaker can respond to the fault at the speed proportional to system frequency, the system stability can be improved. This is the same trend as what was discovered in 4.2.2.2 and this conclusion is consolidated by other calculated TRASI and history index in this test. Transient responses of Generator 1 frequency and rotor angle between Generator 1 and 3 are shown in Figure 4.21 and Figure 4.22. All systems in this test are capable of maintaining stability after the fault with the help of constant-cycle circuit breakers.

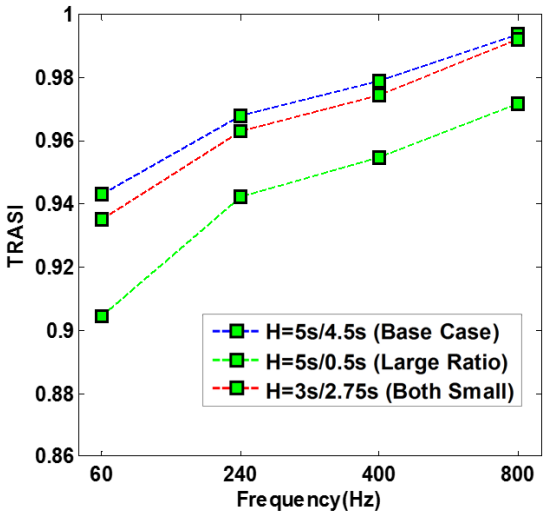

Figure 4.18 TRASI for rotor angle between Generator 1 and 3, under the scenario of Normal Self-Clearing

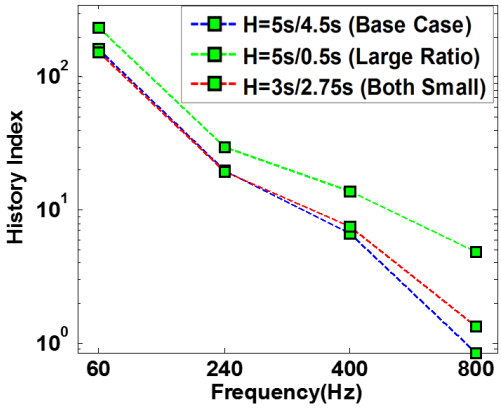

Figure 4.19 History index for rotor angle between Generator 1 and 3, under the scenario of Normal Self-Clearing

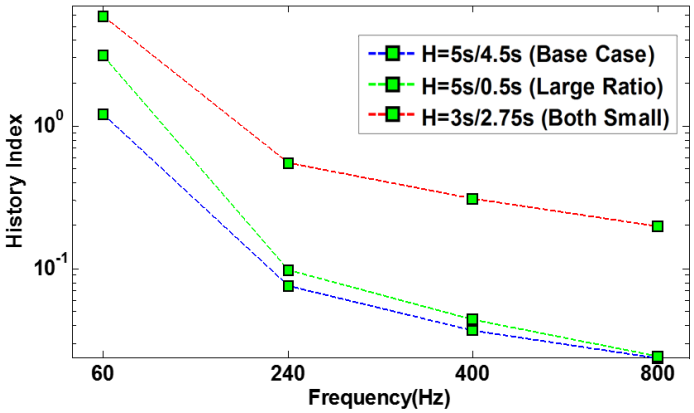

Figure 4.20 History index for frequency of Generator 1, under the scenario of Normal Self-Clearing

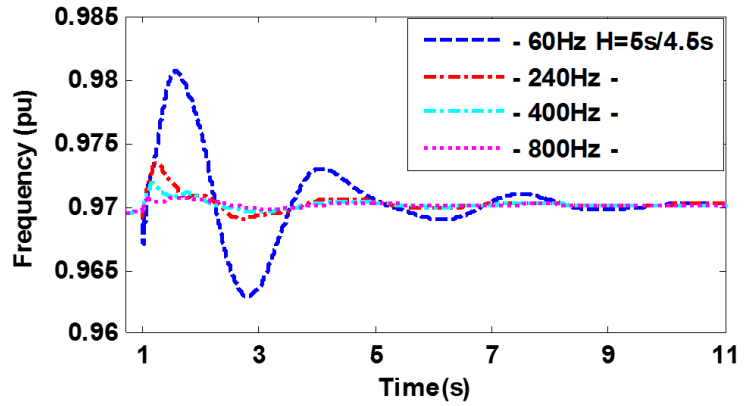

Figure 4.21 Frequency of Generator 1 under the scenarios of Base-Case inertia constants and Normal Self-Clearing

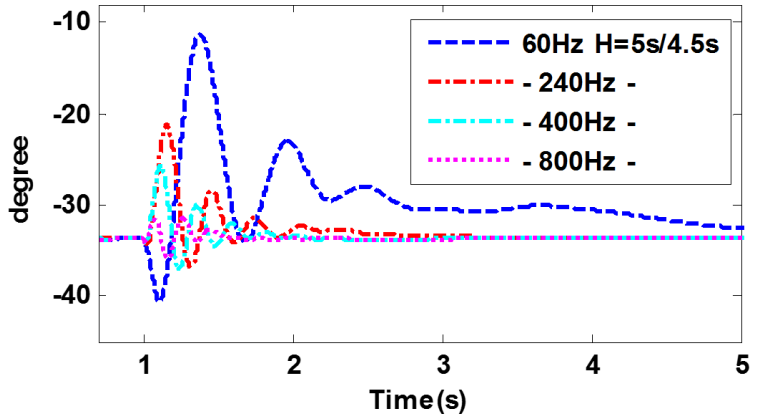

Figure 4.22 Rotor angle between Generator 1 and 3 under the scenarios of Base-Case inertia constants and Normal Self-Clearing

4.3.2.4 Sensitivity of System Stability to System Frequency with Respect to Circuit-Breaker-Speed Using Constant-Speed Circuit Breaker

Unlike the last section, the circuit breaker for 60 Hz system was applied to other frequency systems (240 Hz/ 400 Hz/800 Hz) in this sensitivity test. Three scenarios of fault-self-clearing times, similar to last section, were applied. Figure 4.23 and Figure 4.24 show the TRASI and history index for rotor angle between Generator 1 and 3 under the scenario of Normal Self-Clearing. Figure 4.25 shows the history index for the frequency of Generator 1. There is no fixed trend that can be observed, similar to the conclusions from 4.2.2.4. This can be interpreted as if the speed of circuit breaker cannot be increased proportionally to

system frequency, the stability of higher frequency system may be worse. Figure 4.26 and Figure 4.27 show some transients during the fault. It can be seen that even if the frequency oscillation at higher frequency is a little less (Figure 4.26), the rotor angle accumulates much faster (Figure 4.27) which requires the circuit protection devices to intervene earlier. Figure 4.28 shows the rotor angle between Generator 1 and 4 under the scenario of Large-Ratio inertia constants. It can be seen that the generators in 800 Hz system cannot maintain synchronism after the fault, due to the slow circuit breaker.

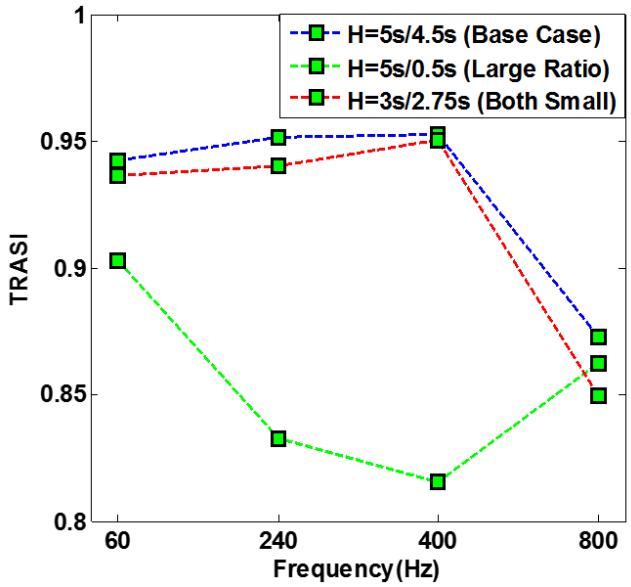

Figure 4.23 TRASI for rotor angle between Generator 1 and 3, under the scenario of Normal Self-Clearing

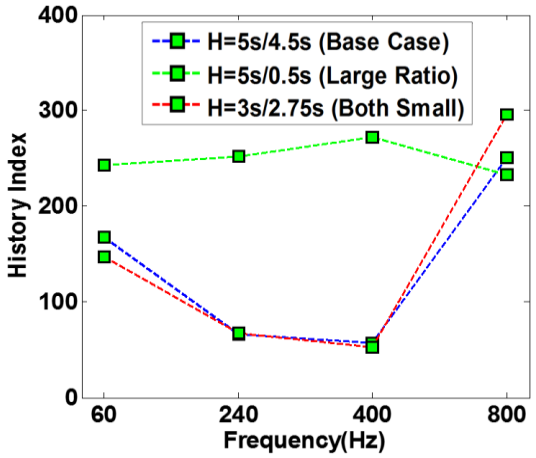

Figure 4.24 History index for rotor angle between Generator 1 and 3, under the scenario of Normal Self-Clearing

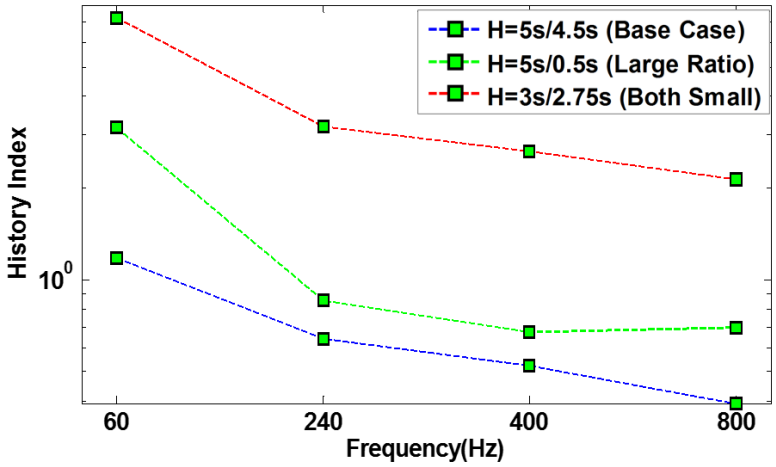

Figure 4.25 History index for frequency of Generator 1, under the scenario of Normal Self-Clearing

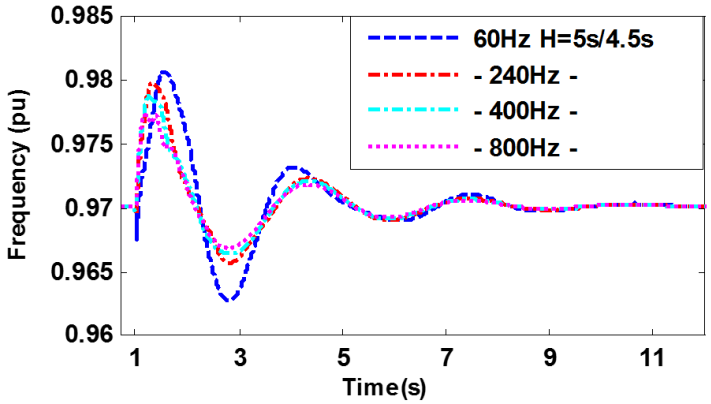

Figure 4.26 Frequency of Generator 1 under the scenarios of Base-Case inertia constants and Normal Self-Clearing

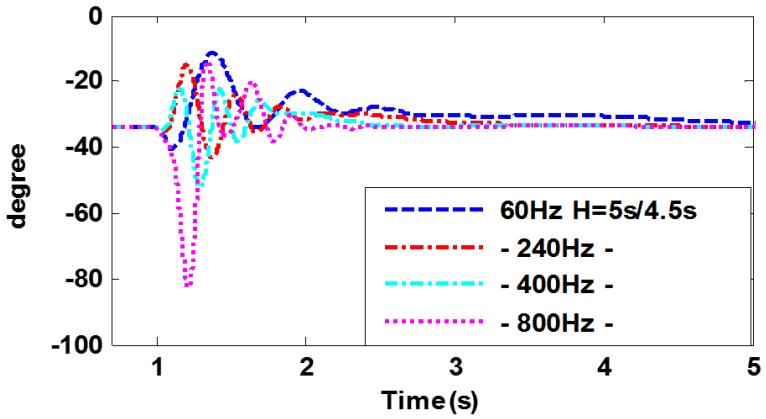

Figure 4.27 Rotor angle between Generator 1 and 3 under the scenarios of Base-Case inertia constants and Normal Self-Clearing

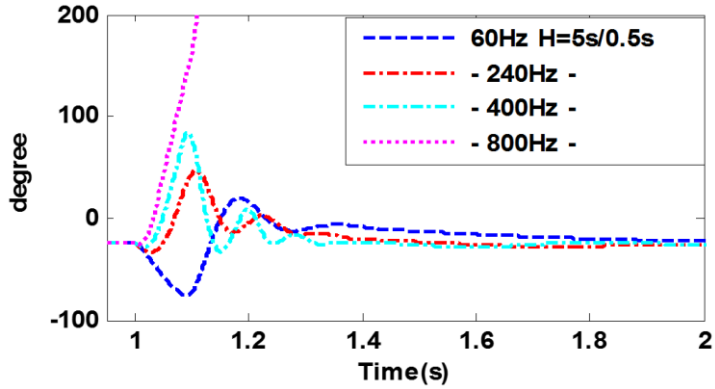

Figure 4.28 Rotor angle between Generator 1 and 4 under the scenarios of Large-Ratio inertia constants and Normal Self-Clearing, the 800 Hz system loses stability after the fault

4.4 ANALYSIS

In this chapter, the transient stability of HFAC power systems was investigated and compared to that of conventional 60 Hz systems. A fundamental analysis was made based on rotor swing equation. Our analytical and simulation studies conclude the following points:

a) Fundamental analysis paints such a picture that it takes less time for rotor angle difference to reach critical rotor degree. From the CCT test it is found that in higher

frequency systems CCT becomes shorter. These indicate that system overcurrent protection in higher frequency systems has less time to isolate the fault.

b) From Constant-Cycle-Circuit-Breaker test, if a fault current can be detected and interrupted within certain number of cycles instead of certain time, the history index and TRASI show that as system frequency increases, the maximum rotor angle difference becomes less and system stability becomes better.

c) From Constant-Time-Circuit-Breaker test, it is found that if it is not possible to interrupt fault currents within certain number of cycles, but instead we rely on circuit breakers with fixed activation times that are independent of system frequency, then frequency oscillations in higher frequency systems are greater than those in lower frequency systems. With the help of fast response voltage regulator, the stability of higher frequency system could be improved, but might still be worse than that of lower frequency system. Considering systems at the same frequency, increasing inertia constants would bring better transient stability performance.

d) The advantages of high frequency generators are compactness and light weight, thus some designs may result in small inertia constants. Generally, low values of inertia constant correspond to large values of maximum rotor swing angle during contingency events and more oscillations on frequency profile after events, so that more rapid corrective action is necessary to keep the swing angle within some defined limits. If the equipment (such as high speed circuit breaker and fast response voltage regulator) fulfilling such corrective action are unavailable, increasing machine inertia would be necessary to maintain a desired level of system stability.

e) Safe and effective use of high frequency generators demands fast-acting overcurrent protection and ideally, comparably-fast generator excitation controls.

4.5 SUMMARY

This chapter analyzed the large-signal stability of HFAC systems. The impacts of system frequency and inertia constants were explored by a fundamental analysis based on swing equation and many simulation tests based on a three-phase-bolted fault. The significance of faster circuit breakers for stable operation of HFAC systems was revealed.

Chapter 5

SMALL SIGNAL STABILITY OF HFAC POWER SYSTEMS

This chapter will discuss the small-signal stability characteristics of HFAC power system and study the impact from several key parameters. First, the method for assessing small-signal stability of HFAC power system will be introduced. Then the reference system will be described. Thirdly, tests for sensitivity of system small-signal stability to some system parameters will be performed. Stability regions will be discovered and trends with changes in dominating parameters will be presented.

5.1 METHODOLOGY

Small-signal stability studies if a power system could maintain synchronism after a small disturbance. This disturbance is small enough so that mathematical equations describing system responses can be linearized around a specific operating point. The dynamic of a power system can be described by a set of nonlinear differential equations in the following form [22]:

$$\dot{\boldsymbol{x}} = \boldsymbol{f}(\boldsymbol{x}, \boldsymbol{u}, t) \tag{5.1}$$

$$\boldsymbol{y} = \boldsymbol{g}(\boldsymbol{x}, \boldsymbol{u}) \tag{5.2}$$

where $\boldsymbol{x}$ is the state vector composed of n entries (termed state variables, $x_1, x_2, \ldots, x_n$), $\boldsymbol{u}$ is the system input vector, $\boldsymbol{y}$ is the output vectors, $\boldsymbol{g}$ is the vector of nonlinear functions relating state and input variables to output variables.

If we linearize the system nonlinear equations around the equilibrium point x_0, following equations can be obtained for describing system dynamics around this equilibrium point:

$$\Delta\dot{\boldsymbol{x}} = \boldsymbol{A}\Delta\boldsymbol{x} + \boldsymbol{B}\Delta\boldsymbol{u} \tag{5.3}$$

$$\Delta\boldsymbol{y} = \boldsymbol{C}\Delta\boldsymbol{x} + \boldsymbol{D}\Delta\boldsymbol{u} \tag{5.4}$$

$$\boldsymbol{A} = \begin{bmatrix} \frac{\partial f_1}{\partial x_1} & \cdots & \frac{\partial f_1}{\partial x_n} \\ \cdots & \cdots & \cdots \\ \frac{\partial f_n}{\partial x_1} & \cdots & \frac{\partial f_n}{\partial x_n} \end{bmatrix} \quad \boldsymbol{B} = \begin{bmatrix} \frac{\partial f_1}{\partial u_1} & \cdots & \frac{\partial f_1}{\partial u_r} \\ \cdots & \cdots & \cdots \\ \frac{\partial f_n}{\partial u_1} & \cdots & \frac{\partial f_n}{\partial u_r} \end{bmatrix}$$

$$\boldsymbol{C} = \begin{bmatrix} \frac{\partial g_1}{\partial x_1} & \cdots & \frac{\partial g_1}{\partial x_n} \\ \cdots & \cdots & \cdots \\ \frac{\partial g_m}{\partial x_1} & \cdots & \frac{\partial g_m}{\partial x_n} \end{bmatrix} \quad \boldsymbol{D} = \begin{bmatrix} \frac{\partial g_1}{\partial u_1} & \cdots & \frac{\partial g_1}{\partial u_r} \\ \cdots & \cdots & \cdots \\ \frac{\partial g_m}{\partial u_1} & \cdots & \frac{\partial g_m}{\partial u_r} \end{bmatrix} \tag{5.5}$$

where A is the state matrix, B is the input matrix, C is the output matrix, and D is the feed forward matrix. Treated by Laplace Transform, (5.3) and (5.4) become:

$$s\Delta\boldsymbol{x}(s) - \Delta\boldsymbol{x}(\boldsymbol{0}) = \boldsymbol{A}\Delta\boldsymbol{x}(s) + \boldsymbol{B}\Delta\boldsymbol{u}(s) \tag{5.6}$$

$$\Delta\boldsymbol{y}(s) = \boldsymbol{C}\Delta\boldsymbol{x}(s) + \boldsymbol{D}\Delta\boldsymbol{u}(s) \tag{5.7}$$

Rearranging (5.6), the following equation is obtained:

$$(s\boldsymbol{I} - \boldsymbol{A})\Delta\boldsymbol{x}(s) = \Delta\boldsymbol{x}(0) + \boldsymbol{B}\Delta\boldsymbol{u}(s) \tag{5.8}$$

Therefore, the characteristic equation of matrix A is:

$$det(s\boldsymbol{I} - \boldsymbol{A}) = 0 \tag{5.9}$$

The values of *s* satisfying characteristic equation are termed eigenvalues of system matrix A. Information for system stability characteristics can be obtained from the analysis of eigenproperties of state matrix. The small-signal stability study is to analyze the root

locus of eigenvalues of state matrix. If one of the eigenvalues enters the right-half plane, the system is defined as unstable. The root locus for the largest eigenvalue will be observed to determine the trend of system stability.

5.2 REFERENCE SYSTEM MODEL FOR SMALL-SIGNAL STABILITY STUDY

The reference system for small-signal stability is the two-generator system as shown in Figure 4.2 of Chapter 4. The generator model adopted in this analysis is a two-axis model [24][27]:

$$\begin{cases} T'_{q0i}\dot{E'_{di}} = -E'_{di} - \left(x_{qi} - x'_i\right)I_{qi} \\ T'_{d0i}\dot{E'_{qi}} = E_{FDi} - E'_{qi} + (x_{di} - x'_i)I_{di} \\ \tau_i\dot{\omega_i} = T_{mi} - \left(I_{di}E'_{di} + I_{qi}E'_{qi}\right) - K_{Di}\omega_i - K_{Si}\delta_i \\ \dot{\delta_i} = \omega_i - 1 \end{cases} \tag{5.10}$$

In this model, T_m is a system input. The governor model was not included under the consideration that during the small-disturbance period, the slow governor will not respond fast enough to affect the output of the generator. The detailed excitation system model which includes Automatic Voltage Regulator (AVR) and Power System Stabilizer (PSS) were not included in the generator model. Fixed values for K_D (damping torque coefficient) and K_S (synchronizing torque coefficient) were used to represent the effect of the exciter and PSS. There are two reasons for doing so. The exciter contributes a certain amount of K_S to system small-signal stability depending on its parameters, which helps improve transient stability, especially for exciters with high ceiling voltage and fast-response AVR [24]. But it also brings negative impact on damping torque by applying the high gain in the AVR. The PSS was introduced dated back in the 1950s and it was proposed to address this problem: to bring more damping to power systems. In real application, PSS's structure and parameters

are tuned according to the specific parameters of the exciter and the generator. In this study, in order to represent as many cases as possible and to make the results more general without limiting to a certain structure and parameters of exciter and PSS, we assume that for different generators and system parameters, the exciter and PSS pose the same effect on small-signal stability. Therefore, the values of K_D and K_S were incorporated in the generator model, rather than using the models for the exciter and PSS. The process for deriving state-space equation and the system base parameters are documented in Appendix A. The final system state-space equations, the state variables, and system inputs are shown in below.

$$\dot{\boldsymbol{X}} = \boldsymbol{AX} + \boldsymbol{BY} \tag{5.11}$$

$$\boldsymbol{X} = \begin{bmatrix} \Delta \mathrm{E}'_{d1} \\ \Delta \mathrm{E}'_{q1} \\ \Delta\omega_1 \\ \Delta \mathrm{E}'_{d2} \\ \Delta \mathrm{E}'_{q2} \\ \Delta\omega_2 \\ \Delta\delta_1 \\ \Delta\delta_2 \end{bmatrix} \tag{5.12}$$

$$\boldsymbol{Y} = \begin{bmatrix} 0 \\ \Delta E_{FD1} \\ \Delta T_{m1} \\ 0 \\ \Delta E_{FD2} \\ \Delta T_{m2} \\ 0 \\ 0 \end{bmatrix} \tag{5.13}$$

5.3 SENSITIVITY TESTS

Before assessing the small-signal stability, initial operating points were obtained by power flow analysis. Then system stability was evaluated by analyzing eigenvalues of system state matrix. Numerous tests have been carried out for investigating the sensitivity

of system stability to each system parameter. Some of the parameters show little to no influence on system stability. Some of the parameters appear to affect the system stability in similar patterns. Thus, this section will only cover some significant results instead of introducing every single test. Among all parameters, it is found that the synchronizing torque and damping torque coefficients exert the most significant effect on system small-signal stability. Twenty percent change in those coefficients may trigger fifty percent change in stability region while one hundred percent change in other parameters such as generator reactance may only bring changes of less than three percent. In this section, the sensitivity of other important system parameters will also be discussed, including generator inertia constant, the ratio of power ratings of two generators, and cable length. The test range of frequency is from 60 Hz to 6000 Hz. 3D figures will be used to demonstrate stability region.

5.3.1 Sensitivity of System Stability to Synchronizing Torque Coefficient (K_S) and Damping Torque Coefficient (K_D)

Figure 5.1 shows the stability boundary for the systems with frequency in the range of 60 Hz to 6000 Hz, and both K_S and K_D in the range of 0 to 5. Both generators have the same K_S and K_D in their rotor angle equations. The color on the stability boundary indicates the frequency where the system becomes unstable. It could be learned that only if K_S is larger than a certain value (it is in the vicinity of 1 in this figure), the reference system starts to become stable. Figure 5.2 to Figure 5.4 shows the details of different cross-sections in Figure 5.1 to help better understand the impact of frequency, K_D, and K_S. Figure 5.2 indicates that the boundary between unstable and stable regions moves to the right and the stable region shrinks from 68.8% to 45.6% as frequency increases from 60 Hz to 3000 Hz. Figure 5.3 discusses the impact of K_D. It could be seen that larger K_D results in larger stable region.

For systems at higher frequencies, they could only maintain stability while K_D reaches a certain value. Figure 5.4 shows a similar picture for the impact of K_S: larger K_S allows higher frequency systems to be stable and generates more stable regions.

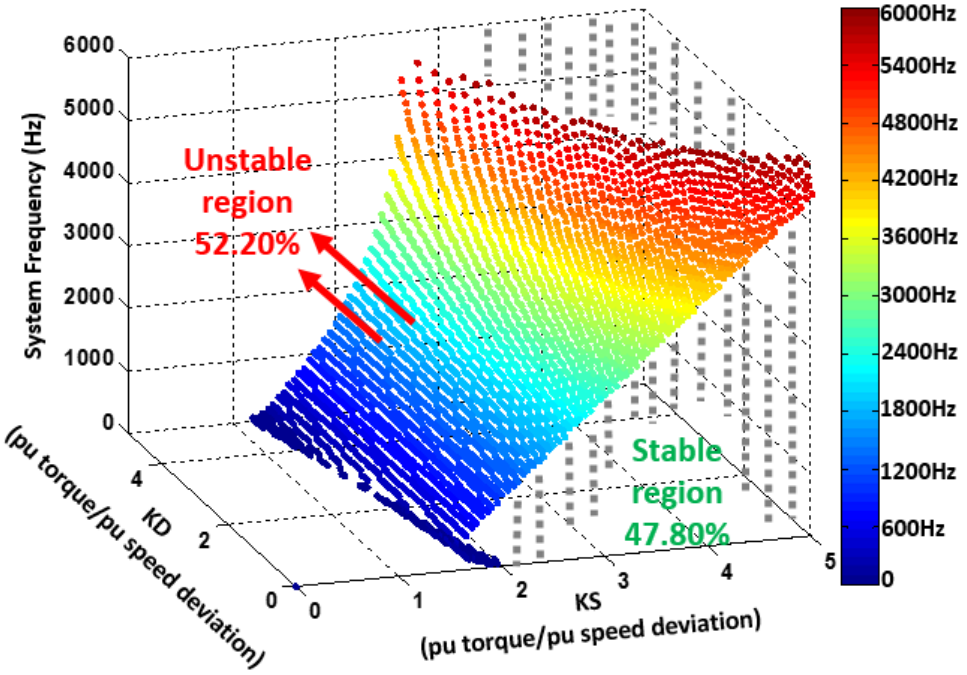

Figure 5.1 Stable and unstable regions with frequency, K_D, and K_S varying for the reference system with base parameters

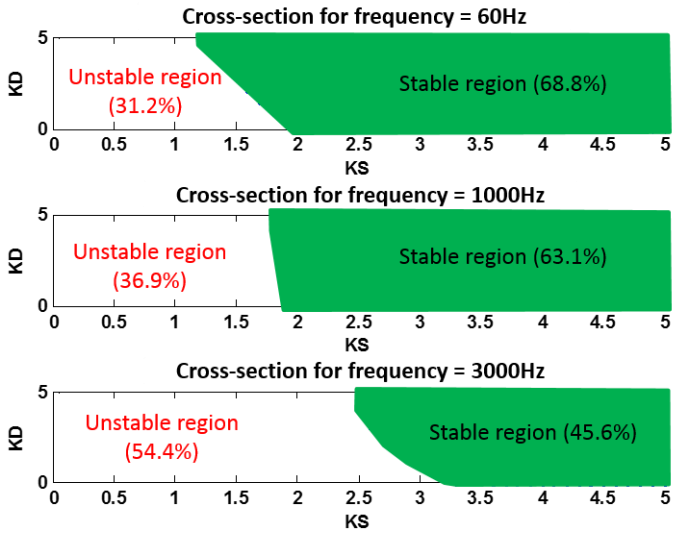

Figure 5.2 Three cross-sections in Figure 5.1: K_S vs K_D for different frequencies

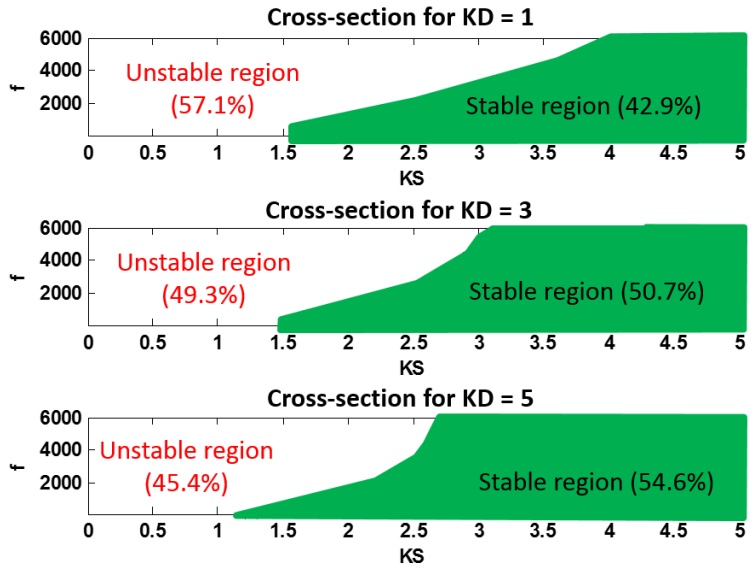

Figure 5.3 Three cross-sections in Figure 5.1: K_S vs. frequency for different K_Ds

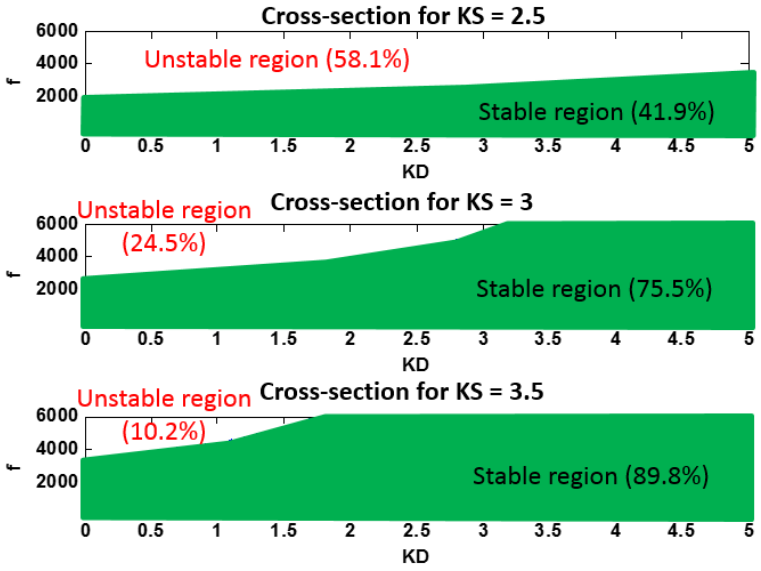

Figure 5.4 Three cross-sections in Figure 5.1: K_D vs. frequency for different K_Ss

The improvement from K_S and K_D on system small-signal stability could be explained by using the concept of participation factor [24] [33]. Let us pick some points out of Figure 5.1 to start the discussion. Figure 5.5 plots the root locus of the largest eigenvalues (7^{th} and 8^{th} in this case) when system frequency increases from 60 Hz to 6000 Hz. For plotting this figure, K_S and K_D are chosen as 2.5 and 0.375 correspondingly and the other parameters are

the base ones listed in Appendix A. It can be learned that these two complex eigenvalues pass through imaginary axis at the frequency of 1920 Hz and the system starts to become unstable after that. Figure 5.6 shows the participation factors associated with the two eigenvalues mentioned above. Each subplot presents the information about the contribution from eight state variables to this mode. Each column in the subplot stands for the change of the participation factor of a state variable in this mode. The higher value of the participation factor, the larger the contribution from the corresponding state variable. The color represents the movement of the participation factor when frequency moves from 60 Hz to 6000 Hz – starts from black, travels at blue, and ends at red. For example, the 6^{th} column in the first subplot represents the participation factor of the 6^{th} state variable (the speed of Generator 2) in the 7^{th} mode (the top eigenvalue in Figure 5.5). At the beginning, its contribution from the 6th state variable is very little (close to 0). But as frequency increases, it starts to contribute to majority of that oscillatory mode (ends at 0.8), especially at the frequency where the system becomes unstable. The same trend could be obtained from the 8^{th} column (the rotor angle of Generator 2) in the first subplot. Therefore, this oscillatory mode can be called as "Generator 2 rotor angle" mode. The stability can be improved by adding more damping and synchronizing torque to Generator 2. The stability of the reference system at frequency higher than 1920 Hz will be restored if this oscillatory mode can be damped out effectively.

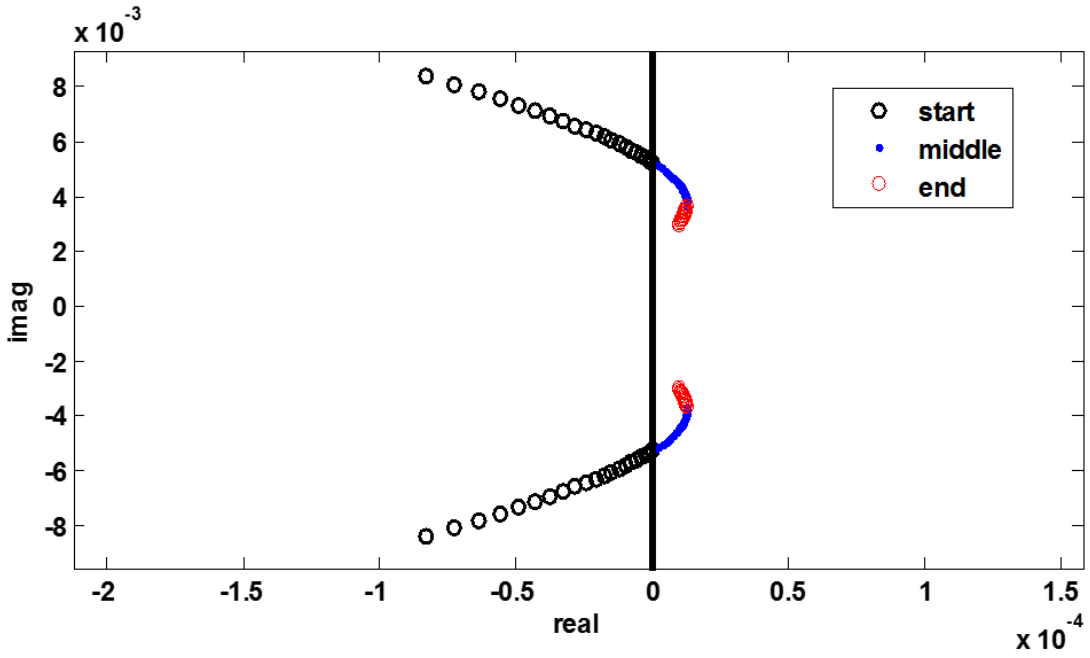

Figure 5.5 Rootlocus for largest eigenvalue (7th and 8th in this case)

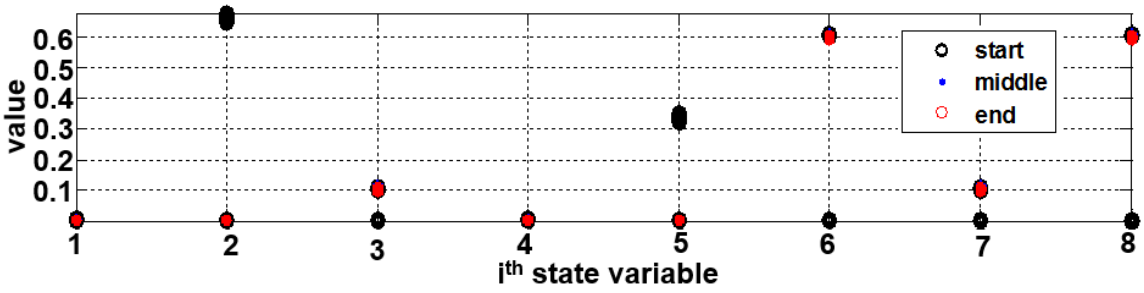

(a) Participation factors of eight state variables corresponding to the 7th Eigenvalue

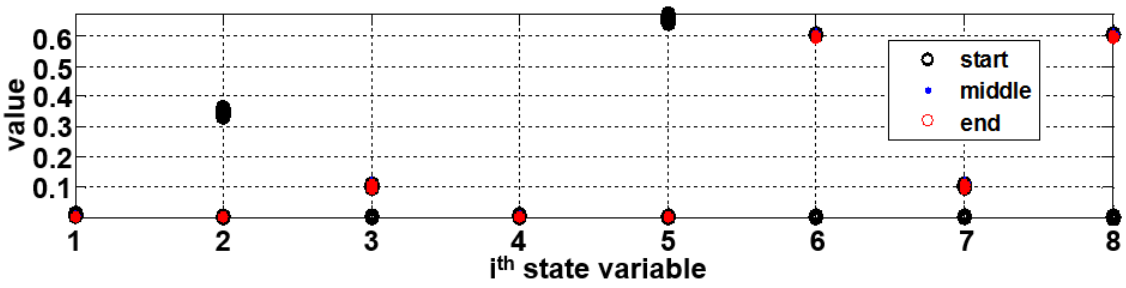

(b) Participation factors of eight state variables corresponding to the 8th Eigenvalue

Figure 5.6 Participation factors associated with largest eigenvalues (7th and 8th)

Four measures have been tried to improve the small-signal stability for systems at high frequencies: increasing K_{D2}, K_{S2}, K_{D1}, and K_{S1}. Note that, in Figure 5.6, although the 3rd (the speed of Generator 1) and 7th (the rotor angle of Generator 1) state variables participate significantly less than in this oscillatory mode, increasing K_{S1} and K_{D1} may also be effective solutions because they will help damp out system oscillation to some extent.

Figure 5.7 shows the root locus of the oscillatory complex eigenvalues which cause instability (shown in Figure 5.5) after we increase the K_{S2} by 200%. The trend is the same as before – as frequency increases, eigenvalues move towards the imaginary axis. But at this time the system maintains stable within the investigated frequency range (60~6000 Hz) due to the larger synchronizing torque coefficient.

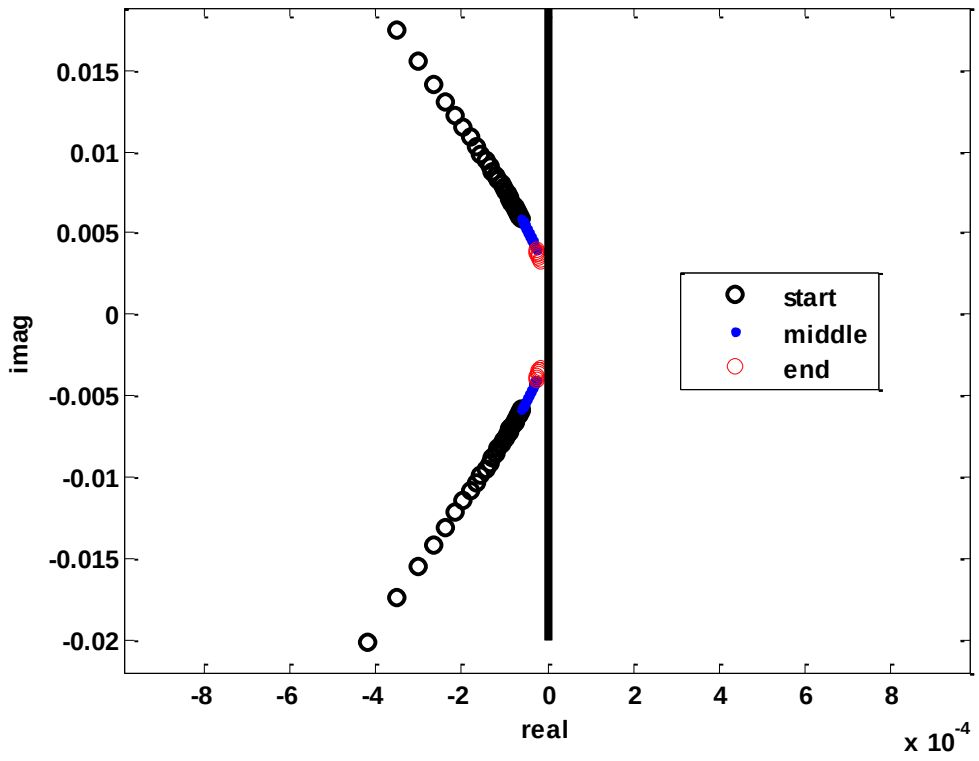

Figure 5.7 Root locus of 7th and 8th Eigenvalues for the case that the K_{S2} increase by 200%

The second test was to increase K_{D2} by 200% to see whether it will help improve stability. As shown in Figure 5.8, the root locus of the largest eigenvalues associated with the "Generator 2 rotor angle" mode does not change too much from Figure 5.5, except the fact that the stability boundary is pushed a little further from 1920 Hz to 2040 Hz. Increasing K_{D2} in this case does not improve stability significantly.

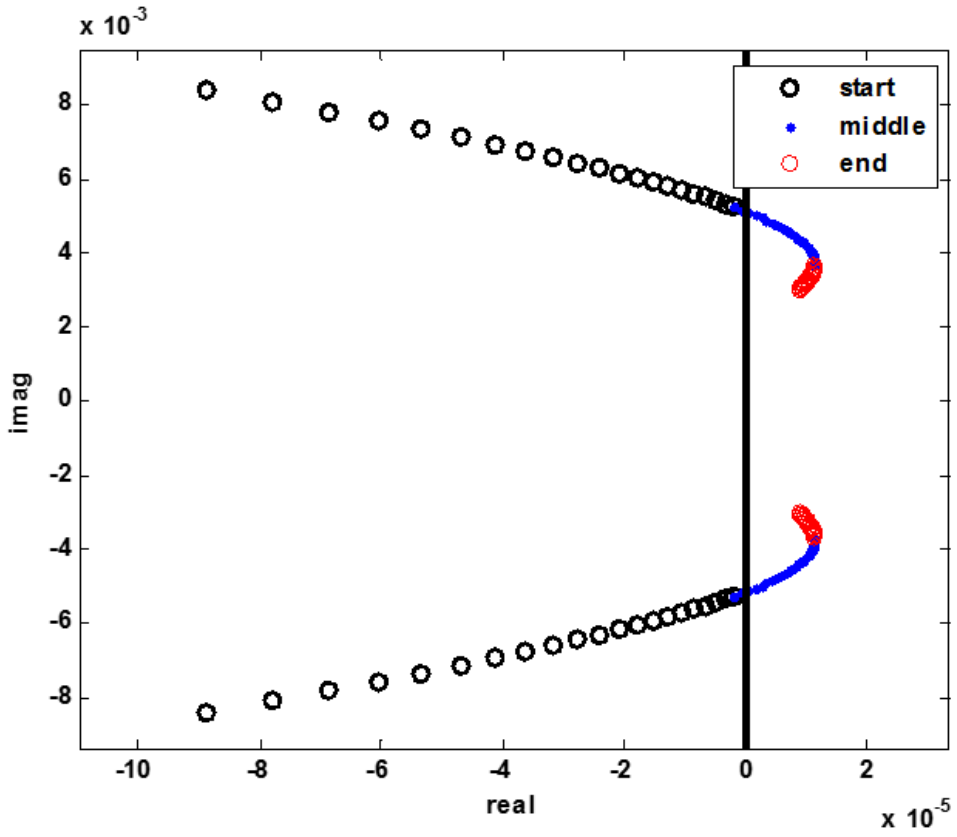

Figure 5.8 Root locus of 7th and 8th Eigenvalues for the case that the K_{D2} increase by 200%

The effect of increasing K_{S1} is shown in Figure 5.9. This measure is more helpful than K_{D2} but not as effective as increasing K_{S2}. It successfully defers the stability boundary from 1920 Hz to 4620 Hz.

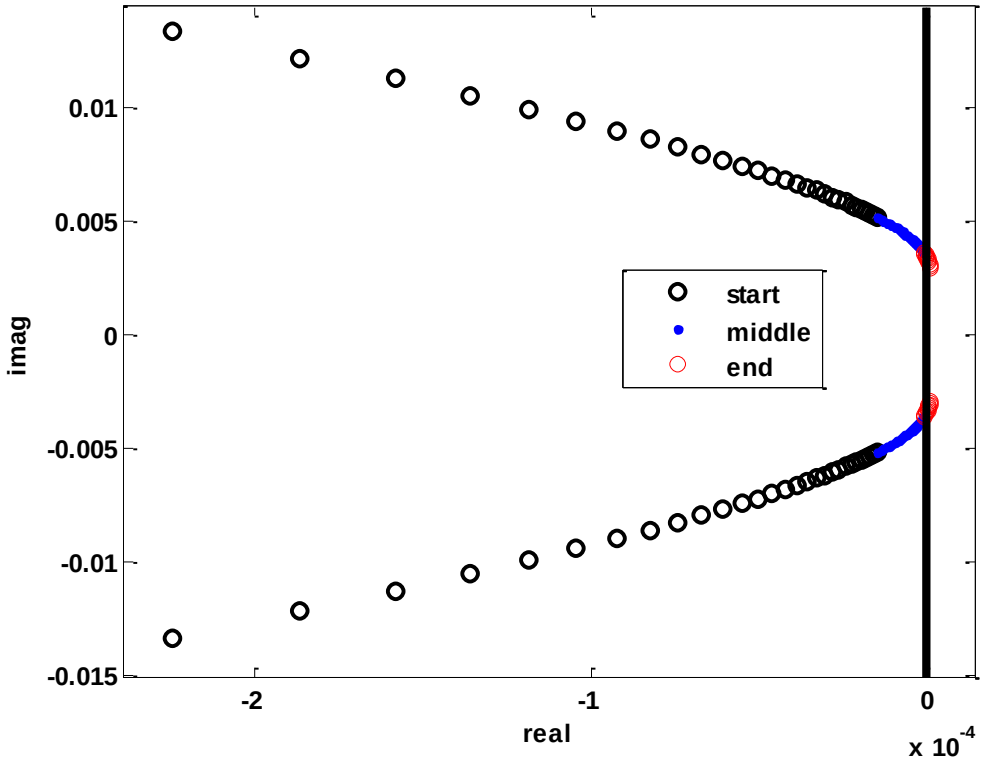

Figure 5.9 Root locus of 7th and 8th Eigenvalues for the case that the K_{S1} increase by 200%

Figure 5.10 shows the result of increasing K_{D1} by 200%. There is no improvement observed. Stability boundary is still the same as the original case, as shown in Figure 5.5.

In general, increasing K_S of either generator helps improve system stability. But increasing K_D is not an effective method in this case. It should be also noted that even if the newly-grown stable HFAC systems are "saved" by the larger K_S, as the red dots shown in Figure 5.7 and Figure 5.9, they may still not be stable enough to successfully sustain through certain disturbances because their eigenvalues are too close to the imaginary axis.

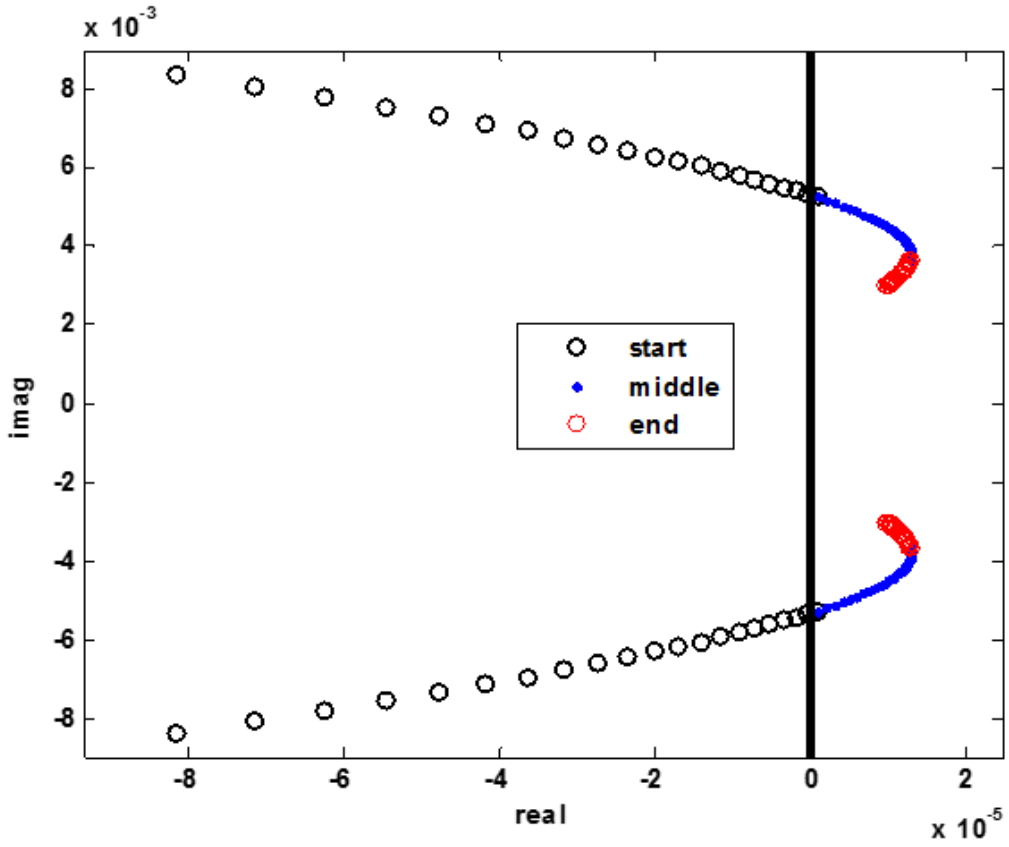

Figure 5.10 Root locus of 7th and 8th Eigenvalues for the case that the K_{D1} increase to 200%

5.3.2 Sensitivity of System Stability to the Ratio of Power Ratings of Two Generators

In this section we tested the sensitivity of system stability to the ratio of power ratings of two generators. 3D figures were drawn for four cases when the ratio drops from 9:1 (the base case plotted in Figure 5.1) to 6:1, 3:1, 1.5:1 and 1:1, as shown in Figure 5.11, Figure 5.12, Figure 5.14, and Figure 5.14 correspondingly. Comparing Figure 5.1, Figure 5.11, and Figure 5.12, it can be observed that stable regions do not change too much for the cases of 9:1 (stable region = 47.80%), 6:1 (44.81%) and 3:1 (46.35%). But when the ratio gets close to 1:1, the stable region increases dramatically to 76.45% and more stable region starts to appear especially in high frequency area, as shown in Figure 5.14. It can be learned that in

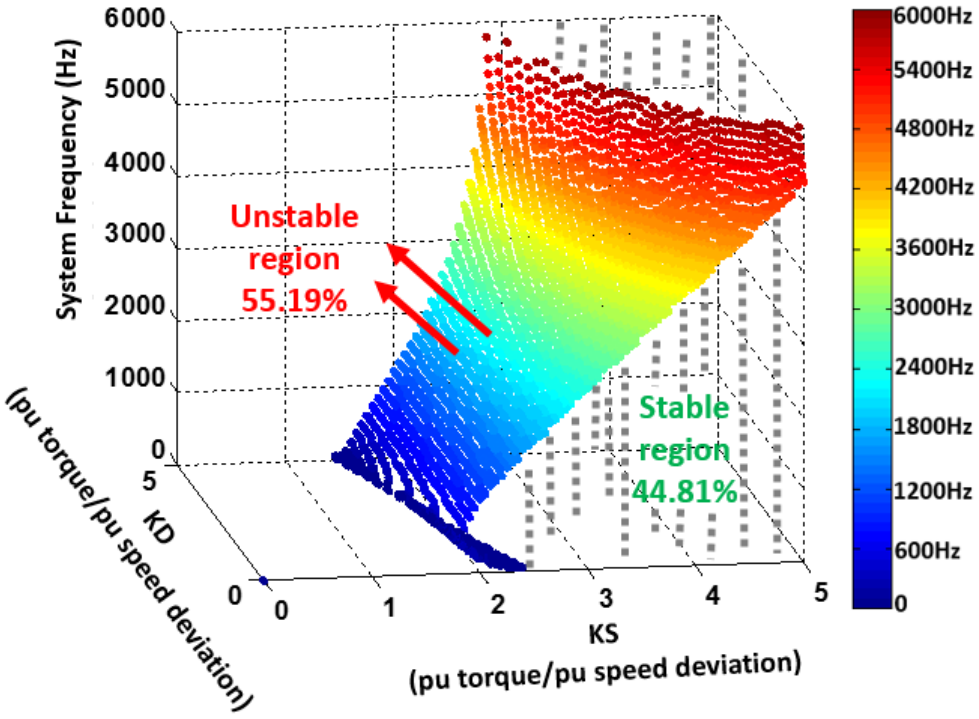

Figure 5.11 Ratio of power ratings of two generators is 6:1

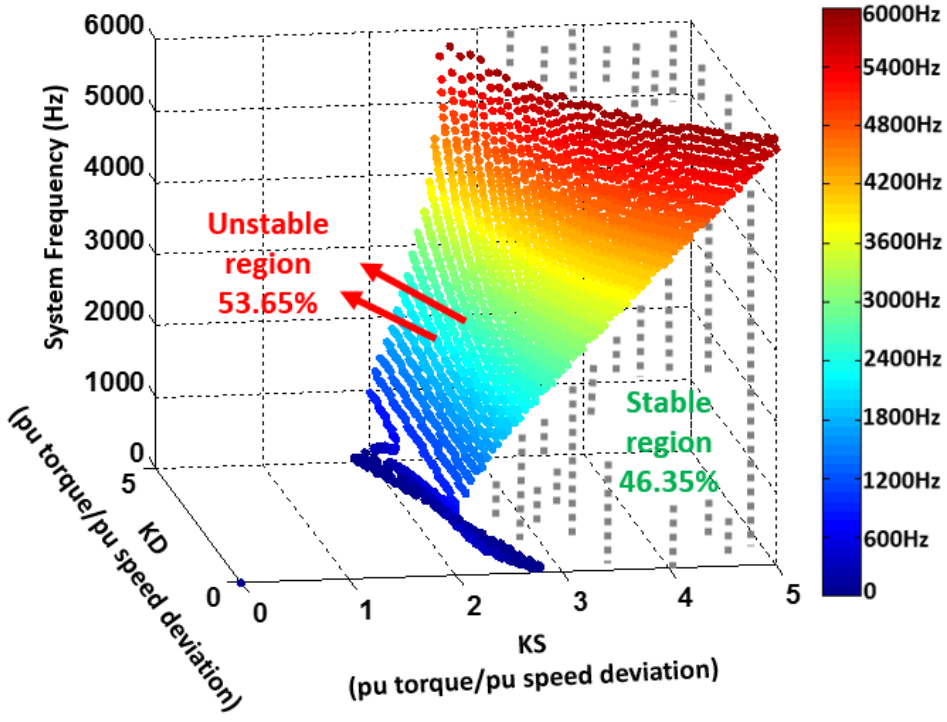

Figure 5.12 Ratio of power ratings of two generators is 3:1

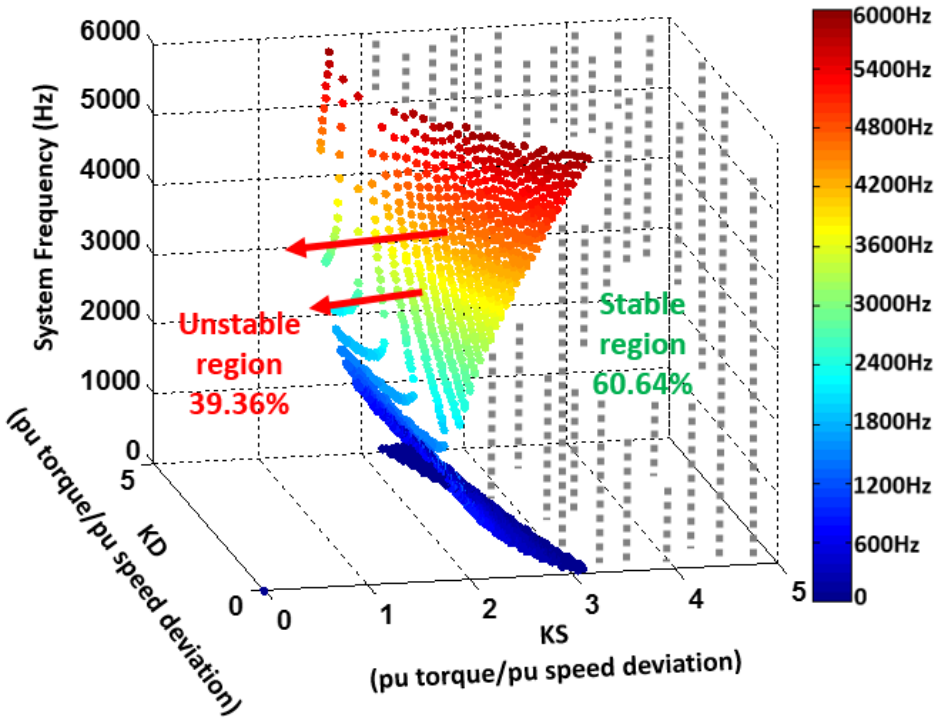

Figure 5.13 Ratio of power ratings of two generators is 1.5:1

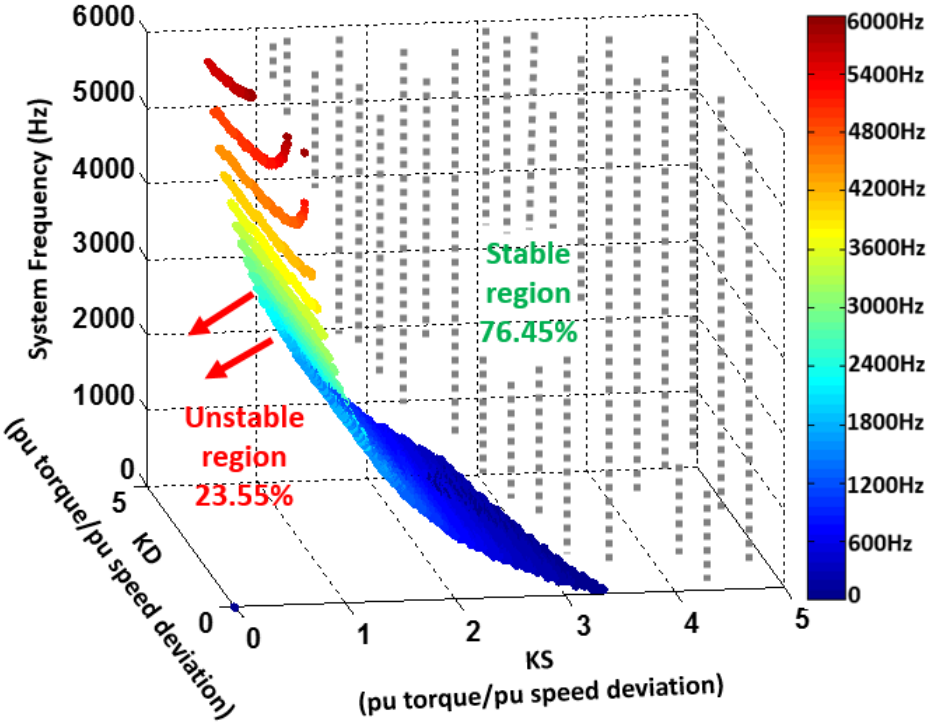

Figure 5.14 Ratio of power ratings of two generators is 1:1, stable region increases dramatically

terms of small-signal stability, HFAC systems are in favor of generators with similar power ratings.

5.3.3 Sensitivity of System Stability to Inertia Constant

This section studies the sensitivity of system stability to generator inertia constant (*H*). The previous section has concluded that K_D and K_S are very important parameters affecting system small-signal stability. In this section, one axis of Figure 5.1 (K_D or K_S) will be replaced by "*scaleH"* to study the impact of *H*s. "*scaleH*" means to scale *H*s of both generators by the same percentage simultaneously. The test results are shown in Figure 5.15 and Figure 5.16. In both figures, the axis of *scaleH* ranges from 10% to 200% with the base values of *H*s of two generators listed in Appendix A. In order to better understand the 3D figures, Figure 5.17 and Figure 5.18 are plotted to expand the cross-sections in Figure 5.15 and Figure 5.16 correspondingly. One apparent observation based on the two figures is that the stable region shrinks as the values of *H*s of both generators (*scaleH*) increase. Higher frequency systems, such as those above 4000 Hz, tend to become unstable as the value of *H*s double. This founding matches with the small-signal stability characteristics of one-machine-infinite-bus system where the eigenvalue analysis shows that the oscillatory roots of the swing equation move toward the imaginary axis as the *H* increases [22]. The other conclusion that can be drawn from these two figures is that the stability of higher frequency systems is subject to change more easily while lower frequency systems can maintain stability with a wider range of parameters.

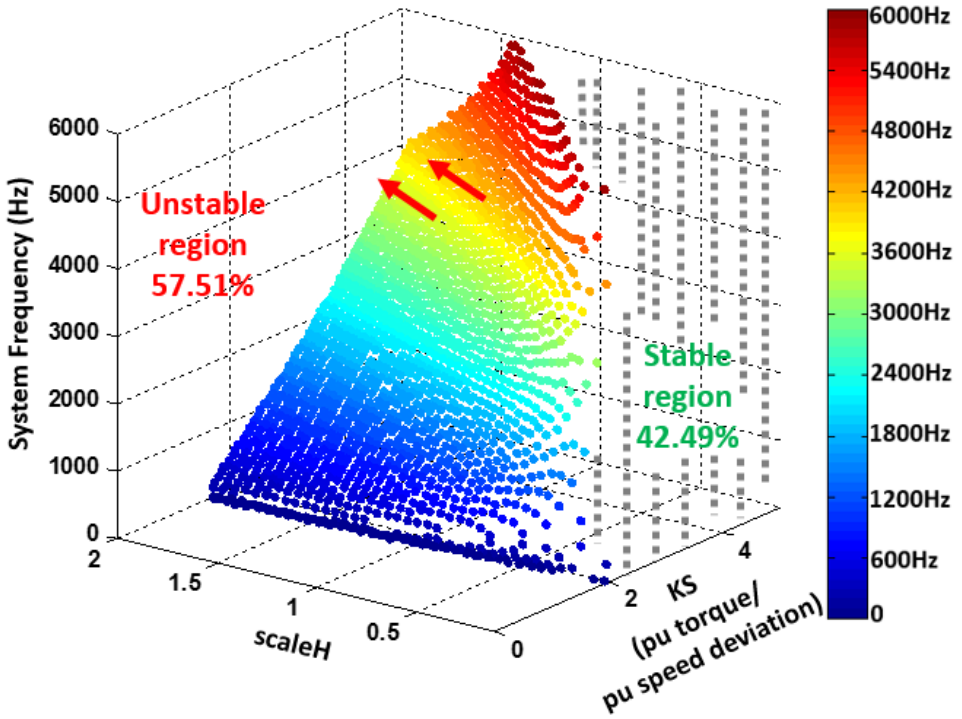

Figure 5.15 *scaleH* vs. K_S vs. *f* with base parameter

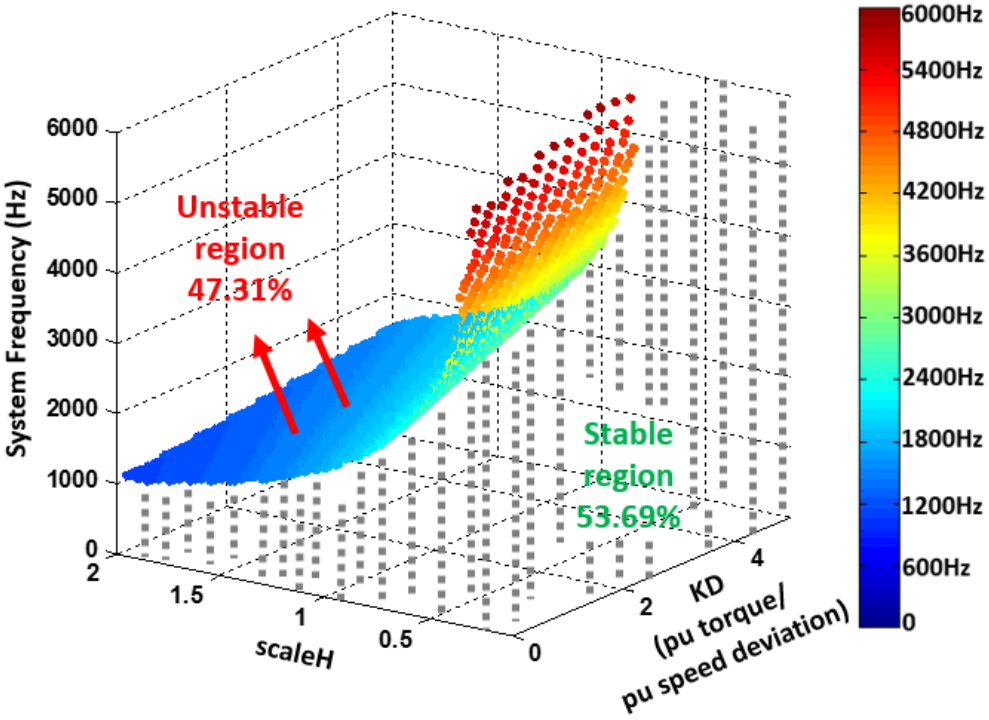

Figure 5.16 *scaleH* vs. K_D vs. *f*, with base parameters and K_S = 2.5

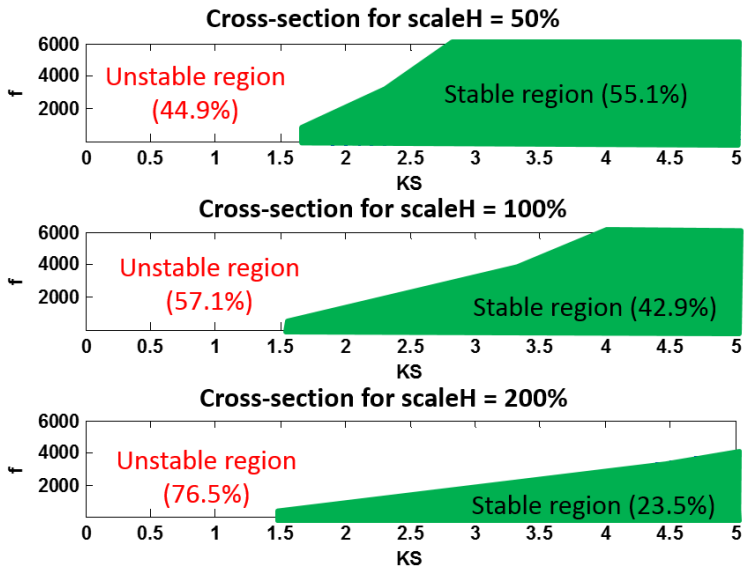

Figure 5.17 Three cross-sections in Figure 5.15: K_S vs. f for different values of *scaleH*

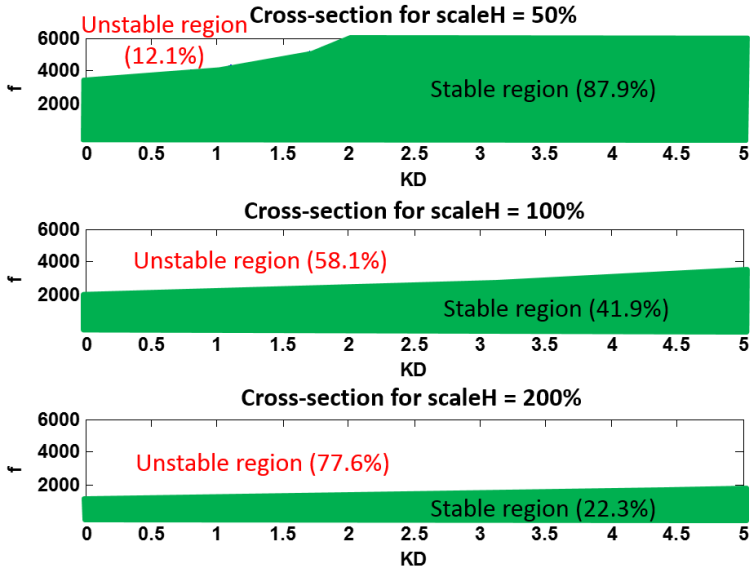

Figure 5.18 Three cross-sections in Figure 5.16: K_D vs. f for different values of *scaleH*

Two more 3D figures, Figure 5.19 and Figure 5.20, are plotted to prove this trend. They compare the stable regions when *scaleH*s are 50% and 200%. It can be concluded that larger *H*s of both generators push the stability boundary to the right resulting in a smaller stable region.

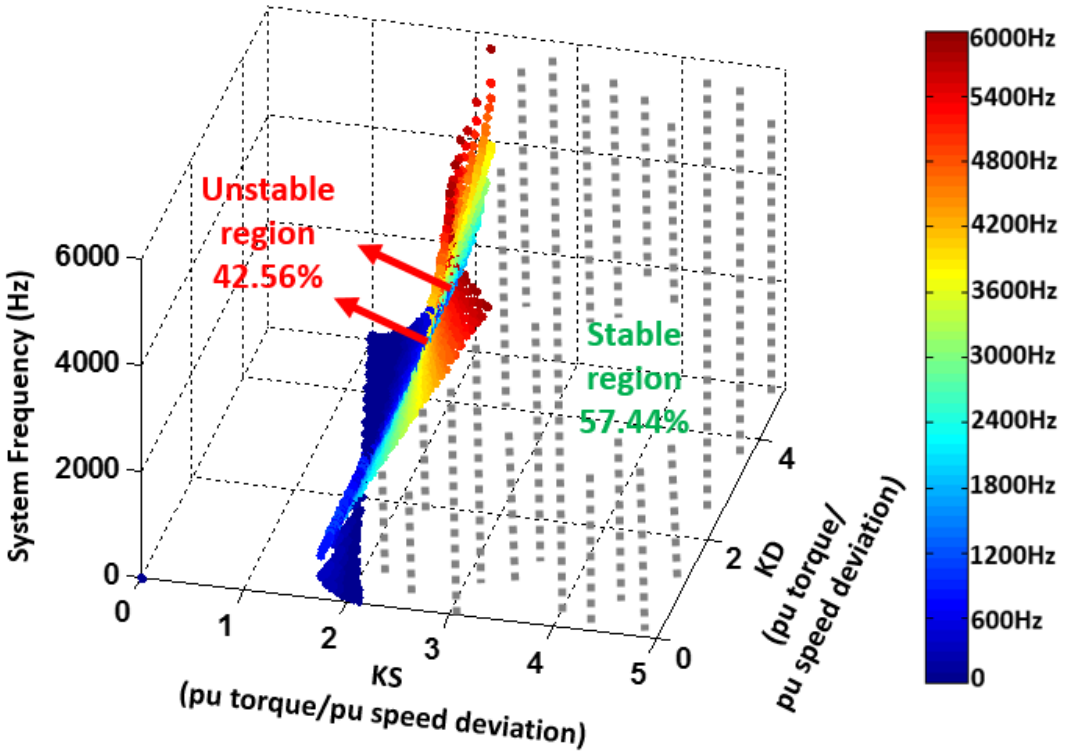

Figure 5.19 K_S vs. K_D vs. f with *scaleH*=50%

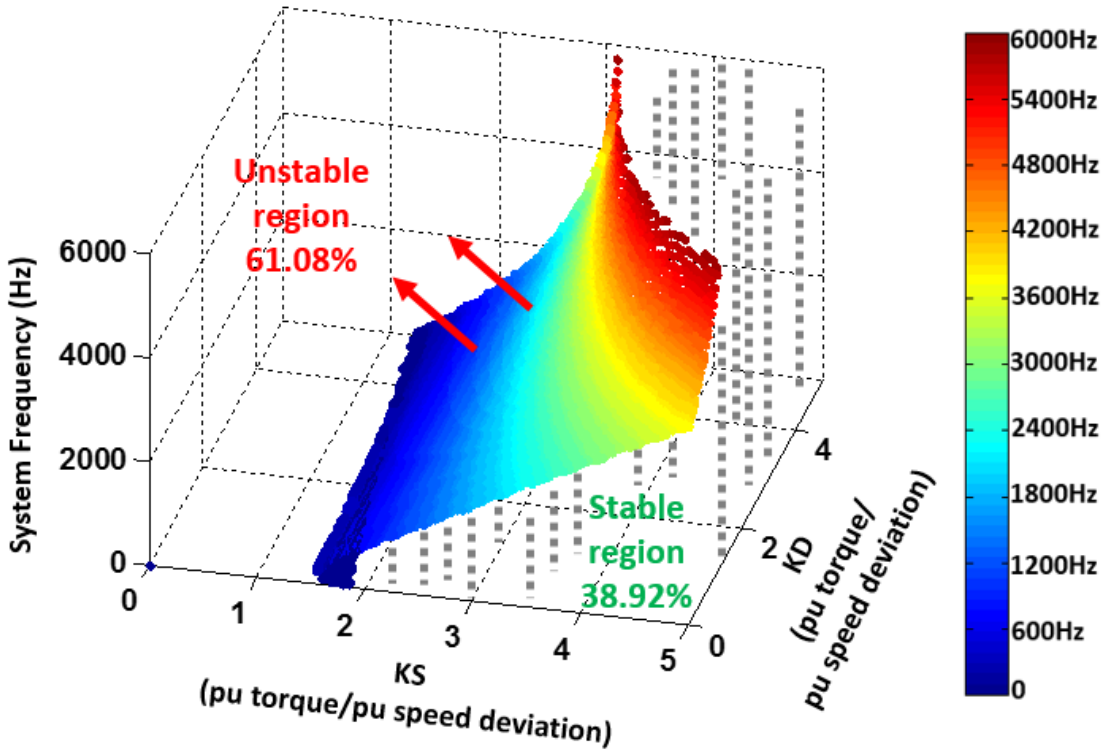

Figure 5.20 K_S vs. K_D vs. f with *scaleH*=200%

5.3.4 Sensitivity of System Stability to Cable Length

Sensitivity of system stability to cable length will be discussed in this section. The test results are shown in Figure 5.21 and Figure 5.22. Figure 5.21 shows the stable region when cable lengths between two generators and the Point-of-Common-Coupling (PCC) are 40 m and 30 m while in Figure 5.22 those lengths are 100 times longer – 4000 m and 3000 m. The reason that we do not extend the cable length any longer is the following. In our reference system, reactive impedance of cable dominates the overall cable impedance at high frequency since it is proportional to system frequency. Therefore, the voltage drop over the cable becomes very significant at high frequency. According to our tests when frequency reaches 6000 Hz and the cable lengths between generators and PCC are longer than 4000 m and 3000 m, the generator excitation system will no longer be able to maintain rated voltage

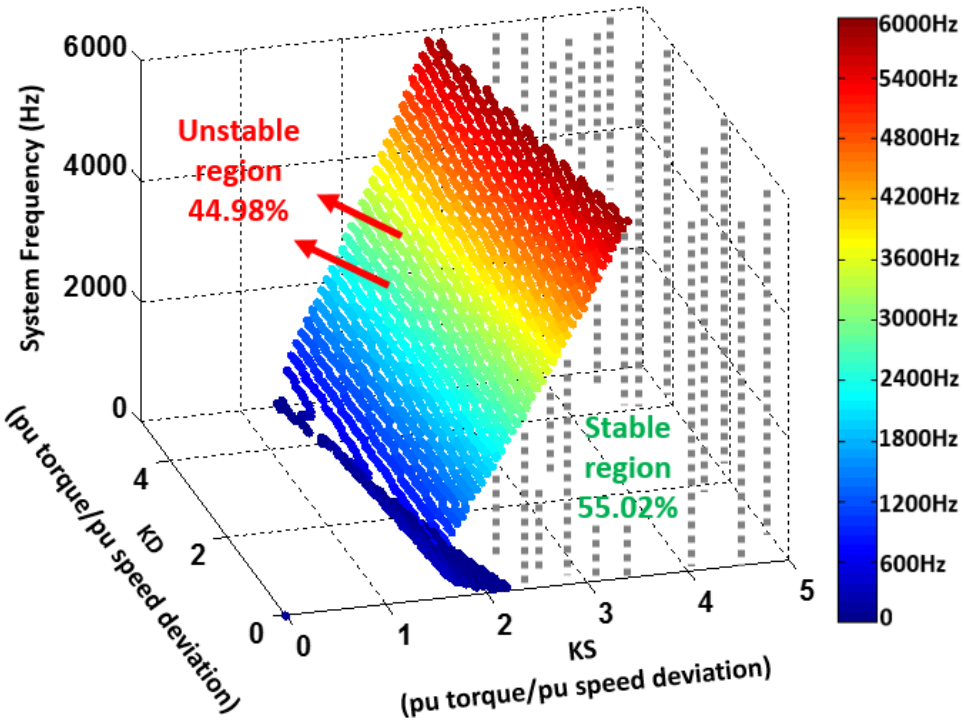

Figure 5.21 Cable lengths between generators and Point-of-Common-Coupling are 40 m and 30 m

at PCC, assuming the help of other voltage supporting equipment is unavailable. Comparing Figure 5.21 and Figure 5.22, the stable region drops from 55.02% to 47.8%. Most of the areas that change from "stable" to "unstable" are at high frequency.

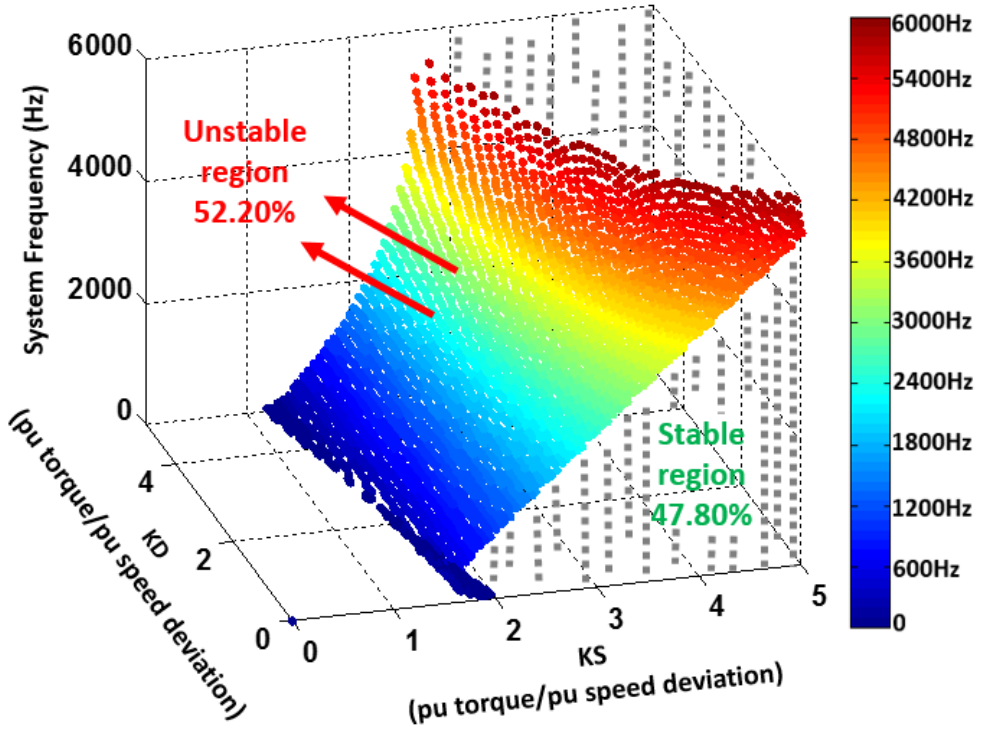

Figure 5.22 Cable length between generators and Point-of-Common-Coupling are 4000 m and 3000 m

5.3.5 Analysis

Based on the previous tests, for the reference system with base parameters, K_D and K_S are proved to be significant to determine whether the system can maintain small-signal stability. The stability boundary is drawn in Figure 5.1.

With system parameters changing, the shape of stability boundary may change. Most changes occur in systems with higher frequencies which means higher frequency systems are more sensitive and dependent on system parameters. Meanwhile, HFAC systems in

those newly-grown stable areas may not be stable enough to successfully sustain through small disturbances because their eigenvalues are still too close to the imaginary axis.

5.4 SUMMARY

Following the previous chapter, this chapter analyzed the other important aspect of rotor angle stability: small-signal stability. Eigenanalysis was the method deployed to study the small-signal stability of HFAC systems. The two-axis model of generators were utilized to establish system state equation. Four sensitivity analyses discussing the impact of system key parameters were presented. Lots of 3D figures were drawn to aid the analysis.

Chapter 6

CONCLUSION AND FUTURE WORK

6.1 CONCLUSION

This work discovered the frequency limit in HFAC systems and examined the impact of increasing system frequency on the rotor angle stability of HFAC systems.

First, we derived the trend lines for defining the feasibility area of high frequency generators, and for scaling power density against frequency. An equation for quick estimating inertia constants of high frequency generators was derived which allows the system engineers to study system stability without having extensive knowledge of generator design. The inertia constants of high frequency generators were found to be less than two-second easily which may potentially threaten system stability.

Rotor angle stability concerning that if multiple generators with different sizes can operate in synchronism is critical to HFAC systems. In this research the analysis for rotor angle stability of HFAC systems covered both large-signal (transient) stability and small-signal stability. Discovered trends from both categories of power system stability showed that increasing frequency deteriorates stability of HFAC systems.

Fundamental analysis found the mathematical relation between Critical Clearing Time (CCT) and system parameters, such as system frequency, inertia constants, and the ratio of inertia constants of different generators. It was found that higher frequency, lower inertia constants, and generators with much different inertia constants tend to shorten CCT, which

leave less time for circuit protection devices to identify the fault and intervene. The frequency limit can be calculated based on the CCT and the speed of protection devices. The findings from fundamental analysis were proved by transient stability analysis.

Transient stability analysis, studied via extensive simulation tests that covered many scenarios, revealed that micro-grids with low inertia constants are potentially more unstable than normal 60 Hz systems, and the problem worsens as frequency increases. Rotor angle exceeds the critical value faster in HFAC systems. The simulation results also suggested that when building HFAC systems, it is desirable to avoid selecting generators with significantly different inertia constants. Quantified stability indices illustrated that faster circuit breaker whose speed is proportional to system frequency, and faster excitation control systems are powerful tools for improving transient stability of HFAC systems.

As another critical aspect of stability of HFAC systems, small signal stability was investigated by analyzing the eigen-properties of system state-space equation. Compared to normal 60 Hz power systems, HFAC systems appear to have much stronger dependency on system key parameters including synchronizing torque coefficient, damping torque coefficient, inertia constants, and cable length. The higher the frequency, the stronger the dependency. The systems within a few hundred Hz are much less sensitive than those at a few thousand Hz. Increasing inertia constants which benefits transient stability tends to worsen small-signal stability, especially at higher frequency. The range of system parameters to ensure stable operation of HFAC systems is much narrower than normal 60 Hz system. The requirement for accurate tuning of system controllers such as AVR and PSS is much more critical.

In order to successfully implement HFAC systems, the following issues are suggested to address beforehand:

- Development of fast circuit breakers that can operate at speeds proportional to system frequency
- Extremely careful tuning of AVR and PSS to ensure adequate synchronizing torque and damping torque over the complete system operation range
- Avoid using generators with much different inertia constants
- Protection coordination systems need to be designed carefully to ensure timely intervene to faults in every location of the system

6.2 FUTURE WORK

This work discovered that the frequency limit of HFAC systems comes from the opening times of protection devices. Future work may take into account certain types of popular circuit breakers, such as SF6 and vacuum circuit breakers. Discussion based on the principle of these circuit breakers to derive the potential relation between the circuit breaker characteristics and frequency limit of HFAC systems may be valuable.

In this work, the small-signal stability of HFAC systems was studied based on a two-machine system. Future work may consider to study a larger scale HFAC system. More useful trends may be revealed by such a study.

REFERENCES

[1] I. Takahashi and G. J. Su, "A 500Hz power system - power converter and transmission lines," in *Proc. 1989 Industry Applications Society Annual Meeting*, San Diego, CA, Oct. 1989, pp. 988-995.

[2] I. Takahashi and G. J. Su, "A 500Hz power system – applications," in *Proc. 1989 Industry Applications Society Annual Meeting*, San Diego, CA, Oct. 1989, pp. 996-1002.

[3] R. Strzelecki, *Power Electronics in Smart Electrical Energy Network*. New York, NY: Springer-Verlag Inc., 2008.

[4] N. Doerry. (2007, Nov.). Next generation integrated power system: NGIPS technology development road map. Available: http://www.doerry.org/norbert/papers/090106usna-ngips-final.pdf

[5] S. C. LaGrone, M. C. Griggs, and M. Bressani, "Application of a 5500 RPM high speed induction motor and drive in a 7000 HP natural gas compressor installation," in *Proc. 1992 Petroleum and Chemical Industry Conference*, San Antonio, TX, Sep. 1992, pp. 141-146.

[6] I. G. Hansen, "Status of 20kHz space station power distribution technology," NASA Technical Memorandum, 1988.

[7] A. F. Forestieri and C. R. Baraona, "Space station power system," *IEEE Trans. on Aerospace and Electronic Systems*, vol. AES-20, no. 6, pp. 666-671, Nov. 1984.

[8] A. Tessarolo, G. Zocco, and C. Tonello, "Design and Testing of a 45-MW 100-Hz Quadruple-Star Synchronous Motor for a Liquefied Natural Gas Turbo-Compressor Drive," *IEEE Trans. on Industry Applications*, vol. 47, no. 3, pp. 1210-1219, May/Jun. 2011.

[9] K. John. (2013). Electric Ship Office. Naval power systems technology development roadmap PMS 320.

[10] J. Langstone, M. Steurer, J. Crider, S. Sudhoff, Y. Lee, E. Zivi, R. Dougal, Y. Zhang, R. Hebner, and A. Ouroua, "Waveform-level time-domain simulation comparison study of three shipboard power system architectures," in *Proc. 2012 Summer Computer Simulation Conference*, Genoa, Italy, 2012.

[11] P. K. Sood and T. A. Lipo, "Power conversion distribution system using a high-frequency ac link," *IEEE Trans. on Industry Applications*, vol. 24, no. 2, pp. 288-300, Mar/Apr. 1988.

[12] R. T. Leskovich and I. G. Hansen, "The effects of nonlinear loading upon the space station freedom 20kHz power system," in *Proc. 1989 Intersociety Energy Conversion Engineering Conference*, Washington, DC, Aug. 1989, pp. 555-560.

[13] A. F. Forestieri and C. R. Baraona, "Space station power system," *IEEE Trans. on Aerospace and Electronic Systems*, vol. AES-20, no. 6, pp. 666-671, Nov. 1984.

[14] S. Chakraborty and M. G. Simoes, "Advanced active filtering in a single phase high frequency ac microgrid," in *Proc. IEEE 36th Power Electronics Specialists Conference*, Recife, Brazil, Jun. 2005, pp. 191-197.

[15] J. M. Correa, S. chakraborty, M. G. Simoes, and F. A. Farret, "A single phase high frequency ac microgrid with an unified power quality conditioner," in *Proc. 2003 Industry Applications Conference*, Oct. 2003, pp. 956-962.

[16] S. Chakraborty, M. D. Weiss, and M. G. Simoes, "Distributed intelligent energy management system for a single-phase high-frequency ac microgrid," *IEEE Trans. on Industrial Electronics*, vol. 54, no. 1, pp. 97-109, Feb. 2007.

[17] J. H. Beno, R. E. Hebner, and A. Ouroua, "High-frequency power generation and distribution in multi-megawatt power systems," in *Proc. 2011 Electric Ship Technologies Symposium*, Alexandria, VA, Apr. 2011, pp. 84-89.

[18] R. M. Calfo, J. A. Fulmer, and J. E. Tessaro, "Generators for use in electric marine ship propulsion systems," in *Proc. 2002 IEEE Power Engineering Society Summer Meeting*, Chicago, IL, Jul. 2002, pp. 254-259.

[19] R. M. Calfo, M. B. Smith, and J. E. Tessaro, "High-speed generators for power-dense, medium-power, gas turbine generator sets," *Naval Engineering Journal*, vol. 119, no. 2, pp. 63-81, Nov. 2007.

[20] R. M. Calfo, G. E. Poole, and J. E. Tessaro, "High frequency ac power system," *Naval Engineering Journal*, vol. 120, no. 4, pp. 45-54, Dec. 2008.

[21] R. M. Calfo, G. E. Poole, and J. E. Tessaro, "Affordability of power density," ASNE Day, 2008.

[22] P. Kundur, *Power System Stability and Control*. New York, NY: McGraw-Hill, 1994.

[23] P. Kundur, J. Paserba, and S. Vitet, "Overview on definition and classification of power system stability," in *Proc. 2003 CIGRE/IEEE PES International Symposium*, Oct. 2003, pp. 1-4.

[24] J. Machowski, J. W. Bialek, and J. R. Bumby, *Power System Dynamics Stability and Control*, 2nd ed. New York, NY: John Wiley & Sons Inc., 2008.

[25] M. A. Pai, *Power System Stability*. New York, NY: North-Holland Publishing Company, 1981.

[26] M. A. Pai, *Energy Function Analysis for Power System Stability*. Boston, MA, Kluwer Academic Publishers, 1989.

[27] P. M. Anderson and A. A. Fouad, *Power System Control and Stability*. Hoboken, NJ: John Wiley & Sons, 2003.

[28] C. P. Steinmetz, "Power control and stability of electric generating stations," *AIEE Trans*., vol. XXXIX, no. 2, pp. 1215-1287, Jul. 1920.

[29] R. D. Evans and R. C. Bergvall, "Experimental analysis of stability and power limitations," *AIEE Trans*., vol. 43, no. 4, pp. 39-58, Apr. 1924.

[30] R. Wilkins, "Practical aspects of system stability," *AIEE Trans*., vol. 45, no. 2, pp. 142-151, Feb. 1926.

[31] R. D. Evans and C. F. Wagner, "Further studies of transmission system stability," *AIEE Trans*., vol. 45, no. 2, pp. 51-80, Feb. 1926.

[32] G. S. Vassell, "Northeast blackout of 1965," *IEEE Power Engineering Review*, vol. 11, no. 1, pp. 4-8, Jan. 1991.

[33] D. Gautam, V. Vittal, and T. Harbour, "Impact of increased penetration of DFIG-based wind turbine generators on transient and small signal stability of power systems," *IEEE Trans. on Power Systems*, vol. 24, No. 3, pp. 1426-1434, Aug. 2009.

[34] S. Dahal, N. Mithulananthan, and T. Saha, "Investigation of small signal stability of a renewable energy based electricity distribution system," in *Proc. 2010 IEEE Power and Energy Society General Meeting*, Minneapolis, MN, Jul. 2010, pp. 1-8.

[35] H. Liu, L. Jin, D. Le, and A. A. Chowdhury, "Impact of high penetration of solar photovoltaic generation on power system small signal stability," in *Proc. 2010 International Conference on Power System Technology*, Oct. 2010, pp. 1-7.

[36] L. Meegahapola and D. Flynn, "Impact on transient and frequency stability for a power system at very high wind penetration," in *Proc. 2010 IEEE Power and Energy Society General Meeting*, Minneapolis, MN, Jul. 2010, pp. 1-8.

[37] Q. Li, "AC system stability analysis and assessment for shipboard power systems," Ph.D. dissertation, Texas A&M University, College Station, TX, 2004.

[38] C. W. Taylor, *Power System Voltage Stability*. New York, NY: McGraw-Hill, 1994.

[39] S. D. Sudhoff, S. F. Glover, S. H. Zak, S. D. Pekarek, E. J. Zivi, D. E. Delisle, and D. Clayton, "Stability analysis methodologies for dc power distribution systems," in *Proc. 13th International Ship Control Systems Symposium*, Orlando, Florida, Apr. 2003.

[40] J. O. Flower and C. G. Hodge, "Stability and transient-behavioral assessment of power-electronics based dc-distribution systems, Part 1:the root-locus technique," in *Proc. 1st WSEAS Int. Sub-Conference on Electroscience and Technology for Naval Engineering and All Electric Ship*, Athens, Greece, Jul. 2004, pp. 13-21.

[41] V. Arcidiacono, A. Monti, and G. Sulligoi, "An innovative generation control system for improving design and stability of shipboard medium-voltage dc integrated power system," in *Proc. 2009 Electric Ship Technologies Symposium*, Baltimore, MD, Apr. 2009, pp. 152-156.

[42] S. Rosado, R. Burgos, F. Wang, and D. Boroyevich, "Large-signal stability analysis in power systems with a synchronous generator connected to a large motor drive," in *Proc. 2007 Electric Ship Technologies Symposium*, Arlington, VA, May 2007, pp. 42-47.

[43] J. V. Amy Jr., "Composite system stability methods applied to advanced shipboard electric power systems," Ph.D. dissertation, Massachusetts Institute of Technology, Cambridge, MA, 1992.

[44] J. F. Gieras, *Advancements in Electric Machines*. New York, NY: Springer-Verlag Inc., 2008.

[45] A. Arkkio, T. Jokinen, and E. Lantto, "Induction and permanent-magnet synchronous machines for high-speed applications," in *Proc. 2005 8th International Conference on Electrical Machines and Systems*, Nanjing, China, Sep. 2005, pp. 871-876.

[46] Hiperco 50 data sheet. Available: http://www.cartech.com.

[47] M. Lokhandwalla, K. S. Haran, and J. P. Alexander, "Scaling studies of high speed high temperature superconducting generator," in *Proc. 2012 International Conference on Electrical Machines*, Marseile, Sep. 2012, pp. 751-756.

[48] M. Ali, M. Andrus, R. Dougal, O. Faruque, B. Hebner, R.Hovsapian, J. Langston, A. Ouroua, K. Schoder, and M.Steurer, "Cross-platform validation of notional baseline architecture models of naval electric ship power systems," in *Proc. 2011 IEEE Electric Ship Technologies Symposium*, Alexandria, VA, Apr. 2011, pp. 78-83.

[49] IEEE Recommended Practice for Excitation System Models for Power System Stability Studies, IEEE Standard 421.5, 2005.

[50] H. Zheng, R. A. Dougal, and M. H. Ali, "Transient stability of high frequency ac power systems," in *Proc. 2013 IEEE Electric Ship Technologies Symposium*, Arlington, VA, Apr. 2013, pp. 292-298.

[51] L. Qi and S. Woodruff, "Stability analysis and assessment of integrated power systems using RTDS," *Electric Ship Technologies Symposium*, 2005

[52] J. Pyrhonen, T. Jokinen, and V. Hrabovcova, *Design of Rotating Electrical Machines*. New York, NY: John Wiley & Sons Inc., 2008.

Appendix A MODELS FOR SMALL-SIGNAL STABILITY ANALYSIS

The reference system for small-signal stability is the two-generator system as shown in Figure 4.2 of Chapter 4. The generator model adopted in this analysis is a two-axis model [24][27]:

$$\begin{cases} T'_{q0i}\dot{E'_{di}} = -E'_{di} - \left(x_{qi} - x'_i\right)I_{qi} \\ T'_{d0i}\dot{E'_{qi}} = E_{FDi} - E'_{qi} + \left(x_{di} - x'_i\right)I_{di} \\ \tau_i\dot{\omega_i} = T_{mi} - \left(I_{di}E'_{di} + I_{qi}E'_{qi}\right) - K_{Di}\omega_i - K_{Si}\delta_i \\ \dot{\delta_i} = \omega_i - 1 \end{cases} \tag{A.1}$$

In this model, T_m is a system input. The governor model was not included under the consideration that during the small-disturbance period, the slow governor will not respond fast enough to affect the output of the generator. The detailed excitation system model which includes Automatic Voltage Regulator (AVR) and Power System Stabilizer (PSS) were not included in the generator model. Fixed values for K_D and K_S are used to represent the effect of the exciter and PSS. There are two reasons for doing so. The exciter contributes a certain amount of synchronizing torque (K_S) to system small-signal stability depending on its parameters which helps improve transient stability, especially for exciters with high ceiling voltage and fast-response AVR [22]. But it also brings negative impact on damping torque by applying the high gain in the AVR. The PSS was introduced back in the 1950s and it was proposed to address this problem: to bring more damping to power systems. In a real application, PSS's structure and parameters are tuned according to the specific parameters

of the exciter and the generator. In this study, in order to represent as many cases as possible and to make the results more general without limiting to a certain structure and parameters of exciter and PSS, we assume that for different generators and system parameters, the exciter and PSS pose the same effect on small-signal stability. Therefore, the values of K_D and K_S are incorporated in the generator model, rather than using the models for the exciter and PSS.

The base generator parameters utilized in this small-signal stability assessment are listed in Table A.1. The subscripts "1" and "2" denote Generator 1 and Generator 2.

Table A.1 Base parameters utilized in small-signal stability analysis

Symbol	Definition	Value
T'_{q01} / T'_{q02}	Transient q-axis open-circuit time constant in second	0.27 / 0.1353
T'_{d01} / T'_{d02}	Transient d-axis open-circuit time constant in pu	2.4094 / 2.8529
H_1 / H_2	Inertia constant in second	4 / 3
x_{q1} / x_{q2}	Synchronous reactance in q-axis in pu	1.5 / 1.0
x_{d1} / x_{d2}	Synchronous reactance in d-axis in pu	1.5 / 1.0
x'_1 / x'_2	Transient reactance (ignore saliency, $x'_d = x'_q$) in pu	0.1926 / 0.1196
K_{S1} / K_{S2}	Synchronizing torque coefficient in pu torque/pu speed deviation	1 / 1
K_{D1} / K_{D2}	Damping torque coefficient in pu torque/pu speed deviation	1 / 1

After linearizing the generator model in (5.10) we can write the reference two-generator system model for the purpose of small-signal stability analysis as following:

$$\begin{cases} T'_{q01}\Delta\dot{E}'_{d1} = -\Delta E'_{d1} - \left(x_{q1} - x'_1\right)\Delta I_{q1} \\ T'_{d01}\Delta\dot{E}'_{q1} = \Delta E_{FD1} - \Delta E'_{q1} + \left(x_{d1} - x'_1\right)\Delta I_{d1} \\ \tau_1\Delta\dot{\omega}_1 = \Delta T_{m1} - \left(I_{d10}\Delta E'_{d1} + I_{q10}\Delta E'_{q1} + E'_{d10}\Delta I_{d1} + E'_{q10}\Delta I_{q1}\right) - K_{D1}\Delta\omega_1 - K_{S1}\Delta\delta_1 \\ T'_{q02}\Delta\dot{E}'_{d2} = -\Delta E'_{d2} - \left(x_{q2} - x'_2\right)\Delta I_{q2} \\ T'_{d02}\Delta\dot{E}'_{q2} = \Delta E_{FD2} - \Delta E'_{q2} + \left(x_{d2} - x'_2\right)\Delta I_{d2} \\ \tau_2\Delta\dot{\omega}_2 = \Delta T_{m2} - \left(I_{d20}\Delta E'_{d2} + I_{q20}\Delta E'_{q2} + E'_{d20}\Delta I_{d2} + E'_{q20}\Delta I_{q2}\right) - K_{D2}\Delta\omega_2 - K_{S2}\Delta\delta_2 \\ \Delta\dot{\delta}_1 = \Delta\omega_1 \\ \Delta\dot{\delta}_2 = \Delta\omega_2 \end{cases} \tag{A.2}$$

Arrange (A.2) into the following succinct form for further manipulation:

$$\begin{cases} \Delta\dot{E}'_{d1} = a_1\Delta E'_{d1} + a_2\Delta I_{q1} \\ \Delta\dot{E}'_{q1} = b_1\Delta E_{FD1} + b_2\Delta E'_{q1} + b_3\Delta I_{d1} \\ \Delta\dot{\omega}_1 = c_1\Delta T_{m1} + c_2\Delta\omega_1 + c_3\Delta E'_{d1} + c_4\Delta E'_{q1} + c_5\Delta I_{d1} + c_6\Delta I_{q1} + c_7\Delta\delta_1 \\ \Delta\dot{E}'_{d2} = d_1\Delta E'_{d2} + d_2\Delta I_{q2} \\ \Delta\dot{E}'_{q2} = e_1\Delta E_{FD2} + e_2\Delta E'_{q2} + e_3\Delta I_{d2} \\ \Delta\dot{\omega}_2 = f_1\Delta T_{m2} + f_2\Delta\omega_2 + f_3\Delta E'_{d2} + f_4\Delta E'_{q2} + f_5\Delta I_{d2} + f_6\Delta I_{q2} + f_7\Delta\delta_2 \\ \Delta\dot{\delta}_1 = \Delta\omega_1 \\ \Delta\dot{\delta}_2 = \Delta\omega_2 \end{cases} \tag{A.3}$$

where intermediate variables of *a* through *f* are expressed as following:

$$\begin{cases} a_1 = \dfrac{-1}{T'_{q01}} \\ a_2 = \dfrac{-x_{q1} + x'_1}{T'_{q01}} \end{cases} \tag{A.4}$$

$$\begin{cases} b_1 = \dfrac{1}{T'_{d01}} \\ b_2 = \dfrac{-1}{T'_{d01}} \\ b_3 = \dfrac{-x_{d1} + x'_1}{T'_{d01}} \end{cases} \tag{A.5}$$

$$\begin{cases} c_1 = \dfrac{1}{\tau_1} \\ c_2 = \dfrac{-K_{D1}}{\tau_1} \\ c_3 = \dfrac{-I_{d10}}{\tau_1} \\ c_4 = \dfrac{-I_{q10}}{\tau_1} \\ c_5 = \dfrac{-E'_{d10}}{\tau_1} \\ c_6 = \dfrac{-E'_{q10}}{\tau_1} \\ c_7 = \dfrac{-K_{S1}}{\tau_1} \end{cases} \tag{A.6}$$

$$\begin{cases} d_2 = \dfrac{-1}{T'_{q02}} \\ d_2 = \dfrac{-x_{q2} + x'_2}{T'_{q02}} \end{cases} \tag{A.7}$$

$$\begin{cases} e_1 = \dfrac{1}{T'_{d02}} \\ e_2 = \dfrac{-1}{T'_{d02}} \\ e_3 = \dfrac{-x_{d2} + x'_2}{T'_{d02}} \end{cases} \tag{A.8}$$

$$\begin{cases} f_1 = \dfrac{1}{\tau_2} \\ f_2 = \dfrac{-K_{D2}}{\tau_2} \\ f_3 = \dfrac{-I_{d20}}{\tau_2} \\ f_4 = \dfrac{-I_{q20}}{\tau_2} \\ f_5 = \dfrac{-E'_{d20}}{\tau_2} \\ f_6 = \dfrac{-E'_{q20}}{\tau_2} \\ f_7 = \dfrac{-K_{S2}}{\tau_2} \end{cases} \tag{A.9}$$

To linearize the equation relating voltages and currents, the following equations can be obtained:

$$\begin{cases} \Delta I_{q1} = g_1\Delta E'_{d1} + g_2\Delta E'_{q1} + g_3\Delta\delta_1 + g_4\Delta E'_{d2} + g_5\Delta E'_{q2} + g_6\Delta\delta_2 \\ \Delta I_{d1} = h_1\Delta E'_{d1} + h_2\Delta E'_{q1} + h_3\Delta\delta_1 + h_4\Delta E'_{d2} + h_5\Delta E'_{q2} + h_6\Delta\delta_2 \\ \Delta I_{q2} = j_1\Delta E'_{d1} + j_2\Delta E'_{q1} + j_3\Delta\delta_1 + j_4\Delta E'_{d2} + j_5\Delta E'_{q2} + j_6\Delta\delta_2 \\ \Delta I_{d2} = k_1\Delta E'_{d1} + k_2\Delta E'_{q1} + k_3\Delta\delta_1 + k_4\Delta E'_{d2} + k_5\Delta E'_{q2} + k_6\Delta\delta_2 \end{cases} \tag{A.10}$$

where

$$\begin{cases} g_1 = -B_{11} \\ g_2 = G_{11} \\ g_3 = Y_{12}\left[\sin(\theta_{12} - \delta_{120})\, E'_{q20} + \cos(\theta_{12} - \delta_{120})\, E'_{d20}\right] \\ g_4 = -Y_{12}\sin(\theta_{12} - \delta_{120}) \\ g_5 = Y_{12}\cos(\theta_{12} - \delta_{120}) \\ g_6 = -g_3 \end{cases} \tag{A.11}$$

$$\begin{cases} h_1 = G_{11} \\ h_2 = B_{11} \\ h_3 = Y_{12}\left[\sin(\theta_{12} - \delta_{120})\, E'_{d20} - \cos(\theta_{12} - \delta_{120})\, E'_{q20}\right] \\ h_4 = Y_{12}\cos(\theta_{12} - \delta_{120}) \\ h_5 = Y_{12}\sin(\theta_{12} - \delta_{120}) \\ h_6 = -h_3 \end{cases} \tag{A.12}$$

$$\begin{cases} j_1 = -Y_{12}\sin(\theta_{12}+\delta_{120}) \\ j_2 = Y_{12}\cos(\theta_{12}+\delta_{120}) \\ j_3 = -Y_{12}\left[\sin(\theta_{12}+\delta_{120})\,E'_{q10} + \cos(\theta_{12}+\delta_{120})\,E'_{d10}\right] \\ j_4 = -B_{22} \\ j_5 = G_{22} \\ j_6 = -j_3 \end{cases} \tag{A.13}$$

$$\begin{cases} k_1 = Y_{12}\cos(\theta_{12}+\delta_{120}) \\ k_2 = Y_{12}\sin(\theta_{12}+\delta_{120}) \\ k_3 = Y_{12}\left[\cos(\theta_{12}+\delta_{120})\,E'_{q10} + \sin(\theta_{12}+\delta_{120})\,E'_{d10}\right] \\ k_4 = G_{22} \\ k_5 = B_{22} \\ k_6 = -k_3 \end{cases} \tag{A.14}$$

where B, G, Y are the elements of the admittance matrix of the two-generator system including transmission line impedance, generator synchronous reactance and transient reactance. When calculating the admittance matrix, Node 1 and 2 are behind the d/q axis steady-state or transient-state voltage. θ_{12} is the angle of the element of the admittance matrix at Column 2, Array 1. δ_{120} is the initial relative rotor angle between generator 1 and 2 before perturbation.

Finally, the system state-space equations in matrix form can be obtained by substituting (A.10) into (A.3) and necessary algebraic manipulation:

$$\dot{\boldsymbol{X}} = \boldsymbol{AX} + \boldsymbol{BY} \tag{A.15}$$

$$\boldsymbol{A} = \begin{bmatrix} \boldsymbol{a_1 + a_2 g_1} & \boldsymbol{a_2 g_1} & \boldsymbol{0} & \boldsymbol{a_2 g_4} & \boldsymbol{a_2 g_5} & \boldsymbol{0} & \boldsymbol{a_2 g_7} & \boldsymbol{a_2 g_8} \\ \boldsymbol{b_3 h_1} & \boldsymbol{b_2 + b_3 h_2} & \boldsymbol{0} & \boldsymbol{b_3 h_4} & \boldsymbol{b_3 h_5} & \boldsymbol{0} & \boldsymbol{b_3 h_7} & \boldsymbol{b_3 h_8} \\ \boldsymbol{c_3 + c_5 h_1 + c_6 g_1} & \boldsymbol{c_4 + c_5 h_2 + c_6 g_2} & \boldsymbol{c_2} & \boldsymbol{c_5 h_4 + c_6 g_4} & \boldsymbol{c_5 h_5 + c_6 g_5} & \boldsymbol{0} & \boldsymbol{c_5 h_7 + c_6 g_7 + c_7} & \boldsymbol{c_5 h_8 + c_6 g_8} \\ \boldsymbol{d_2 j_1} & \boldsymbol{d_2 j_2} & \boldsymbol{0} & \boldsymbol{d_1 + d_2 j_4} & \boldsymbol{d_2 j_5} & \boldsymbol{0} & \boldsymbol{d_2 j_7} & \boldsymbol{d_2 j_8} \\ \boldsymbol{e_3 k_1} & \boldsymbol{e_3 k_2} & \boldsymbol{0} & \boldsymbol{e_3 k_4} & \boldsymbol{e_2 + e_3 k_5} & \boldsymbol{0} & \boldsymbol{e_3 k_7} & \boldsymbol{e_3 k_8} \\ \boldsymbol{f_5 k_1 + f_6 j_1} & \boldsymbol{f_5 k_2 + f_6 j_2} & \boldsymbol{0} & \boldsymbol{f_3 + f_5 k_4 + f_6 j_4} & \boldsymbol{f_4 + f_5 k_5 + f_6 j_5} & \boldsymbol{f_2} & \boldsymbol{f_5 k_7 + f_6 j_7} & \boldsymbol{f_7 + f_5 k_8 + f_6 j_8} \\ \boldsymbol{0} & \boldsymbol{0} & \boldsymbol{1} & \boldsymbol{0} & \boldsymbol{0} & \boldsymbol{0} & \boldsymbol{0} & \boldsymbol{0} \\ \boldsymbol{0} & \boldsymbol{0} & \boldsymbol{0} & \boldsymbol{0} & \boldsymbol{0} & \boldsymbol{1} & \boldsymbol{0} & \boldsymbol{0} \end{bmatrix}$$

$$\boldsymbol{X} = \begin{bmatrix} \Delta \mathrm{E}'_{d1} \\ \Delta \mathrm{E}'_{q1} \\ \Delta\omega_1 \\ \Delta \mathrm{E}'_{d2} \\ \Delta \mathrm{E}'_{q2} \\ \Delta\omega_2 \\ \Delta\delta_1 \\ \Delta\delta_2 \end{bmatrix} \qquad \boldsymbol{Y} = \begin{bmatrix} 0 \\ \Delta E_{FD1} \\ \Delta T_{m1} \\ 0 \\ \Delta E_{FD2} \\ \Delta T_{m2} \\ 0 \\ 0 \end{bmatrix} \qquad \boldsymbol{B} = diag[0 \quad b_1 \quad c_1 \quad 0 \quad e_1 \quad f_1 \quad 0 \quad 0]$$